Investigating the impact of pre-harvesting sprouting on maize hardness using near infrared (NIR) hyperspectral imaging and X-ray micro-computed tomography (µCT)

by

Tshepiso Mokhoro

Thesis presented in partial fulfilment of the requirements for the degree

MASTER OF SCIENCE IN FOOD SCIENCE

in the Faculty of AgriSciences

at Stellenbosch University

Supervisor: Prof Marena Manley

Co-supervisors: Prof Paul Geladi

Dr Anton du Plessis

Dr Glen Fox

March 2016

DECLARATION

By submitting this thesis electronically, I declare that the entirety of the work contained therein is my own, original work, that I am the sole author thereof (save to the extent explicitly otherwise stated), that reproduction and publication thereof by Stellenbosch University will not infringe any third party rights and that I have not previously in its entirety or in part submitted it for obtaining any qualification.

Tshepiso Mokhoro
March 2016

Table of Contents

Language and style used in this thesis are in accordance with the requirements of the International Journal of Food Science and Technology. This thesis represents a compilation of manuscripts where each chapter is an individual entity and some repetition between chapters has, therefore, been unavoidable.

Acknowledgements

This thesis is dedicated to my son Thato Tshepo and my mother Louisa Masoabi Mokhoro (1954-2005). So don't get tired of doing what is good, don't get discouraged and give up, for you will reap a harvest of blessings at the appropriate time (Gal 6:9 NLT). This verse has been experienced through this thesis.

I would like to give all praise to the heavenly Father for providing me with the following individuals and institutions, without which this thesis would not have been possible to assemble:

- my supervisor, Prof Manley whose critic ensured that a good document was produced at the end of this study, for the patience and push to complete this study;
- my co-supervisor, Prof Geladi for his expertise on NIR hyperspectral imaging and chemometrics;
- my co-supervisor, Dr Du Plessis, for assistance with X-ray micro computed tomography (X-ray µCT and reviewing my work to provide me with feedback;
- my co-supervisor, Dr Glen Fox for helping with editing the compiled chapters;
- the staff of CAF including Stephan le Roux, Olwethu Majodina, for X-ray µCT assistance and analysis;
- Umbio AB (Umeå, Sweden) for the use of their Umbio Inspector SWIR pushbroom hyperspectral imaging system; and
- Sasko, a division of Pioneer Foods (Pty) Ltd (Paarl, South Africa), for the use of their research and development facilities supplying samples used in the study.

I would also like to acknowledge the financial contributions of:

- Department of Agriculture Forestry and Fisheries (DAFF)
- Belgian Technical Corporation (BTC)

On a more personal note, I would like to thank my family, Mr Khotso Mpitso, my Parmalat colleagues, Mr C Ng'andwe for always encouraging me to continue when I wanted to give up. For always being there to carry me through the patches when I felt discouraged.

To my dear sisters Setsoana Moorosi and Pontsho Moorosi, I could not be more grateful than I am right now for having both of you in my life. As we say in Sesotho "Poho pedi ha e hlolwe ke morwalo" translated there is no amount of work is too intense for the masses. Even though we were in different countries at the time, those skype calls really helped with the late nights that I sometimes had to pull for this work. Love you immensely.

Abstract

Maize forms an integral part of the human energy intake in South Africa and its quality should always be maintained. A quality attribute important to the dry milling industry is maize hardness. In the milling industry, hard maize hybrids are described as kernels with a higher ratio of vitreous endosperm in comparison to floury endosperm. Certain circumstances such as agricultural conditions (e.g. pre-harvest germination), post-harvest conditions and improper treatments (e.g. no irrigation during periods of insufficient rain or improper drying procedures) will have a negative impact on maize hardness. This study focused on the impact of pre-germination on maize hardness, subsequently observations on the rate of the pre-germination process on three hardness variants (hard, intermediate and soft) were noted. Six maize hybrids with varying hardness levels were pre-germinated (from 0 – 22 h) bi-hourly and three imaging techniques (Scanning electron microscopy (SEM), near-infrared (NIR) hyperspectral imaging and X-ray micro computed tomography (X-ray µCT)) used to investigate the impact of the process on hardness.

From the NIR hyperspectral imaging technique, principal component analysis (PCA) score plots and score images were employed in the investigations due to the amount of data obtained. Three types of endosperm (vitreous, intermediate or floury) were observed in the first principal component (PC1) of the score images. PCA classification plots revealed the three types of endosperm present within a maize kernel. Classification plots (both score plots and images) allowed for the isolation of the vitreous endosperm by removing the two clusters representing the floury and intermediate endosperm. PCA score images depicted decreasing trend in the content of the vitreous endosperm as pre-germination took place. Another observation from the PCA score images was that, the soft maize hybrids showed traces of vitreous endosperm after 8 h of pre-germination. The intermediate hybrids showed a decrease in the endosperm content at 12 h and the hard hybrid was noted to be at 18 h. Pixel count (obtained from the PCA score plots) indicated a decreasing trend in all hybrids investigated. The graphs plotted from pixel counts of hard hybrids (i.e. H2 and H3), intermediate (H7) and soft (H9) depicted decreasing curvilinear plots. The rest of the hybrids' graphs (H6 and H5) depicted a decreasing linear trend.

X-ray µCT indicated fissures and shrinkage stress cracks occurring as a results of either or both of the pre-germination and drying processes. Larger fissures were assumed to have developed due to pre-germination and shrinkage stress cracks from the drying process. These (i.e. fissures and shrinkage stress cracks) were observed in all the 10 h and 22 h images, on 2D slices and 3D volumes. The side orientation 2D image slices depicted the intermediate and soft maize hybrids' endosperm integrity as having deteriorated more than the hard hybrid at 10 h and 22 h incubation time period. The top orientation of the 2D slice images indicated the hard and intermediate deteriorated more than the soft hybrids. It was noted that the fissures and shrinkage stress cracks developed throughout the maize kernel.

SEM was used to validate results obtained from the X-ray µCT imaging system, fissures could also be observed on SEM images. Starch and protein matrix deterioration was also observed.

Starch granules and protein matrix developed numerous pores on the surfaces indicating the extent of deterioration.

Single kernel analysis using 2D slices at T8 = 21 h, crevices started to develop and propagated until the end of the pre-germination process at T19 = 143 h. Fissure measurement indicated an increment in all measured areas of the maize kernels, i.e. from the left side of the maize kernel fissures propagated from 1.51 mm at 99 h to 4.22 mm at 143 h, on the right side from 1.86 mm at 99 h to 3.65 mm at 143 h. At T15 = 123 h, a horizontal fissure was observed and measured to be 1.62 mm long while at T19 = 143 h it had propagated to 4.30 mm. The fissures were noted to be pathways used to transport hydrolytic enzymes and monomers (obtained from starch and protein hydrolysis) to the germ where the growing embryo utilises them as a source of nutrition. Volumes of the vitreous endosperm were also determined and a decreasing trend was noticed. At T1 = 0 h the content of the vitreous endosperm was 64.7 mm^3 and at T19 = 143 h the content had decreased to 50.5 mm^3.

Endosperm deterioration due to pre-germination should thus be of great concern to the milling industry as it influences the desired end product.

Abbreviations

2D	Two dimensional
3D	Three dimensional
h	Hours
H	Hybrid
mm	Millimetre
NIR hyperspectral imaging	Near-infrared hyperspectral imaging
PC	Principal component
PCA	Principal component analysis
SEM	Scanning electron microscope
SNV	standard normal variate
T	Time
X-ray µCT	X-ray micro computed tomography

List of Tables

Chapter 4

List of Figures

Chapter 2

Chapter 3

Chapter 1

Introduction

Maize (*Zea mays* L.) is the most produced cereal crop in South Africa, followed by wheat, and most adapted to different ecosystems (Serna-Saldivar, 2010). It provides about half of the energy intake of mankind (Pereira *et al.*, 2008; Poutanen, 2012). Based on the maize quality report provided by the Southern African Grain Laboratory, 10 357 961 tonnes of maize were locally produced during the 2012/13 season (Anon., 2013). Over a quarter of the produced tonnes (i.e. 3 558 283) were processed for human consumption and 1 926 364 tonnes were exported to other African countries. Maize is mostly dry milled to produce a range of raw materials such as maize meal and samp which are the staple foods for many South Africans (O'Kennedy, 2011). Maize meal is used as the main ingredient in the production of a porridge commonly known as 'pap' (van der Merwe *et al.*, 2001) and for the production of the traditional Transkei Xhosa beer (Shephard *et al.*, 2005). During the dry milling process, the pericarp and germ are separated from the endosperm. In order to achieve maximum separation, the maize kernel should be of a hard character because hardness influences milling efficiency in addition to quality of the final product (Jindal & Mohsenin, 1978; Almeida- Dominguez *et al.*, 1997; Fox & Manley, 2009; Blandino *et al.*, 2010).

Maize hardness is a quality trait that describes the ability of a kernel to withstand applied force without fracture (Pomeranz *et al.*, 1986a; Pomeranz *et al.*, 1986b; Chandrashekar & Mazhar, 1999). It has also been mainly related to the ratio of the two endosperm types present within a maize kernel. Based on the difference in compactness of the starch granules in the protein matrix, the two types of endosperm (floury and vitreous) have been identified identified and the more vitreous endosperm present within the maize kernel, that kernel is said to be a hard maize kernel (Dombrink-Kurtzman & Bietz, 1993; Almeida-Dominguez *et al.*, 1997; Dombrink-Kurtzman & Knutson, 1997; Lee *et al.*, 2005; Lee *et al.*,2006; Manley *et al.*, 2009; Williams *et al.*, 2009; Blandino *et al.*, 2010).

Due to the amount of maize produced and consumed in South Africa, it is essential that maize kernel integrity be maintained to avoid losses for farmers, millers and consumers. Quality control is one of the most important goals of any industry and with increasing expectations for food products with high quality and safety, the need for accurate, fast and objective determination of product characteristics continues to grow (ElMasry & Sun, 2010).

Near infrared hyperspectral imaging, which combines near infrared (NIR) spectroscopy with digital imaging, has been used to investigate food and agricultural products non-destructively (review Elmasry *et al.*, 2012; Manley, 2014). NIR hyperspectral images provide chemical composition and spatial information of a sample, using a number of NIR wavelengths (Mehl *et al.*, 2004; Lee *et al.*,2005; Reich, 2005; Gowen *et al.*, 2007). Advantages of this method are the ability to depict chemical composition and location of the chemical compounds, minimal sample preparation, no use of chemical substances and fast acquisition times (Orman & Schumann Jr, 1991; Geladi, 2002; Büning- Pfaue, 2003; Baye *et al.*, 2006; Huang *et al.*, 2008). Interpretation of hyperspectral images is possible using chemometrics methods (Gowen *et al.*, 2007).

NIR hyperspectral imaging has been used to classify maize (Manley *et al.*, 2009; Williams *et al.*, 2009; McGoverin & Manley, 2012) and wheat (Du Toit, 2009) kernels based on hardness. Other applications included detection of pre-germinated wheat, barley and sorghum grains (Arngren *et al.*,2011; McGoverin *et al.*, 2011) investigation of food quality (Qiao *et al.*, 2007) and presence of contamination (Siripatrawan *et al.*, 2011) to ensure food safety (Mehl *et al.*, 2004; Gowen *et al.*,2007; Del Fiore *et al.*, 2010; Fernández Pierna *et al.*, 2012; Dale *et al.*, 2013; Di & Sun, 2013; Moghaddam *et al.*, 2013; Williams, 2013).

A more recent technique, i.e. X-ray micro-computed tomography (µCT) that is fast becoming the technique of choice in food research, due to it enabling three-dimensional visualisation of a sample's internal structure non-destructively and non-invasively (Bull, 1993). X-ray µCT has been used to investigate various food products such as meat (Young *et al.*, 2002; Frisullo *et al.*, 2009), fruits and vegetables (Mendoza *et al.*, 2007; Léonard *et al.*, 2008), emulsions and foam products (Lim & Barigou, 2004) as well as coffee (Laverse *et al.*, 2012). The technique has also been used to investigate the crispiness of cornflakes produced using different mechanical and processing (i.e. batch and extruded) conditions (Chaunier *et al.*, 2007). Texture is important in determining the quality of cornflakes and X-ray µCT results correlated with the destructive piston method. In another study, crispiness of products made from maize starch extrudates (e.g. tortilla chips) was correlated with micro-structural data such as air cell wall thickness and cell diameter (Agbisit *et al.*, 2007). X- ray µCT has been used to provide information on texture variability between biscuits made from different solvent-coupled flavours (Yang *et al.*, 2012).

During high rainfall seasons, germination of the kernels on the maize ear is likely to be initiated with subsequent starch hydrolysis. When germination or sprouting takes place prior to the maize being harvested, it is termed pre-harvest sprouting (PHS) and is signalled by visible evidence of the protruding radicle (Fincher, 1989; Bewley & Black, 1994; Ceccato *et al.*, 2011; DePauw *et al.*, 2011). PHS is a well-studied occurrence for cereal grains such as barley (Brookes, 1980; Jensen *et al.*, 1984; Evers & Millar, 2002; Jacobsen *et al.*, 2002; Gualano & Benech-Arnold, 2009; Engelbrecht, 2011; McGoverin *et al.*, 2011) and wheat (Bewley & Black, 1994; Evers *et al.*, 1995; Skerritt & Heywood, 2000; Gelin *et al.*, 2006; Fang & Chu, 2008; Xing *et al.*, 2009; Arngren *et al.*, 2011; Engelbrecht, 2011) as it decreases malting and baking quality, respectively. The extent of the concern regarding PHS is indicated by the International Symposium on pre-harvest sprouting in cereals held every three to four years.

Similar to barley and wheat, maize is also prone to PHS (Bewley & Black, 1994). During the sprouting process, endosperm contents are utilised for the development of the maize kernel into a new seedling. Maize endosperm is the most important part of the maize kernel for the milling industry. Presently, there is no study that has been conducted to investigate the impact of PHS on the hardness (vitreous endosperm) of maize kernels, as vitreous endosperm is utilised for energy during the PHS process. Thus the impact of PHS on endosperm texture is of great concern and will be investigated in this study. The non-destructive nature of NIR hyperspectral imaging as well as X-ray µCT, makes these methods ideal for characterising whole maize kernels. Maize kernels used in this study were subjected to sprouting under controlled conditions, therefore the term pre-germination will be used rather than PHS. The objectives of this study were thus to:

- investigate the effect of pre-germination on the vitreous endosperm in maize kernels differing in hardness, using NIR hyperspectral imaging; and
- evaluate the effect of pre-germination on the microstructure of whole maize kernels, differing in hardness, using X-ray µCT.

References

Abdelrahman, A. & Hoseney, R. (1984). Basis for hardness in pearl millet, grain sorghum, and corn. *Cereal Chemistry*, **61**, 232-235.

Agbisit, R., Alavi, S., Cheng, E., Herald, T. & Trater, A. (2007). Relationships between microstructure and mechanical properties of cellular cornstarch extrudates. *Journal of Texture Studies*, **38**,199-219.

Aldrich, S.R. & Leng, E.R. (1965). Modern corn production. *Modern corn production.*

Almeida-Dominguez, H.D., Suhendro, E.L. & Rooney, L.W. (1997). Factors affecting rapid visco analyser curves for the determination of maize kernel hardness. *Journal of Cereal Science*,**25**, 93-102.

Anonymous (2013). South African maize crop: Quality report 2012/2013 season. [WWW document]. http://www.sagl.co.za/Maize/Maizereports/20122013Season.aspx. 02/02/2014

Arngren, M., Hansen, P.W., Eriksen, B., Larsen, J. & Larsen, R. (2011). Analysis of pre-germinated barley using hyperspectral image analysis. *Journal of Agricultural and Food Chemistry*, **21**,11385-11394.

Baye, T.M., Pearson, T.C. & Settles, A.M. (2006). Development of a calibration to predict maize seed composition using single kernel near infrared spectroscopy. *Journal of Cereal Science*, **43**, 236-243.

Bewley, J.D. & Black, M. (1994). *Seeds: physiology of development and germination.* Pp. 372. NewYork: Plenum Publishing Corporation.

Blandino, M., Mancini, M.C., Peila, A., Rolle, L., Vanara, F. & Reyneri, A. (2010). Determination of maize kernel hardness: comparison of different laboratory tests to predict dry-milling performance. *Journal of the Science of Food and Agriculture*, **90**, 1870-1878.

Brookes, P.A. (1980). The significance of pre-harvest sprouting of barley in malting and brewing. *Cereal Research Communications*, **8**, 29-38.

Bull, C. (1993). A review of sensing techniques which could be used to generate images of agricultural and food materials. *Computers and Electronics in Agriculture*, **8**, 1-29.

Büning-Pfaue, H. (2003). Analysis of water in food by near infrared spectroscopy. *Food Chemistry*, **82**, 107-115.

Ceccato, D.V., Daniel Bertero, H. & Batlla, D. (2011). Environmental control of dormancy in quinoa (Chenopodium quinoa) seeds: two potential genetic resources for pre-harvest sprouting tolerance. *Seed Science Research*, **21**, 133.

Chandrashekar, A. & Mazhar, H. (1999). The biochemical basis and implications of grain strength in sorghum and maize. *Journal of Cereal Science*, **30**, 193-207.

Chaunier, L., Della Valle, G. & Lourdin, D. (2007). Relationships between texture, mechanical properties and structure of cornflakes. *Food Research International*, **40**, 493-503.

Dale, L.M., Thewis, A., Boudry, C., Rotar, I., Dardenne, P., Beaten, V. & Pierra, J.A.F. (2013). Hyperspectral imaging applications in agriculture and agro-food product quality and safety control: a review. *Applied Spectroscopy Reviews*, **48**, 142-159.

Del Fiore, A., Reverberi, M., Ricelli, A., Pinzari, F., Serranti, S., Fabbri, A.A., Bonifazi, G. & Fanelli,C. (2010). Early detection of toxigenic fungi on maize by hyperspectral imaging analysis.*International Journal of Food Microbiology*, **144**, 64-71.

DePauw, R., Knox, R., Singh, A., Fox, S., Humphreys, D. & Hucl, P. (2011). Developing standardized methods for breeding preharvest sprouting resistant wheat, challenges and successes in Canadian wheat. *Euphytica*, 1-8.

Di, W. & Sun, D.-W. (2013). Advanced applications of hyperspectral imaging technology for food quality and safety analysis and assessment: a review-part II: applications. *Innovative Food Science and Emerging Technologies*, **19**, 15-28.

Dombrink-Kurtzman, M. & Bietz, J.A. (1993). Zein composition in hard and soft endosperm of maize.*Cereal Chemisty*, **70**, 105-108.

Dombrink-Kurtzman, M. & Knutson, C. (1997). A study of maize endosperm hardness in relation to amylose content and susceptibility to damage. *Cereal Chemistry*, **74**, 776-780.

Du Toit, G. (2009). Near infrared hyperspectral imaging and chemometrics for exploration and classification of whole wheat kernels. Stellenbosch: University of Stellenbosch.

Elmasry, G., Kamruzzaman, M., Sun, D.-W. & Allen, P. (2012). Principles and applications of hyperspectral imaging in quality evaluation of agro-food products: a review. *Critical reviews in food science and nutrition*, **52**, 999-1023.

ElMasry, G. & Sun, D.-W. (2010). Principles of hyperspectral imaging technology. In: *Hyperspectral Imaging for Food Quality Analysis and Control* (edited by S. Professor Da-Wen). Pp. 3-43. San Diego: Academic Press.

Engelbrecht, P. (2011). Near infrared hyperspectral imaging as detection method for pre-germination in whole wheat, barley and sorghum grains. Stellenbosch: University of Stellenbosch.

Evers, A.D., Flintham, J. & Kotecha, K. (1995). Alpha-amylase and grain size in wheat. *Journal of Cereal Science*, **21**, 1-3.

Evers, T. & Millar, S. (2002). Cereal grain structure and development: some implications for quality. *Journal of Cereal Science*, **36**, 261-284.

Fang, J. & Chu, C. (2008). Abscisic acid and the pre-harvest sprouting in cereals. *Plant signaling & behavior*, **3**, 1046.

Fernández Pierna, J.A., Vermeulen, P., Amand, O., Tossens, A., Dardenne, P. & Baeten, V. (2012). NIR hyperspectral imaging spectroscopy and chemometrics for the detection of undesirable substances in food and feed. *Chemometrics and Intelligent Laboratory Systems*, **117**, 233-239.

Fincher, G.B. (1989). Molecular and cellular biology associated with endosperm mobilization in germinating cereal grains. *Annual review of plant biology*, **40**, 305-346.

Fox, G. & Manley, M. (2009). Hardness methods for testing maize kernels. *Journal of Agricultural and Food Chemistry*, **57**, 5647-5657.

Frisullo, P., Laverse, J., Marino, R. & Nobile, M.D. (2009). X-ray computed tomography to study processed meat microstructure. *Journal of Food Engineering*, **94**, 283-289.

Geladi, P. (2002). Some recent trends in the calibration literature. *Chemometrics and Intelligent Laboratory Systems*, **60**, 211-224.

Gelin, J.R., Elias, E.M. & Kianian, S.F. (2006). Evaluation of two durum wheat (Triticum turgidum L. var. durum) crosses for pre-harvest sprouting resistance. *Field Crops Research*, **97**, 188-196.

Gowen, A.A., O'Donnell, C.P., Cullen, P.J., Downey, G. & Frias, J.M. (2007). Hyperspectral imaging – an emerging process analytical tool for food quality and safety control. *Trends in Food Science and Technology*, **18**, 590-598.

Gualano, N.A. & Benech-Arnold, R.L. (2009). Predicting pre-harvest sprouting susceptibility in barley: Looking for “sensitivity windows” to temperature throughout grain filling in various commercial cultivars. *Field Crops Research*, **114**, 35-44.

Huang, H., Yu, H., Xu, H. & Ying, Y. (2008). Near infrared spectroscopy for on/in-line monitoring of quality in foods and beverages: A review. *Journal of Food Engineering*, **87**, 303-313.

Huber, K. & BeMiller, J. (2000). Channels of maize and sorghum starch granules. *Carbohydrate polymers*, **41**, 269-276.

Jacobsen, J.V., Pearce, D.W., Poole, A.T., Pharis, R.P. & Mander, L.N. (2002). Abscisic acid, phaseic acid and gibberellin contents associated with dormancy and germination in barley. *Physiologia Plantarum*, **115**, 428-441.

Jensen, S.A., Munck, L. & Kruger, J. (1984). A rapid fluorescence method for assessment of pre-harvest sprouting of cereal grains. *Journal of Cereal Science*, **2**, 187-201.

Jindal, V.K. & Mohsenin, N.N. (1978). Dynamic hardness determination of corn kernels from impact tests. *Journal of Agricultural Engineering Research*, **23**, 77-84.

Laverse, J., Mastromatteo, M., Frisullo, P. & Del Nobile, M.A. (2012). X-ray microtomography to study the microstructure of mayonnaise. *Journal of Food Engineering*, **108**, 225-231.

Lee, K.-M., Bean, S.R., Alavi, S., Herrman, T.J. & Waniska, R.D. (2006). Physical and biochemical properties of maize hardness and extrudates of selected hybrids. *Journal of Agricultural and Food Chemistry*, **54**, 4260-4269.

Lee, K.M., Herrman, T.J., Lingenfelser, J. & Jackson, D.S. (2005). Classification and prediction of maize hardness-associated properties using multivariate statistical analyses. *Journal of Cereal Science*, **41**, 85-93.

Léonard, A., Blacher, S., Nimmol, C. & Devahastin, S. (2008). Effect of far-infrared radiation assisted drying on microstructure of banana slices: an illustrative use of X-ray microtomography in microstructural evaluation of a food product. *Journal of Food Engineering*, **85**, 154-162.

Lim, K. & Barigou, M. (2004). X-ray micro-computed tomography of cellular food products. *Food Research International*, **37**, 1001-1012.

Manley, M. (2014). Near-infrared spectroscopy and hyperspectral imaging: non-destructive analysis of biological materials. *Chemical Society Reviews*, **43**, 8200-8214.

Manley, M., Williams, P., Nilsson, D. & Geladi, P. (2009). Near infrared hyperspectral imaging for the evaluation of endosperm texture in whole yellow maize (Zea maize L.) kernels. *Journal of Agricultural and Food Chemistry*, **57**, 8761-8769.

McGoverin, C.M., Engelbrecht, P., Geladi, P. & Manley, M. (2011). Characterisation of non-viable whole barley, wheat and sorghum grains using near-infrared hyperspectral data and chemometrics. *Analytical and Bioanalytical Chemistry*, 1-7.

McGoverin, C.M. & Manley, M. (2012). Classification of maize kernel hardness using near infrared hyperspectral imaging. *Journal of Near Infrared Spectroscopy*, **20**, 529-535.

Mehl, P.M., Chen, Y.-R., Kim, M.S. & Chan, D.E. (2004). Development of hyperspectral imaging technique for the detection of apple surface defects and contaminations. *Journal of Food Engineering*, **61**, 67-81.

Mendoza, F., Verboven, P., Mebatsion, H.K., Kerckhofs, G., Wevers, M. & Nicolaï, B. (2007). Three- dimensional pore space quantification of apple tissue using X-ray computed microtomography. *Planta*, **226**, 559-570.

Mestres, C. & Matencio, F. (1996). Biochemical basis of kernel milling characteristics and endosperm vitreousness of maize. *Journal of Cereal Science*, **24**, 283-290.

Moghaddam, T.M., Razavi, S.M. & Taghizadeh, M. (2013). Applications of hyperspectral imaging in grains and nuts quality and safety assesment: a review. *Journal of Food Measurement and Characterization*, **7**, 129-140.

O'Kennedy, K. (2011). Characterisation of zein from South African maize of varying endosperm texture. MSc in Food Science, University of Stellenbosch: Stellenbosch.

Orman, B.A. & Schumann Jr, R.A. (1991). Comparison of near-infrared spectroscopy calibration methods for the prediction of protein, oil, and starch in maize grain. *Journal of agricultural and food chemistry*, **39**, 883-886.

Pereira, R.C., Davide, L.C., Pedrozo, C.A., Carneiro, N.P., Souza, I.R. & Paiva, E. (2008). Relationship between structural and biochemical characteristics and texture of corn grains. *Genetics and Molecular Research*, **7**, 498-508.

Pomeranz, Y., Czuchajowska, Z. & Lai, F. (1986a). Comparison of methods for determination of hardness and breakage susceptibility of commercially dried corn. *Cereal chemistry*, **63**, 39- 43.

Pomeranz, Y., Hall, G., Czuchajowska, Z. & Lai, F. (1986b). Test weight, hardness, and breakage susceptibility of yellow dent corn hybrids. *Cereal chemistry*, **63**, 349-351.

Poutanen, K. (2012). Past and future of cereal grains as food for health. *Trends in Food Science & Technology*, **25**, 58-62.

Qiao, J., Ngadi, M.O., Wang, N., Gariépy, C. & Prasher, S.O. (2007). Pork quality and marbling level assessment using a hyperspectral imaging system. *Journal of Food Engineering*, **83**, 10-16.

Reich, G. (2005). Near-infrared spectroscopy and imaging: Basic principles and pharmaceutical applications. *Advanced Drug Delivery Reviews*, **57**, 1109-1143.

Robutti, J., Borrás, F., González, R., Torres, R. & De Greef, D. (2002). Endosperm properties and extrusion cooking behavior of maize cultivars. *LWT - Food Science and Technology*, **35**, 663- 669.

Serna-Saldivar, S.O. (2010). *Cereal grains: properties, processing, and nutritional attributes.* CRC Press Inc.

Shephard, G.S., van der Westhuizen, L., Gatyeni, P.M., Somdyala, N.I.M., Burger, H.M. & Marasas, W.F.O. (2005). Fumonisin mycotoxins in traditional Xhosa maize beer in South Africa. *Journal of Agricultural and Food Chemistry*, **53**, 9634-9637.

Williams, P.J. (2013). Near infrared (NIR) hyperspectral imaging and X-ray computed tomography combined with statistical and multivariate data analysis to study Fusarium infection in maize. Stellenbosch: University of Stellenbosch.

Xing, J., Van Hung, P., Symons, S., Shahin, M. & Hatcher, D. (2009). Using a Short Wavelength Infrared (SWIR) hyperspectral imaging system to predict alpha amylase activity in individual Canadian western wheat kernels. *Sensing and Instrumentation for Food Quality and Safety*, **3**, 211-218.

Yang, N., Fisk, I.D., Linforth, R., Brown, K., Walsh, S., Mooney, S., Sturrock, C. & Hort, J. (2012). Impact of flavour solvent on biscuit micro-structure as measured by X-ray micro-Computed Tomography and the distribution of vanillin and HMF (HPLC). *European Food Research and Technology*, **235**, 1083-1091.

Young, M., Lewis, R., Jones, H. & Wolf, B.T. (2002). The use of X-ray computer tomography for measuring the muscularity of live sheep. *Animal Science*.

Chapter2

Literature review

2.0. Introduction

Maize (*Zea mays* L.) is a tall annual plant that belongs to the Poaceae (earlier called Gramineae) grass family. It is the most produced cereal crop in the world (Serna-Saldivar, 2010) and a single maize seed or kernel can develop into a plant that can grow to be 2 to 3.5 m tall in a few weeks. The maize plant prefers abundant sunlight, moisture and temperatures between 10 and 45°C (ideally
30°C) for optimal growth. Commercially, maize plants can grow ears that contain 300 to 1000 developed kernels arranged in rows along a rachis, commonly called a cob (Watson, 1987). Maize kernels can be processed into food products in three ways, i.e. distilling (for ethanol production), wet-milling (to produce starches and sweeteners) and dry-milling (for maize meal and grits) (Radosavljević *et al.*, 2000; Blandino *et al.*, 2010). Maize processing industries are particular about the quality of maize for different end-products. Different levels of maize kernel hardness are needed for the production of ethanol, starches, meal or grits. It is thus imperative that breeders develop grains suitable to the end-use process (Jindal & Mohsenin, 1978; Almeida-Dominguez *et al.*, 1997; Lee *et al.*, 2005; Williams *et al.*, 2009).

Kernel hardness is an inherited property that can be affected by several factors such as agricultural practices, pre- and post-harvest conditions as well as improper treatments (Watson,
1987). In this chapter, the composition of the maize kernel followed by kernel hardness and how it is being measured will be reviewed. In addition pre-germination, its effect on maize quality and detection thereof will be reviewed. This literature review will be concluded with a brief review of non- destructive measurement methods, i.e. (near infrared) NIR hyperspectral imaging and X-ray micro- computed tomography (µCT) as potential methods to detect pre-germination in whole maize kernels.

2.1. Maize kernel composition

A maize kernel constitutes of the pericarp (2% of the dry maize kernel weight) which protects the enclosed germ and endosperm), the germ (10% of the dry maize kernel weight) which consists of the initial parts of the young plant) and the endosperm (80 to 85% of the dry maize

kernel weight) which acts as a storage organ at maturity (Fig. 2.1). The endosperm is an essential part of the kernel and provides energy for the developing embryo and most importantly serves as food for humans, once processed (Watson, 1987; Mestres *et al.*, 1991; Johnson, 2000; van der Merwe *et al.*, 2001; Boyer & Shannon, 2003; Serna-Saldivar, 2010; Tetlow, 2011).

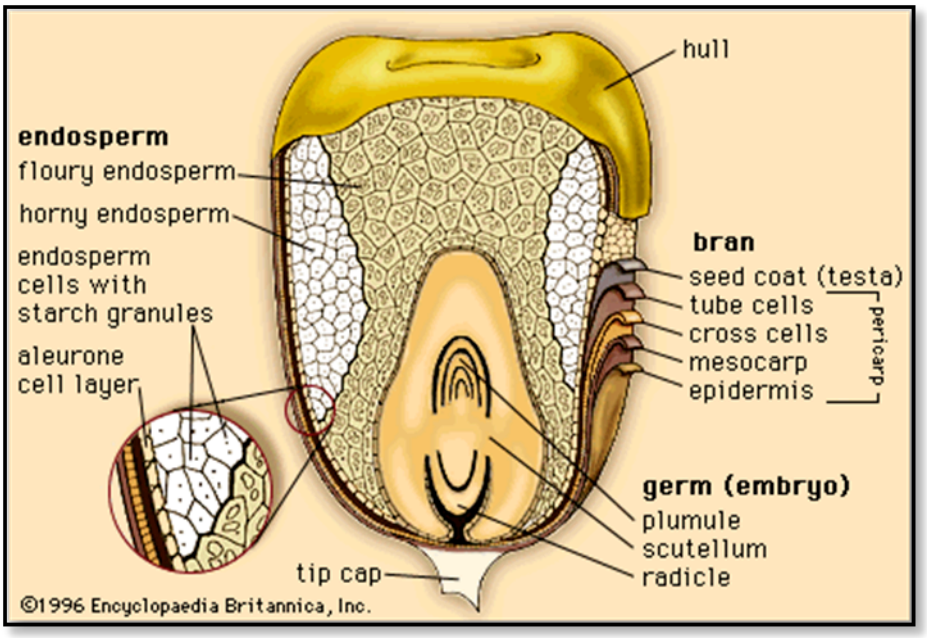

Figure. 2.1 Detailed structure and composition of a maize kernel (Anon., 1996).

The endosperm is characterised by starch granules embedded in a protein matrix (Evers & Millar, 2002). The starch granules are synthesised from sucrose deposited in cells called amyloplasts. The sucrose is then polymerised with the help of enzymes such as Adinosine diphosphate-glucose pyrophosphorylase (AGPase), starch synthase, starch branching as well as starch debranching to form amylose and amylopectin (Singletary *et al.*, 1994; Sabelli & Larkins,
2009). Maize starch is made up of different ratios of amylose (linear structures) and amylopectin (branched structures) (Dombrink-Kurtzman & Knutson, 1997; Lee *et al.*, 2006). Zein (alcohol-soluble proteins that form with the help of polyribosomes and assemble into protein bodies) are split into α- (alpha), β- (beta), γ- (gamma), and δ- (delta) classes.

There are two types of endosperm within a maize kernel, i.e. floury (situated at the central region) and vitreous (situated at the peripheral area) (Watson, 1987). Floury endosperm is regarded as soft endosperm due to minute air pockets present between the starch granules. These air pockets form during drying of the kernels, when the thin protein matrix surrounding the round starch granules shrinks and breaks.

The floury endosperm appears opaque to the naked eye due to the refraction of light by the minute air pockets (Watson, 1987; Fincher, 1989).

In the vitreous endosperm the protein matrix is thicker and remains intact during drying. This protein matrix causes the starch granules to change form and become polyhedral in shape. Lack of refracting light gives the vitreous endosperm a glassy or translucent appearance. The thickness of the protein matrix of the vitreous endosperm is due to the filling pattern that takes place during endosperm development (Fincher,1989). The ratio of the floury-to-vitreous endosperm within the maize kernel impart an important traitcalled maize hardness in the milling industry (Chandrashekar & Mazhar, 1999).

2.2. Maize kernel hardness

Maize kernel hardness or grain strength is a quality property that has been well researched. Maize hardness influences the efficiency of production and quality of the final product (Radosavljević *et al.*,2000; Fox & Manley, 2009; Blandino *et al.*, 2010). The term maize hardness came about because engineers in the cereal industry required knowledge on the measure of strength needed for the handling and processing of maize (Jindal & Mohsenin, 1978). A number of different methods to measure maize hardness are in use and have been studied (Tran *et al.*, 1981; Pomeranz *et al.*,1984; Robutti, 1995; Dombrink-Kurtzman & Knutson, 1997; Hampton *et al.*, 2000; Correa *et al.*,2002; Lee *et al.*, 2005; Gaytán-Martínez *et al.*, 2006; Lee *et al.*, 2006; Tallada *et al.*, 2009), compared(Pomeranz *et al.*, 1986a; Blandino *et al.*, 2010) and reviewed (Chandrashekar & Mazhar, 1999; Fox & Manley, 2009). Methods include relating maize hardness to breakage susceptibility and milling performance (Paulsen & Hill, 1985; Pomeranz *et al.*, 1986b; Wehling *et al.*, 1996), endosperm type (Gupta *et al.*, 1989; Li *et al.*, 1996; Mestres & Matencio, 1996; Robutti *et al.*, 2002).

Maize is wet-milled to produce modified starches. Starch and protein should thus be easy to recover separately (Radosavljević *et al.*, 2000; Blandino *et al.*, 2010). Soft maize is predominately preferred in the wet milling industry as the removal of starch granules is easier from soft kernels. For dry milling, hard maize kernels are preferred for the production of maize grits (large particles). For this purpose soft maize kernels are deemed to have poor milling quality because they produce more flour (small particles) which results in losses during the dry milling process. Thus, during dry milling an intact endosperm recovery is extremely important (Oldewage-Theron *et al.*, 2006; O'Kennedy, 2011).

In South Africa maize is mostly dry milled to produce products such as samp and maize meal (the raw material for traditional beers and porridge) (van der Merwe *et al.*, 2001; Helland *et al.*, 2002; Shephard *et al.*, 2005; Oldewage-Theron *et al.*, 2006; O'Kennedy, 2011). De-germing is usually applied during dry milling.

Intrinsically, maize kernel hardness has been linked with endosperm type ratio, with the higher the vitreous endosperm content, the harder the maize hybrid. Maize hardness has also been linked to amylose content, i.e. the higher the amylose content, the harder the maize hybrid. Very hard hybrids that comprise 75% amylose, called amylose extenders (Chen *et al.*, 2013), have been bred for specific end-products requiring very hard maize. (Jindal & Mohsenin, 1978; Watson, 1987; Almeida-Dominguez *et al.*, 1997; Lee *et al.*, 2005; Williams *et al.*, 2009).

The starch granules are utilised for energy during germination. It is likely that, due to adverse weather conditions, germination could take place before harvesting. This will impact on endosperm integrity as starch is being utilised during germination.

2.3. Pre-germination

Germination is an essential growth process in nature as it ensures the survival of the maize crop, but seeds (intended for food production) that undergo the germination process prior to the harvesting period could lead to major economic losses (Skerritt & Heywood, 2000; Evers & Millar, 2002). Pre- germination is the untimely germination of mature maize kernels that have been subjected to wet or humid conditions prior to the harvest period (Smail *et al.*, 2006) (Fig. 2.2).

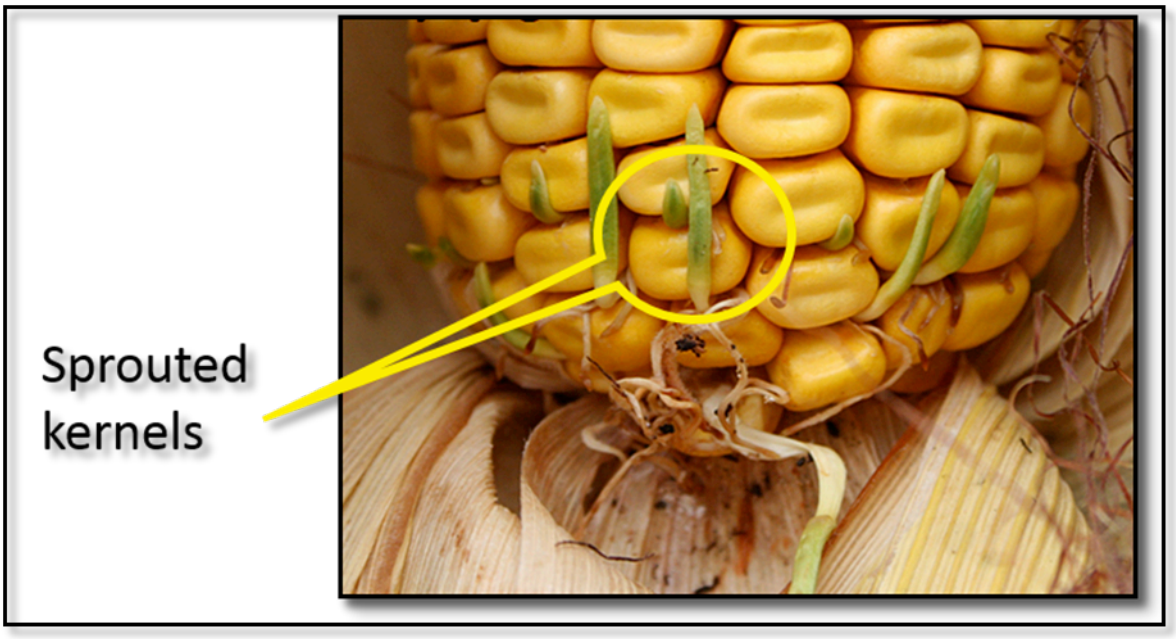

Figure 2.2. Sprouted/pre-germinated maize ear (adapted from Anon., 2012)

Pre-germination decreases grain weight, yield and functionality (Mohan, 2008) due to endosperm contents being broken down and mobilised to the embryo (Harvey & Oaks, 1974). Pre-germination in maize occurs in three phases (Fig. 2.3), namely (1) imbibition and activation; (2) intra-seminal growth; and (3) embryo protrusion (Labouriau & Osborn, 1984; Bewley, 1997; Gallardo *et al.*, 2002; Finch-Savage & Leubner-Metzger, 2006). The aleurone layer (situated on the peripheral area of the endosperm) and the scutellar epithelium (situated on the interface of the embryo and endosperm) play a significant role in the activation and continuance of the germination process(Harvey & Oaks, 1974; Fincher, 1989; Nonogaki *et al.*, 2010).

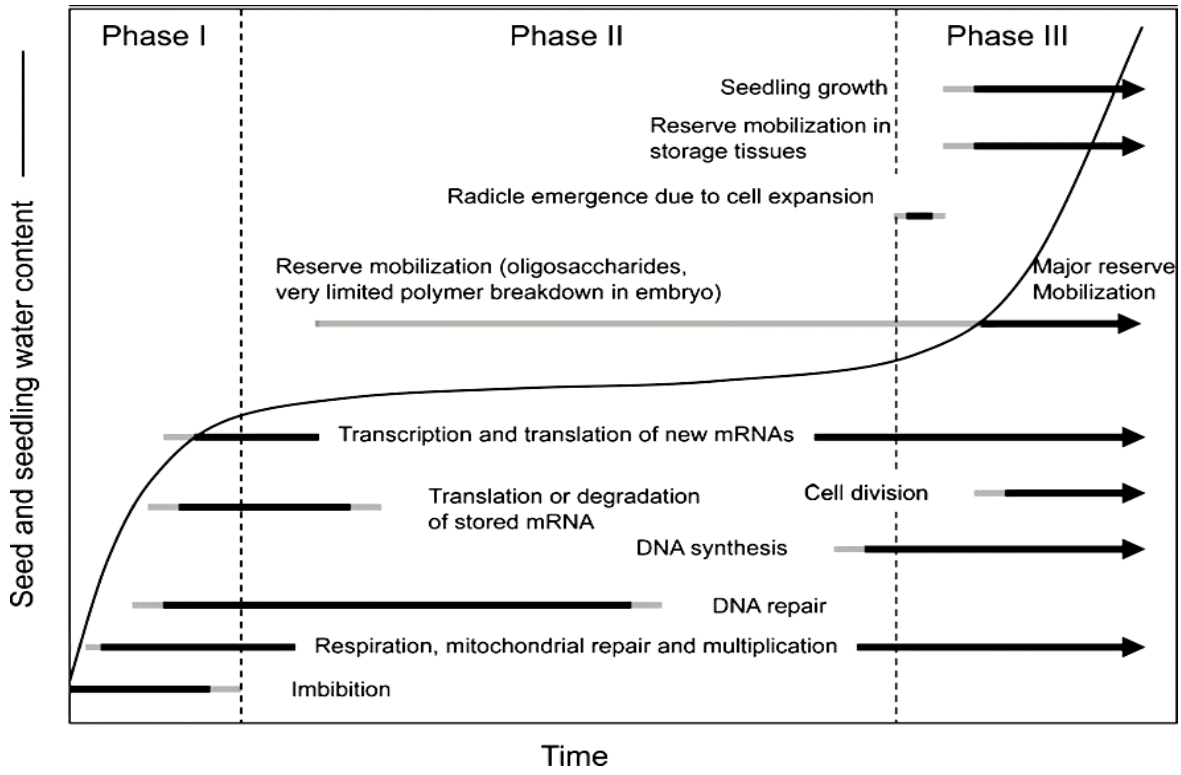

Figure. 2.3. Illustration of the three phases of the germination process (Nonogaki *et al.*, 2010).

Imbibition and activation involves the reintroduction of water into the kernel. This results in sufficient metabolic activities including respiratory activity, perturbations of membranes to leak solutes and low molecular weight metabolites into the surrounding imbibition solution (Bewley, 1997). Upon water uptake, the embryo is stimulated to release the hormone gibbelleric acid which diffuses through to the aleurone layer to stimulate the production of hydrolytic enzymes (Harvey & Oaks, 1974; Fincher, 1989; Ritchie *et al.*, 2000). The phospholipid components of the aleurone layer change from a gel phase to a hydrated liquid crystalline state (Crowe & Crowe, 1992; Nonogaki *et al.*, 2010). The aleurone layer contains carbohydrates (raffinose, sucrose and fructans), endo- peptidases (responsible for proteolitic activation) and exo-peptidases (deposited in the protein bodies of the aleurone layer)

which assists in production of hydrolytic enzymes (Fincher, 1989; Ritchie *et al.*, 2000). Reserve proteins, carbohydrates, lipids, phosphates and cations produce primary or 'house-keeping' hydrolytic enzymes (Fincher, 1989; Ritchie *et al.*, 2000; Tnani *et al.*, 2011). The 'house-keeping' enzymes together with co-factors degrade mitochondria (responsible for metabolic activity) and the intracellular membrane system of the aleurone layer. Simultaneously, the activation of a protein synthesising system (responsible for the synthesis of amino acids that make up endosperm hydrolytic enzymes) takes place (Fincher, 1989; Ritchie *et al.*, 2000; Subedi & Bhattarai, 2003). The protein matrix of the aleurone layer disappears and the protein bodies that were embedded in the matrix coalesce to form vacuoles, due to the lipid bodies surrounding them. As pre-germination progresses, the lipid bodies decrease in amount and become smaller, exposing the protein bodies which then release the hydrolytic enzymes responsible for endosperm starch degradation (Fincher, 1989; Ritchie *et al.*, 2000). Endosperm cell walls have no secondary thickening and no lignin, which makes them more susceptible to rapid hydrolysation (Fincher, 1989).

The scutellar epithelium performs a dual role in that it releases enzymes responsible for endosperm degradation and facilitates the transportation of assimilates into the growing embryo (Fincher, 1989; Ritchie *et al.*, 2000; Tnani *et al.*, 2011). Three distinct types of enzymes are produced by the scutellar epithelium: (1) 'house-keeping' enzymes that help provide adenosine triphosphate for the production of the hydrolytic enzymes and mobilisation enzymes; (2) hydrolytic enzymes that are responsible for endosperm hydrolysis; and (3) mobilisation enzymes that help transport assimilates from the endosperm to the growing embryo (Fincher, 1989; Ritchie *et al.*, 2000). During *intra-seminal growth* the embryo continues to grow until the endosperm contents are depleted (Ritchie *et al.*, 2000) while *embryo protrusion* indicates the culmination of the pre-germination process.

Pre-germination can however be interrupted by means of drying the maize kernels. In spite of no visible signs of pre-germination (Gordon, 1970), irreversible endosperm degradation will have taken place. The increased amounts of starch and protein degrading enzymes (synthesized during pre-germination) lead to increased amounts of soluble sugars and amino acids. This will consequently leads to favourable conditions for microbial and insect contamination which will eventually lead to decreased grain quality and functionality (Pagano *et al.*, 1997; Lijavetzky *et al.*,
2000; Singh *et al.*, 2009).

Pre-germination in barley and sorghum grains destined for malting, would render the grains non-viable (Pagano *et al.*, 1997; Lijavetzky *et al.*, 2000; Arngren *et al.*, 2011; Engelbrecht, 2011; McGoverin *et al.*, 2011) as the grains will not re-germinate during the steeping process

(the first step in the malting process). In wheat, pre-germination lowers the baking quality of the wheat flour (Barnard & Smith, 2009) and therefore causes losses for the millers, grain dealers and bakers (Neethirajan *et al.*, 2007). An excessive amount of alpha-amylase (produced during pre- germination) degrades starch to complex dextrins and simple sugars. This will result in a decreases in the dough's water holding capacity, creating a slack dough (Skerritt & Heywood, 2000; Groos *et al.*, 2002) and sticky crumb (Moot & Every, 1990). The impact of germination, of maize kernels while still on the cob in the field, on maize kernel hardness has not been studied and no reports on this could be found.

Several destructive and non-destructive methods have been employed for the study of maize kernel hardness as well as methods to determine if pre-germination had taken place in cereal grains such as barley, sorghum and wheat.

2.4. Kernel hardness testing methods

2.4.1. Destructive hardness determination methods

Destructive methods such as the texture analyser, Stenvert hardness test, tangential abrasive dehulling device (TADD), particle size index (PSI) and scanning electron microscopy (SEM) have been used to investigate maize kernel hardness. The texture analyser relates kernel hardness to the measure of a compression force, to a pre-requisite depth, required to deform a kernel (Pomeranz *et al.*, 1986a; Gaytán-Martínez *et al.*, 2006; Blandino *et al.*, 2010). The Stenvert hardness test relates maize hardness to the time required to collect 17 mL of ground maize meal (Kirleis & Stroshine, 1990; Ohnson & Fox, 1991; Cavanaugh *et al.*, 1995; Fox & Manley, 2009: review). Wehling *et al.* (1996) and Almeida-Dominguez *et al.* (1997) investigated maize kernel hardness using the TADD which relates hardness to abrading maize kernels for 10 minutes and measuring the mass of the material removed from the kernels. A high amount of material removed indicated soft maize samples. The PSI method uses milled maize samples to relate maize hardness to particle size distribution (Pomeranz *et al.*, 1986a). According to Symes (1961) the relation of hard and/or soft cereal grains (particularly wheat) to hardness dates back as far as 1908 and the first documented research was in 1935 by Cutler and Brinson. These researchers observed that different types of cereal grains fractured differently when subjected to a destructive force, thereby giving birth to a technique termed particle size index analysis. A certain weight of maize kernels would be milled, then fractionated using various sieve mesh sizes, e.g. 150 µm (to trap coarse particles) and 75 µm and a receiving pan (to trap fine particles). The ratio between the coarse and fine particles (C/F ratio) would be determined to obtain the PSI values, and lower PSI values indicated hard maize samples while higher values indicated soft maize kernels (Fox & Manley, 2009 (review); Blandino *et al.*, 2010; O'Kennedy, 2011). To date the PSI method is still used to

determine maize kernel hardness (Blandino *et al.*, 2010). In snacks and cereal industries where extrudates are produced from maize meal, particle size is important as it impacts on the expansion of the extruded products. For instance, it is known that larger particles expanded more thus important to ensure that the right size particle is used for the desired extrusion volume (de la Hera *et al.*, 2013; Gumbira-Sa'id *et al.*,2013; Jozinović *et al.*, 2013).

2.4.1.1. Scanning electron microscopy

The SEM technique has been used to investigate maize microstructure in relation to maize hardness (Dombrink-Kurtzman & Knutson, 1997; Figueroa Cárdenas *et al.*, 2006; Gaytán-Martínez *et al.*,2006). Its utilisation was successful in the investigation and illustration of maize endosperm topography (Fig. 2.4), particularly in determining the variation between hard and soft endosperm. The scanning electron microscope is able to generate 2D images from collected signals created from various elastic scattering processes (Bull, 1993; Fazaeli *et al.*, 2012). The elastic scattering processes results from deflected high energy primary electrons or low energy secondary electrons, after having interacted with the sample's dry surface, coated with a thin layer of carbon or metal such as gold or copper (Hearle *et al.*, 1973). Apart from being destructive, other limitations of SEM are that it requires a skilled operator and temperature increase will also occur as a result of electron-sample material interaction (Wang & Petrova, 2012) which could lead to alteration of the sample.

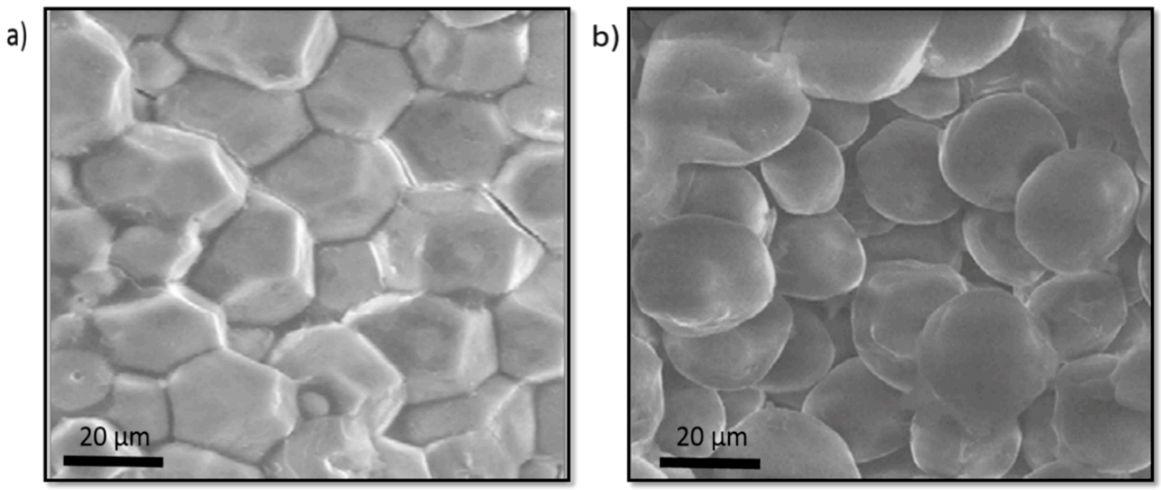

Figure 2.4 Scanning electron microscopy (SEM) image of a) tightly packed starch granules of hard maize endosperm and b) loosely packed starch granules of soft maize endosperm (adapted from Gaytán-Martínez *et al.* (2006))

2.4.2. Non-destructive hardness determination methods

Non-destructive methods relate maize kernel hardness to kernel weight or density using

the thousand-kernel weight, floatation, pycnometer methods as well as near infrared (NIR) hyperspectral imaging and X-ray micro-computed tomography (μCT). The latter two methods will be reviewed in more detail. The thousand-kernel weight method relates maize kernel hardness to the weight of a 1000 maize kernels, counted in sections of 100 kernels (Sahai *et al.*, 2001). The floatation method is based on the notion that soft kernels would float in a beaker filled with a sodium nitrate solution (of concentrations such as 41% (m/v) at a specific gravity of 1.25) while the hard kernels would remain at the bottom of the beaker (Almeida-Dominguez *et al.*, 1997; Gaytán-Martínez *et al.*, 2006; Lozano-Alejo *et al.*, 2007). The gas pycnometer method is based on Archimedes' principle which stated that the force of the fluid acting upwardly upon a partially or fully submerged object will be equal in magnitude to the displaced fluid, thereby giving the volume of the object (Bierman & Kincanon, 2003). The gas pycnometer method relates maize kernel hardness to the determined maize kernel density using the equation **ρ=m/V** where mass (m) is obtained from the weight of the maize kernels and volume (V) obtained from the volume of the displaced helium gas (Chang, 1988; Ohnson & Fox, 1991; Lee *et al.*, 2005).

2.4.2.1. Near infrared hyperspectral imaging

NIR spectroscopy is a spectroscopic technique that utilizes the NIR region of the electromagnetic spectrum with the wavelength range of 780 to 2526 nm as per the American Society of Testing Materials (Reich, 2005; Cen & He, 2007). The NIR electromagnetic radiation interacts with atoms and molecules of the –CH, –NH, –OH and –SH functional groups, to provide chemical and physical information of the sample. The chemical information obtained has been described as finger printing as the information acquired is unique to the particular sample being analysed (ElMasry & Sun, 2010).

Any compound with a covalent bond, whether it be organic or inorganic can absorb various frequencies of electromagnetic radiation in the infrared region of the electromagnetic spectrum (Donald *et al.*, 1996). The frequencies are then automatically translated into wavelength information observed in spectral data. The spectral bands obtained from using NIR spectroscopy arise from stretching and bending vibrations (taking place in the bonds of the functional groups) in the form of overtones and combination bands (ElMasry & Sun, 2010).

The use of NIR spectroscopy grew dramatically since the 1960s (Blanco *et al.*, 1998 (review); Reich, 2005) and its ability to be used at-, on- or in-line has allowed it to be one of the most efficient and advanced tools for monitoring and controlling continuous processes and product quality (Huang *et al.*, 2008). NIR spectroscopy is used to determine quality in products

such as fruits and vegetables (Nicolaï *et al.*, 2007), dairy (Fagan *et al.*, 2009) and meat (Shackelford *et al.*, 2004; Sierra *et al.*, 2008). In the cereal industry the technique had been applied using the wavelength range from 400 to 2500 nm at 2 nm intervals to determine, amongst others, maize protein (Orman & Schumann, 1991), maize starch, carotene and oil content (Cozzolino *et al.*, 2001; Baye *et al.*, 2006), kernel rot and mycotoxins (Berardo *et al.*, 2005) and aflotoxins (Fernández-Ibañez *et al.*, 2009).

NIR spectroscopy possesses four major advantages as an analytical method for quality control within any industry: 1) it enables spectral information to be acquired with minimal or no sample preparation; 2) spectral information obtained provides chemical and physical information of the sample; 3) the method is non-destructive; and 4) results can be obtained in seconds (Blanco *et al.*, 1998; Macho & Larrechi, 2002; Reich, 2005; Liebmann *et al.*, 2010). The NIR technique is however flawed on its own, in that it does not provide the spatial information and sensitivity towards minor constituents is limited (ElMasry & Sun, 2010), hence the development of NIR hyperspectral imaging. Qin (2010) elaborated on the construction of a near infrared hyperspectral imaging system in detail.

NIR hyperspectral imaging combines the strength of NIR spectroscopy technique with digital imaging technique to provide an image made up of hundreds of wavebands that are in close proximity with one another and with spatial information of the property of interest (Gowen *et al.*, 2007; Gowen *et al.*, 2008; ElMasry & Sun, 2010). A hyperspectral image consists of numerous pixels each providing a spectrum in the NIR region of the electromagnetic spectrum. A hyperspectral image is a three-dimensional (3D) set of data called a hypercube, made up from spatial (x,y pixel coordinates obtained from detector array) and spectral (λ) information (Bharati & MacGregor, 1998; Cogdill *et al.*, 2004; Burger & Geladi, 2005; Elmasry *et al.*, 2012). Image data sets can be presented in the form of congruent greyscale or RGB images at different wavelength bands or as numerous pixels with individual spectral profiles (ElMasry & Sun, 2010). There are three approaches to acquiring hyperspectral images, i.e. point/whiskbroom, line/pushbroom and area/turnable/plane scanning (Elmasry *et al.*, 2012). In point scanning, hyperspectral images are produced by measuring a single point of the sample at a time (i.e. pixel-by-pixel) which makes the technique impractical to industries where time is a crucial factor. With line scanning, instead of obtaining a hyperspectral image one pixel at a time as in the case of point scanning, an image of a single line is scanned and an image is built with the help of a 2D light dispersing element and detector array. Line scanning can take up to 20 seconds for a complete image to be acquired depending on the field-of-view and magnification. The pushbroom configuration can be fitted on a conveyor belt for industrial applications (Mehl *et al.*, 2004; Manley *et al.*, 2009). With area scanning, the whole sample is scanned at a single wavelength at a time (based on the spectrograph's and detector

capabilities) to produce a complete hyperspectral image for each wavelength. This can take a few minutes to complete an entire scan.

The ability of the hyperspectral technique to gather greyscale images at each and every preselected wavelength or generate mixed spectral profiles from measuring numerous spots on the sample indicates that enormous amounts of data are generated. The researcher would then have to translate the data obtained into a set that relates mainly the desired information by using data reduction methods such as principal component analysis (PCA). PCA is an unsupervised multivariate data analysis technique, commonly used in situations where there is no *a priori* knowledge about the samples (Ifarraguerri & Chang, 2000). PCA has the ability to reduce the original set of correlated variables to a smaller number of orthogonal variables while capturing the larger part of the variability in the data. This action is performed so that the data obtained can be visualised in a lower dimensional space.

Before data reduction, the hypercube is unfolded and reorganised into a matrix X (containing x,y and λ information), mean-centred and then decomposed into a scores matrix (**T**), a loading matrix (**P**) and a residual matrix (**E**) (Amigo *et al.*, 2013), i.e. **X=TP'+E** (Wold *et al.*, 1987). The scores matrix (**T**) can be used to construct scores plots with scores values depicted in the form of principal components (PC) plotted against each other. The scores matrix are also refolded into scores images presented as contour maps of the imaged sample (Amigo *et al.*, 2013). Typical imaging software packages such as Evince allows the scores image (called the contour 2D plot in the software) and scores plot (called the scatter 2D density plot in the software) to be analysed interactively. When pixels are highlighted in the scores plot, the position of the pixels also becomes highlighted in the scores image. In this manner, PCA can also be used as a classification technique (ElMasry & Sun, 2010), allowing parts of the imaged sample to be assigned a colour corresponding with the selected pixels on the scores image. This way of using PCA for classification purposes was illustrated by McGoverin and Manley (2012). The authors used PCA to illustrate that maize hardness was related to the ratio of the vitreous-to-floury endosperm within a maize kernel. The results were validated by manually dissecting the maize kernel and weighing each endosperm type separately. Figure 2.5 provides an illustration of the use of PCA for classification. Based on the information provided by the authors, the impact of PHS on the vitreous endosperm should be observable using the NIR hyperspectral technique considering that images of the vitreous endosperm could be clearly observed.

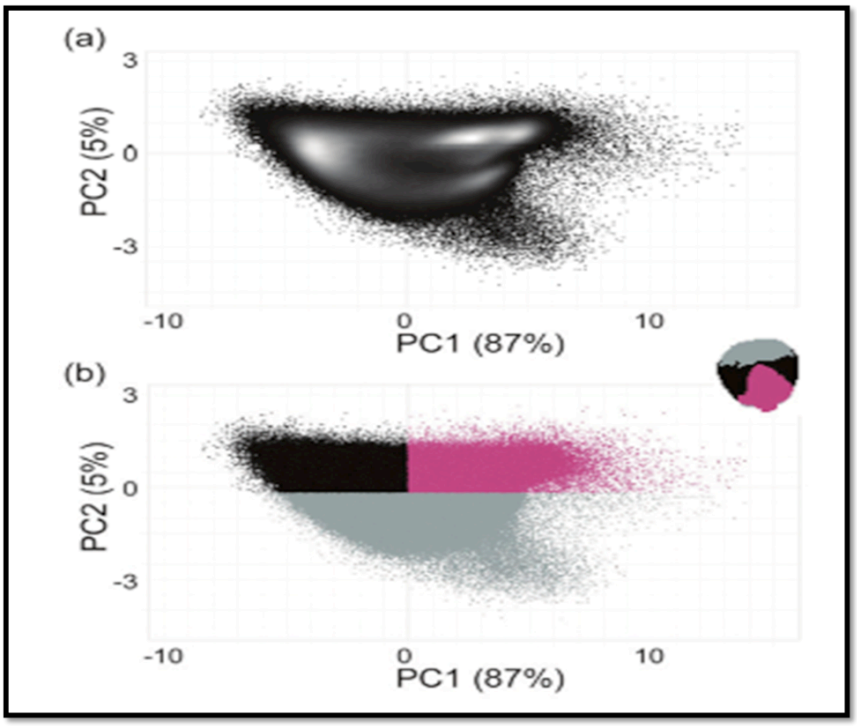

Figure 2.5 a) PCA score plot of PC 1 vs. PC 2, indicating the various parts within maize kernels in 3 clusters and b) classification plot illustrating that the clusters represented the germ (magenta), floury endosperm (grey) and vitreous endosperm (black) (McGoverin & Manley, 2012).

The NIR hyperspectral imaging technique has proven to be highly accurate in assessing cereal grains (Singh *et al.*, 2010) and has been utilised in the classification of wheat hardness (Mahesh *et al.*, 2008; Jayas *et al.*, 2010) and early detection of toxigenic fungi in maize (Del Fiore *et al.*, 2010). It has also been used (Manley *et al.*, 2009); Williams *et al.* (2009) to classify three different hardness categories of maize (i.e. hard, intermediate and soft maize kernels). Williams et al. (2009) used two different hyperspectral imaging instruments, i.e. MatrixNIR camera with spectral range of 960 to 1662 nm and the SisuChema short wave infrared pushbroom imaging system with spectral range of 1000 to 2498 nm. In spite of the limited wavelength range of the MatrixNIR camera the two types of endosperm could be detected, similar to using the short wave infrared SisuChema. In both cases it was possible to use ratio of the two types of endosperm present to classify the maize kernels into different hardness categories. Zhang *et al.* (2012) developed a model to discriminate between six varieties of Chinese maize kernels, using 330 samples, 380 to 1030 nm spectral range including 512 spectral bands. This was done at a reliability of 98.89%. Aside from maize, the technique has been reviewed for usage in evaluating the quality and safety of agricultural products (Elmasry *et al.*, 2012; Dale *et al.*, 2013; Moghaddam *et al.*, 2013; Wu & Sun, 2013a; Wu & Sun, 2013b).

NIR hyperspectral imaging is, however, not without limitations, one of which is inability of the

NIR radiation to provide images of the internal microstructure of the sample. NIR radiation will penetrate to different depts in food products, depending on the scattering and absorption properties which are influenced by the moisture content of the sample (ElMasry & Sun, 2010), while X-rays on the other hand are characterised by short wavelengths and high frequencies which allow them the ability to penetrate through a sample and capture the inner microstructure of the sample (Lim & Barigou, 2004).

2.4.2.2. X-ray micro-computed tomography

X-rays are found in the wavelength region of *ca*. 0.01 to10 nm of the electromagnetic spectrum (Kotwaliwale *et al.*, 2011). Computed tomography is an imaging method that uses multiple two- dimensional (2D) images of the imaged sample to create a virtual three-dimensional (3D) volume (Westneat *et al.* (2008). The first X-ray micro-computed tomography (μCT) scanner was developed in the early 1980's, dedicated to clinical purposes (Ritman, 2004). X-ray μCT (also referred to as high-resolution X-ray μCT) then found its way to the food industry in the 21st century, with the first documented research pertaining to food research reported in 2004. Lim and Barigou (2004) used X-ray μCT to study the structure of cellular food products, namely: aerated chocolate bar, strawberry mouse, honeycomb chocolate bar, chocolate muffin and marshmallow. Advantages of using this technique are: 1) sample scanning can take place at atmospheric pressure; 2) no temperature alteration can take place during the scanning session; 3) all samples can be scanned in their natural state; 4) X-rays can penetrate deep into the sample non-destructively/non-invasively; and 5) three dimensional (3D) detail of the object's microstructure can be obtained (Lim & Barigou, 2004).

X-ray μCT is a combination of microscopy and computing methods ((Mousavi *et al.* (2005); Yin, 2012). The system consists of an X-ray tube, sample holder, a detector with a camera attached and an external computer system that allows visualisation of the projections. Production of the X- ray beam has been described in detail by Curry *et al.* (1990) and Schambach *et al.* (2010). The samples to be imaged are placed in between the X-ray tube and the detector (Salvo *et al.*, 2010), rotates either continuously or in a step scan manner to 180° or 360° while being irradiated with X- ray beams. The sample can then absorb, transmit or scatter the projected X-ray beams (Mendoza *et al.*, 2007; Salvo *et al.*, 2010). The penetration depth of the X-ray depends on its energy and the material of the imaged sample, i.e. soft X-ray (wavelengths range from 0.1 to 10 nm) are low in energy but they are the most suitable for the study of agricultural products which are sensitive to the destructive nature of hard X-rays (Bull, 1993; Renu & Chidanand, 2013).

Transmitted excited photons are then converted into visible light by scintillators in the detector and the cooled couple charge device (CCD) or complimentary metal-oxide semi-conductor (CMOS) cameras record the light, producing projections (Mendoza *et al.*, 2007; Salvo *et al.*, 2010; Baker *et al.*, 2012). The produced multiple two dimensional (2D) projections are recorded and mathematically rendered to form 3D images (Westneat *et al.*, 2008; Salvo *et al.*, 2010).

Soft X-rays have the ability to reveal density variations in the microstructure of agricultural products being imaged (Kotwaliwale *et al.*, 2011). The density variation between the microstructural features in the images are due to absorption of the X-rays by the sample material (Salvo *et al.*, 2010).

The absorption coefficient is based on the density of the material. During the exposure to X-rays,the beam interacts with the sample matter and there is an exponential decrease in the total energy of the beam as it travels through the object (Kotwaliwale *et al.*, 2011). The decrease in energy is known as attenuation, and is affected by the atomic number, the thickness as well as of the density of the object irradiated. The fact that X-ray attenuation is affected by the density of the material being irradiated, makes it ideal to investigate objects with compositional variation (Williams, 2013).

Density dependent attenuation is linear (Baker *et al.*, 2012) with the equation $\mathbf{I/I_0 = exp(-\mu h)}$ where $\boldsymbol{\mu}$ is the linear attenuation coefficient, $\mathbf{I_0}$ and $\mathbf{I}$ are the incident and attenuated X-ray photons and $\mathbf{h}$ is the thickness of the imaged material (Taina *et al.*, 2008). The record of attenuation of the X-ray images is at the point where the X-ray intensity has been reduced by 37% of its original value (Sasov & van Dyck, 1998). The grey image in the form of 2D virtual slices (obtained from 3D images) correspond to the linear attenuation coefficient which are related to densities (Jinorose *et al.*, 2009). With the help of software such as VG Studio Max or Avizo Fire, volume quantification of the region- of-interest (ROI) can be done from 2D virtual slices obtained from any angle of the imaged sample.

X-ray µCT has been utilised for the investigation of food products such as fat content of salami (Laverse *et al.*, 2012). The main variation within the salami samples was the fat content. It was possible to determine the fat content of the salami with the help of a geometric parameter known as percent object volume from X-ray µCT imaging analysis tools. The results were validated with fat determinations of the samples according to an AOAC method (AOAC, 1995). Using a one-way ANOVA ($p<0.05$), no significant difference was found between the conventional chemical method results and those obtained using X-ray µCT. Zhu *et al.* (2012) used the technique to study the kernel structure of rice kernels (wild type and high amylose rice kernels) with varying textures. The wild type rice kernels had more vitreous endosperm while the high amylose rice constituted of mostly floury endosperm.

They also observed that the high amylose rice had texture variation through-out the kernel, i.e. the dorsal and abdomen part of the rice kernel constituted of material of low density as opposed to the material in the mid-area of the kernel. Williams (2013) tracked the deterioration of maize endosperm in maize kernels infected with *F. verticillioides* which produces harmful secondary metabolites. Demirkesen *et al.* (2014) investigated the effect of the different types of gums added to bread dough, during the production of gluten-free breads with a spongy characteristic using X-ray µCT. With the help of image analysis software, X-ray images could be analysed for pore distribution and size in relation to the control bread (gluten bread) successfully. Accurate and precise measurement of single maize kernel density have also been demonstrated by Gustin *et al.* (2013) using X-ray µCT. The volume of interest could also be segmented and measured against the whole single maize kernel. Due to previous studies that correlated maize kernel density to measures of hardness and ratio of vitreous-to-floury endosperm, an indirect relation between kernel density and bulk test weight or hectolitre mass (r = 0.80) could be made (Gustin *et al.*, 2013).

NIR hyperspectral imaging is, however, not without limitations, one of which is inability of the NIR radiation to penetrate through a sample. NIR radiation in the region of 500 to 1900 nm can penetrate to the depth of 2 to 4 mm in food products (ElMasry & Sun, 2010), while X-rays on the other hand are characterised by short wavelengths and high frequencies which allow them the ability to penetrate through a sample and capture the inner microstructure of the sample (Lim & Barigou, 2004).

2.4.2.2. X-ray micro-computed tomography

X-rays are found in the wavelength region of *ca*. 0.01 to10 nm of the electromagnetic spectrum (Kotwaliwale *et al.*, 2011). Computed tomography is an imaging method that uses multiple two- dimensional (2D) images of the imaged sample to create a virtual three-dimensional (3D) volume (Westneat *et al.* (2008). The first X-ray micro-computed tomography (µCT) scanner was developed in the early 1980's, dedicated to clinical purposes (Ritman, 2004). X-ray µCT (also referred to as high-resolution X-ray µCT) then found its way to the food industry in the 21st century, with the first documented research pertaining to food research reported in 2004. Lim and Barigou (2004) used X-ray µCT to study the structure of cellular food products, namely: aerated chocolate bar, strawberry mouse, honeycomb chocolate bar, chocolate muffin and marshmallow. Advantages of using this technique are: 1) sample scanning can take place at atmospheric pressure; 2) no temperature alteration can take place during the scanning session; 3) all samples can be scanned in their natural state; 4) X-rays can penetrate deep into the sample non-destructively/non-invasively; and 5) three dimensional (3D) detail of the object's microstructure can be obtained (Lim & Barigou, 2004).

X-ray µCT is a combination of microscopy and computing methods ((Mousavi *et al.* (2005); Yin, 2012). The system consists of an X-ray tube, sample holder, a detector with a camera attached and an external computer system that allows visualisation of the projections. Production of the X- ray beam has been described in detail by Curry *et al.* (1990) and Schambach *et al.* (2010). The samples to be imaged are placed in between the X-ray tube and the detector (Salvo *et al.*, 2010), rotates either continuously or in a step scan manner to 180° or 360° while being irradiated with X- ray beams. The sample can then absorb, transmit or scatter the projected X-ray beams (Mendoza *et al.*, 2007; Salvo *et al.*, 2010). The penetration depth of the X-ray depends on its energy and the material of the imaged sample, i.e. soft X-ray (wavelengths range from 0.1 to 10 nm) are low in energy but they are the most suitable for the study of agricultural products which are sensitive to the destructive nature of hard X-rays (Bull, 1993; Renu & Chidanand, 2013). Transmitted excited photons are then converted into visible light by scintillators in the detector and the cooled couple charge device (CCD) or complimentary metal-oxide semi-conductor (CMOS) cameras record the light, producing projections (Mendoza *et al.*, 2007; Salvo *et al.*, 2010; Baker *et al.*, 2012). The produced multiple two dimensional (2D) projections are recorded and mathematically rendered to form 3D images (Westneat *et al.*, 2008; Salvo *et al.*, 2010).

Soft X-rays have the ability to reveal density variations in the microstructure of agricultural products being imaged (Kotwaliwale *et al.*, 2011). The density variation between the microstructural features in the images are due to absorption of the X-rays by the sample material (Salvo *et al.*, 2010). The absorption coefficient is based on the density of the material. During the exposure to X-rays,the beam interacts with the sample matter and there is an exponential decrease in the total energy of the beam as it travels through the object (Kotwaliwale *et al.*, 2011). The decrease in energy is known as attenuation, and is affected by the atomic number, the thickness as well as of the density of the object irradiated. The fact that X-ray attenuation is affected by the density of the material being irradiated, makes it ideal to investigate objects with compositional variation (Williams, 2013).

Density dependent attenuation is linear (Baker *et al.*, 2012) with the equation $\mathbf{I/I_0 = \exp(-\mu h)}$ where $\boldsymbol{\mu}$ is the linear attenuation coefficient, $\mathbf{I_0}$ and $\mathbf{I}$ are the incident and attenuated X-ray photons and $\mathbf{h}$ is the thickness of the imaged material (Taina *et al.*, 2008). The record of attenuation of the X-ray images is at the point where the X-ray intensity has been reduced by 37% of its original value (Sasov & van Dyck, 1998). The grey image in the form of 2D virtual slices (obtained from 3D images) correspond to the linear attenuation coefficient which are related to densities (Jinorose *et al.*, 2009). With the help of software such as VG Studio Max or Avizo Fire, volume quantification of the region- of-interest (ROI) can be done from 2D virtual slices obtained from any angle of the imaged sample.

X-ray µCT has been utilised for the investigation of food products such as fat content of salami (Laverse *et al.*, 2012). The main variation within the salami samples was the fat content. It was possible to determine the fat content of the salami with the help of a geometric parameter known as percent object volume from X-ray µCT imaging analysis tools. The results were validated with fat determinations of the samples according to an AOAC method (AOAC, 1995). Using a one-way ANOVA (p<0.05), no significant difference was found between the conventional chemical method results and those obtained using X-ray µCT. Zhu *et al.* (2012) used the technique to study the kernel structure of rice kernels (wild type and high amylose rice kernels) with varying textures. The wild type rice kernels had more vitreous endosperm while the high amylose rice constituted of mostly floury endosperm. They also observed that the high amylose rice had texture variation through-out the kernel, i.e. the dorsal and abdomen part of the rice kernel constituted of material of low density as opposed to the material in the mid-area of the kernel. Williams (2013) tracked the deterioration of maize endosperm in maize kernels infected with *F. verticillioides* which produces harmful secondary metabolites. Demirkesen *et al.* (2014) investigated the effect of the different types of gums added to bread dough, during the production of gluten-free breads with a spongy characteristic using X-ray µCT. With the help of image analysis software, X-ray images could be analysed for pore distribution and size in relation to the control bread (gluten bread) successfully. Accurate and precise measurement of single maize kernel density have also been demonstrated by Gustin *et al.* (2013) using X-ray µCT. The volume of interest could also be segmented and measured against the whole single maize kernel. Due to previous studies that correlated maize kernel density to measures of hardness and ratio of vitreous-to-floury endosperm, an indirect relation between kernel density and bulk test weight or hectolitre mass (r = 0.80) could be made (Gustin *et al.*, 2013).

2.5. Pre-germination testing methods

To determine if pre-germination had taken place in cereal grains, methods such as Falling Number, alpha-amylase assay, Rapid Visco Analyser (RVA) and NIR spectroscopy and hyperspectral imaging have been used.

2.5.1. Destructive pre-germination testing methods

The Falling Number method indirectly determines levels of enzyme presence via measuring rheological properties of a heated starch suspension (Moot & Every, 1990). Flour and water are mixed in a precision test tube and stirred while in a boiling water bath. After 1 min, the stirring rod is allowed to drop inside the viscous suspension, the number of seconds it takes for the rod

to fall to the depth of the suspension is multiplied by 60, giving the Falling Number value. The lower the Falling Number value, the higher the level of enzyme present (Moot & Every, 1990). The alpha- amylase assay takes into account the calorimetric measurements of the starch solution mixed with iodine reagent, incubated for 1 to 10 min at 25°C and absorbance measured at 620 nm. The decrease in absorbance is proportional to the incubation time and the amount of alpha-amylase (Filner & Varner, 1967; Yoo *et al.*, 1986) present. The RVA system has been utilised to measure the viscosity of a heated starch solution in terms of stirring numbers. The presence of alpha-amylase in the starch solution will cause a decrease in viscosity and stirring number (<100) (Bueckert *et al.*, 2007). RVA parameters have also been correlated with NIR spectroscopy spectra to determine maize kernel germination (Juhász *et al.*, 2007). Using wavelengths between 1100 and 2498 nm at 2 nm intervals, physical and chemical changes that take place within maize kernels during the germination process could be determined.

2.5.2. Non-destructive pre-germination testing methods

Using NIR hyperspectral imaging, chemical changes that take place during pre-germination in cereals could be non-destructively detected prior to visible external symptoms (radicle protrusion) (Singh *et al.*, 2009; Xing *et al.*, 2009; Arngren *et al.*, 2011). Using NIR radiation in the wavelength region of 900 to 1700 nm, starch degradation could be compared between pre-germinated barley grains that and sound grains. McGoverin *et al.* (2011) utilised regions between 1000 and 2498 nm to characterise viability of wheat, barley and sorghum grains with induced pre-germination at 0, 6, 9,12, 18 and 24 h (Fig. 2.6).

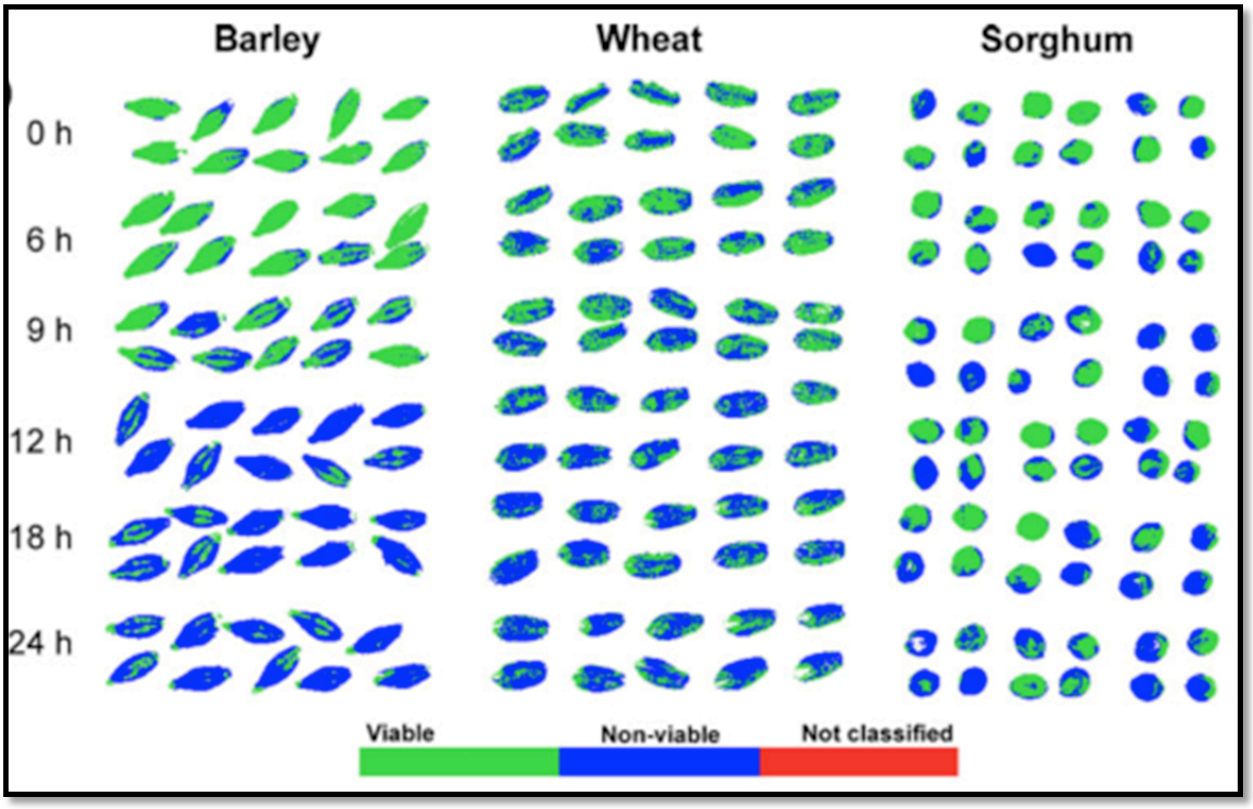

Figure. 2.6. Classification images of barley, wheat and sorghum grains, green hue indicated viable or sound grains whilst the blue hue indicated pre-germinated grains (McGoverin *et al.*, 2011)

Chemical changes have also been observed in single pre-germinated barley kernels. The barley kernels were germinated from 0 to 60 h and imaged with a hyperspectral line-scan NIR camera system in the wavelength range of 900 to 1700 nm (Arngren *et al.*, 2011). Using PCA scores images, chemical changes by means of hue variation between the barley kernels germinated for 0 h through to 60 h could be observed from PC1 to PC5 (Arngren *et al.*, 2011).

2.6. Conclusion

Methods such as X-ray µCT and NIR hyperspectral imaging have shown great potential in hardness analysis and the latter technique has also been successfully used in identifying pre-germinated wheat, barley and sorghum. The NIR hyperspectral imaging technique has the ability to identify chemical changes (i.e. changes in starch and protein contents) that takes place within cereal grains. Unlike SEM, NIR hyperspectral imaging and X-ray µCT take images of the whole sample at once and non-destructively, allowing re-use or additional analysis to be performed on the sample. The scanning time of NIR hyperspectral imaging is shorter than that of X-ray µCT, but the latter has the ability to penetrate through the imaged sample and the results can be

presented as 3D images.The detrimental effects of pre-germination on winter cereals have been documented. The effect of pre-germination on maize quality (particularly maize hardness) might be of concern to the milling industry. This effect on hardness and methods of detection have not been addressed to date.

Both NIR hyperspectral imaging and X-ray µCT seem promising techniques to detect and characterise the effect of pre-germination on maize endosperm and subsequent kernel hardness.

2.7. References

Almeida-Dominguez, H.D., Suhendro, E.L. & Rooney, L.W. (1997). Factors affecting rapid visco analyser curves for the determination of maize kernel hardness. *Journal of Cereal Science*, **25**, 93-102.

Amigo, J.M., Martí, I. & Gowen, A. (2013). Hyperspectral imaging and chemometrics: a perfect combination for the analysis of food structure, composition and quality. In: *Chemometrics in Food Chemistry* (edited by F. Marini). Pp. 343-370. UK: Elsevier.

Anonymous (1996). Corn: layers and structures of corn kernel. [WWW document]. http://www.britannica.com/EBchecked/topic-art/103350/162/The-outer-layers-and-internal-structures-of-a-kernel-of. 29/05/2012

Anonymous (2012). Premature corn kernel sprouting (aka vivipary). [WWW document]. http://extension.entm.purdue.edu/pestcrop/2012/issue25/index.html. 24/01/2014

Arngren, M., Hansen, P.W., Eriksen, B., Larsen, J. & Larsen, R. (2011). Analysis of pre-germinated barley using hyperspectral image analysis. *Journal of Agricultural and Food Chemistry*, **21**, 11385-11394.

Baker, D., Mancini, L., Polacci, M., Higgins, M., Gualda, G., Hill, R. & Rivers, M. (2012). An introduction to the application of X-ray microtomography to the three-dimensional study of igneous rocks. *Lithos*, **148**, 262-276.

Barnard, A. & Smith, M.F. (2009). The effect of rainfall and temperature on the preharvest sprouting tolerance of winter wheat in the dryland production areas of the Free State Province. *Field Crops Research*, **112**, 158-164.

Baye, T.M., Pearson, T.C. & Settles, A.M. (2006). Development of a calibration to predict maize seed composition using single kernel near infrared spectroscopy. *Journal of Cereal Science*, **43**, 236-243.

Berardo, N., Pisacane, V., Battilani, P., Scandolara, A., Pietri, A. & Marocco, A. (2005). Rapid detection of kernel rots and mycotoxins in maize by near-infrared reflectance spectroscopy. *Journal of Agricultural and Food Chemistry*, **53**, 8128-8134.

Bewley, J.D. (1997). Seeds germination and dormancy. *The Plant Cell*, **9**, 1055-1066.

Bharati, M. & MacGregor, J. (1998). Multivariate image analysis for real-time process monitoring and control. *Industrial and Engineering Chemistry Research*, **37**, 4715-4724.

Bierman, J. & Kincanon, E. (2003). Reconsidering Archimedes and apos principle. The Physics Teacher, 41, 340-344.

Blanco, M., Coello, J., Iturriaga, H., Maspoch, S. & De la Pezuela, C. (1998). Near-infrared spectroscopy in the pharmaceutical industry. *Analyst-London-Society of Public Analysts then Royal Society of Chemistry*, **123**, 135R-150R.

Blandino, M., Mancini, M.C., Peila, A., Rolle, L., Vanara, F. & Reyneri, A. (2010). Determination of maize kernel hardness: comparison of different laboratory tests to predict dry-milling performance. *Journal of the Science of Food and Agriculture*, **90**, 1870-1878.

Boyer, C.D. & Shannon, J.C. (2003). Carbohydrates of the kernel. In: *Corn Chemistry and Technology* (edited by P.J. White & L. Johnson). Pp. 289-312. St Paul, Minnesota: American Association of Cereal Chemists.

Bueckert, R.A., Lefol, E.B. & Harvey, B.L. (2007). Early detection of non-visible sprouting in barley seed using rapid visco analysis. *Canadian Journal of Plant Science*, **87**, 3-12.

Bull, C.R. (1993). A review of sensing techniques which could be used to generate images of agricultural products and food material. *Computer and Electronics in Agriculture*, **8**, 1-29.

Burger, J. & Geladi, P. (2005). Hyperspectral NIR image regression part I: calibration and correction. Journal of chemometrics, 19, 355-363.

Cavanaugh, K.J., Zehr, B.E., Nyquist, W.E., Hamaker, B.R. & Crane, P.L. (1995). Responses to selection of endosperm hardness and associated changes in agronomic traits after four cycles of recurrent selection in maize. *Crop science*, **35**, 745-748.

Cen, H. & He, Y. (2007). Theory and application of near infrared reflectance spectroscopy in determination of food quality. *Trends in Food Science and Technology*, **18**, 72-83.

Chandrashekar, A. & Mazhar, H. (1999). The biochemical basis and implications of grain strength in sorghum and maize. *Journal of Cereal Science*, **30**, 193-207.

Chang, C. (1988). Measuring density and porosity of grain kernels using a gas pycnometer. *Cereal chemistry*, **65**, 13-15.

Chen, J., Zhang, J., Lui, Y. & Huang, Y. (2013). Morphologies and microstructure of maize starch granules differed in hardness during development of kernels. *Journal of Food, Agriculture and Environment*, **11**, 125-130.

Cogdill, R.P., Hurburgh, C.R., Rippke, G.R., Bajic, S.J., Jones, R.W., McClelland, J.F., Jensen, T.C. & Liu, J. (2004). Single-kernel maize analysis by near-infrared hyperspectral imaging. American Society of Agricultural Engineers, 47, 311-320.

Correa, C.E.S., Shavert, R.D., Pereira, M.N., Lauer, J.G. & Kohn, K. (2002). Relationship between corn vitreosness and ruminal in situ starch degradability. *Journal of Dairy Science*, **85**, 3008-
3012.

Cozzolino, D., Fassio, A. & Gimenez, A. (2001). The use of near-infrared reflectance spectroscopy (NIRS) to predict the composition of whole maize plants. Journal of the Science of Food and Agriculture, 81, 142-146.

Crowe, J. & Crowe, L. (1992). Membrane integrity in anhydrobiotic organisms: toward a mechanism for stabilizing dry cells. In: *Water and Life* (edited by G. Somero, C. Osmond & C. Bolis). Pp. 87-103. New York: Springer-Verlag Berlin Heidelberg.

Curry, T.S., Dowdey, J.E. & Murry Jr, R.C. (1990). Production of x-rays. In: Christensen's Physics of Diagnonstic Radiology. Pp. 10-117. USA: Lippincott Williams & Wilkins.

Dale, L.M., Thewis, A., Boudry, C., Rotar, I., Dardenne, P., Beaten, V. & Pierra, J.A.F. (2013). Hyperspectral imaging applications in agriculture and agro-food product quality and safety control: a review. Applied Spectroscopy Reviews, 48, 142-159.

de la Hera, E., Rosell, C.M. & Gomez, M. (2013). Effect of water content and flour particle size on gluten-free bread quality and digestibility. *Food Chemistry*, **151**, 526-531.

Del Fiore, A., Reverberi, M., Ricelli, A., Pinzari, F., Serranti, S., Fabbri, A.A., Bonifazi, G. & Fanelli, C. (2010). Early detection of toxigenic fungi on maize by hyperspectral imaging analysis. *International Journal of Food Microbiology*, **144**, 64-71.

Demirkesen, I., Kelkar, S., Campanella, O., Sumnu, G., Sahin, S. & Okas, M. (2014). Characterization of structure of gluten-free breads by using X-ray microtomography. Food Hydrocolloids, 36, 37-44.

Dombrink-Kurtzman, M. & Knutson, C. (1997). A study of maize endosperm hardness in relation to amylose content and susceptibility to damage. *Cereal chemistry*, **74**, 776-780.

Donald, L.P., Lampman, G.M. & Kriz, G.S. (1996). Infrared spectroscopy. In: *Introduction to spectroscopy: a guide for students of organic chemistry*. Pp. 13-101. USA: Thomson Learning.

Elmasry, G., Kamruzzaman, M., Sun, D.-W. & Allen, P. (2012). Principles and applications of hyperspectral imaging in quality evaluation of agro-food products: a review. *Critical reviews in food science and nutrition*, **52**, 999-1023.

ElMasry, G. & Sun, D.-W. (2010). Principles of hyperspectral imaging technology. In: *Hyperspectral Imaging for Food Quality Analysis and Control* (edited by S. Professor Da-Wen). Pp. 3-43. San Diego: Academic Press.

Engelbrecht, P. (2011). Near infrared hyperspectral imaging as detection method for pre-germination in whole wheat, barley and sorghum grains. Stellenbosch: University of Stellenbosch.

Evers, T. & Millar, S. (2002). Cereal grain structure and development: some implications for quality. Journal of Cereal Science, 36, 261-284.

Fagan, C.C., O'Donnell, C.P., Rudzik, L. & Wüst, E. (2009). Milk and dairy products In: Infrared Spectroscopy for Food Quality Analysis and Control. Pp. Pp. 241-273. San Diego: Academic Press.

Fazaeli, M., Tahmasebi, M. & Emam.Djomeh, Z. (2012). Characterization of food texture: application of microscopic technology In: *Current Microscopy Contributions to Advances in Science and Technology* (edited by A. Méndez-Vilas). Pp. 855-871. Spain: Formatex Research Center.

Fernández-Ibañez, V., Soldado, A., Martínez-Fernández, A. & de la Roza-Delgado, B. (2009).Application of near infrared spectroscopy for rapid detection of aflatoxin B1 in maize and barley as analytical quality assessment. Food Chemistry, 113, 629-634.

Figueroa Cárdenas, J., Gaytán Martínez, M., Morales Sánchez, E., Reyes Vega, M. & Rincón Sánchez, F. (2006). Microstructure of starch granule related to kernel hardness in corn. *Revista Fitotecnia Mexicana*, **29**, 135-139.

Filner, P. & Varner, J.E. (1967). A test for the *de novo* synthesis of enzymes: density labeling with H2O18 of barley α-amylase induced by gibberellic acid *Proceedings of the National Academy of Sciences of the United States of America*, **58**, 1520-1526.

Finch-Savage, W.E. & Leubner-Metzger, G. (2006). Seed dormancy and the control of germination. *New Phytologist*, **171**, 501-523.

Fincher, G.B. (1989). Molecular and cellular biology associated with endosperm mobilization in germinating cereal grains. *Annual Review of Plant Physiology and Plant Molecular Biology*, **40**, 305-346.

Fox, G. & Manley, M. (2009). Hardness methods for testing maize kernels. *Journal of Agricultural and Food Chemistry*, **57**, 5647-5657.

Gallardo, K., Job, C., Groot, S.P., Puype, M., Demol, H., Vandekerckhove, J. & Job, D. (2002). Proteomics of Arabidopsis seed germination. A comparative study of wild-type and gibberellin-deficient seeds. Plant Physiology, 129, 823-837.

Gaytán-Martínez, M., Figueroa-Cárdenas, J., Reyes-Vega, M., Rincón-Sánchez, F. & Morales- Sánchez, E. (2006). Microstructure of starch granule related to kernel hardness in corn. *Revista Fitotecnia Mexicana*, 135-139.

Gordon, A.G. (1970). Premature germination in cereal grains. Canadian Journal of Plant Science,50, 191-194.

Gowen, A., O'Donnell, C., Taghizadeh, M., Cullen, P., Frias, J. & Downey, G. (2008). Hyperspectral imaging combined with principal component analysis for bruise damage detection on white mushrooms (Agaricus bisporus). *Journal of chemometrics*, **22**, 259-267.

Gowen, A.A., O'Donnell, C.P., Cullen, P.J., Downey, G. & Frias, J.M. (2007). Hyperspectral imaging – an emerging process analytical tool for food quality and safety control. Trends in FoodScience and Technology, 18, 590-598.

Groos, C., Gay, G., Perretant, M.-R., Gervais, L., Bernard, M., Dedryver, F. & Charmet, G. (2002). Study of the relationship between pre-harvest sprouting and grain color by quantitative trait loci analysis in a white and red grain bread-wheat cross. Theoretical and Applied Genetics,104, 39-47.

Gumbira-Sa'id, E., Sunarti, T.C. & Hariyanto, B. (2013). Improvement particle size fineness of corn flour by addition of papain enzyme and its effects to their hardness, morphology and pasting properties. *Food Science and Quality Management*, **18**, 9-17.

Gupta, H.O., Prakash, O. & Singh, J. (1989). Influence of endosperm texture on milling, chemical composition and nutritive quality in maize. *Plant Foods for Human Nutrition (Formerly Qualitas Plantarum)*, **39**, 235-243.

Gustin, J.L., Jackson, S., Williams, C., Patel, A., Armstrong, P.R., Peter, G.F. & Settles, A.M. (2013).Analysis of maize (Zea mays) kernel density and volume using micro-computed tomography and single-kernel near infrared spectroscopy. Journal of Agricultural and Food Chemistry,61, 10872-10880.

Hampton, J., Opara, L., Hardacre, A., Hill, M. & MacKay, B. (Year). Effects of pre-harvest and post- harvest factors on grain hardness and stress cracking in three maize hybrids. Pp. 83-91. Month and 2000

Harvey, B. & Oaks, A. (1974). The role of gibberellic acid in the hydrolysis of endosperm reserves in Zea mays. Planta, 121, 67-74.

Hearle, J.W.S., Sparrow, J.T. & Cross, P.M. (1973). Specimen preparation. In: *The use of the scanning electron microscope*. Oxford: Parmagon Press Ltd.

Helland, M.H., Wicklund, T. & Narvhus, J.A. (2002). Effect of germination time on alpha-amylase production and viscosity of maize porridge. *Food Research International*, **35**, 315-321.

Huang, H., Yu, H., Xu, H. & Ying, Y. (2008). Near infrared spectroscopy for on/in-line monitoring of quality in foods and beverages: A review. *Journal of Food Engineering*, **87**, 303-313.

Ifarraguerri, A. & Chang, C.I. (2000). Unsupervised hyperspectral image analysis with projection persuit. *Geoscience and Remote Sensing*, **38**, 2529-2538.

Jayas, D.S., Singh, C.B. & Paliwal, J. (2010). Classification of wheat kernels using near-infrared reflectance hyperspectral imaging. In: *Hyperspectral imaging for food quality analysis and control* (edited by D.-W. Sun). Pp. 449-470. UK: Academic Press.

Jindal, V.K. & Mohsenin, N.N. (1978). Dynamic hardness determination of corn kernels from impact tests. *Journal of Agricultural Engineering Research*, **23**, 77-84.

Jinorose, M., Devahastin, S., Blacher, S. & Leonard, A. (2009). Application of image analysis in food drying. In: *Advances in Food Dehydration* (edited by C. Ratti). Pp. 63-96. USA: CRC Press.

Johnson, L. (2000). Corn: the major cereal of the Americans. In: Handbook of Cereal Science and Technology (edited by K. Kulp & J.G.J. Ponte). Pp. 31-80. New York: Marcel Dekker.

Jozinović, A., Šubarić, D., Ačkar, Đ., Babić, J., Planinić, M., Pavoković, M. & Blažić, M. (2013). Effect of screw configuration, moisture content and particle size of corn grits on properties of extrudates. *Croatian Journal of Food Science and Technology*, **4**, 95-101.

Juhász, R., Gergely, S., Szabóki, Á. & Salgó, A. (2007). Correlation between NIR spectra and RVA parameters during germination of maize. Cereal chemistry, 84, 97-101.

Kirleis, A. & Stroshine, R. (1990). Effects of hardness and drying air temperature on breakage susceptibility and dry-milling characteristics of yellow dent corn. *Cereal chemistry*, **67**, 523-
528.

Kotwaliwale, N., Singh, K., Kalne, A., Jha, S.N., Seth, N. & Kar, A. (2011). X-ray imaging methods for internal quality evaluation of agricultural produce. *Journal of Food Science and Technology*, **51**, 1-15.

Labouriau, L.G. & Osborn, J.H. (1984). Temperature dependence of the germination of tomato seeds. *Journal of Thermal Biology*, **9**, 285-294.

Laverse, J., Frisullo, P., Conte, A. & Nobile, M.A. (2012). X-ray microtomography for food quality analysis. In: *Food Industrial Processes - Methods and Equipment* (edited by B. Valdez). Pp. 339-362. Croatia: InTech.

Lee, K.-M., Bean, S.R., Alavi, S., Herrman, T.J. & Waniska, R.D. (2006). Physical and biochemical properties of maize hardness and extrudates of selected hybrids. *Journal of Agricultural and Food Chemistry*, **54**, 4260-4269.

Lee, K.M., Herrman, T.J., Lingenfelser, J. & Jackson, D.S. (2005). Classification and prediction of maize hardness-associated properties using multivariate statistical analyses. *Journal of Cereal Science*, **41**, 85-93.

Li, P.X.P., Hardacre, A., Campanella, O. & Kirkpatrick, K. (1996). Determination of endosperm characteristics of 38 corn hybrids using the Stenvert hardness test. *Cereal chemistry*, **73**, 466-471.

Liebmann, B., Friedl, A. & Varmuza, K. (2010). Applicability of near-infrared spectroscopy for process monitoring in bioethanol production. *Biochemical Engineering Journal*, **52**, 187-193.

Lijavetzky, D., Martinez, M.C., Carrari, F. & Hoop, H.E. (2000). QTL analysis and mapping of pre- harvest sprouting resistance in sorghum. *Euphytica*, **112**, 125-135.

Lim, K.S. & Barigou, M. (2004). X-ray micro-computed tomography of cellular food products. Food Research International, 37, 1001-1012.

Lozano-Alejo, N., Carrillo, G.V., Pixley, K. & Palacios-Rojas, N. (2007). Physical properties and carotenoid content of maize kernels and its nixtamalized snacks. *Innovative Food Science and Emerging Technologies*, **8**, 385-389.

Macho, S. & Larrechi, M.S. (2002). Near-infrared spectroscopy and multivariate calibration for the quantitative determination of certain properties in the petrochemical industry. *Trends in Analytical Chemistry*, **21**, 799-806.

Mahesh, S., Manickavasagan, A., Jayas, D.S., Paliwal, J. & White, N.D.G. (2008). Feasibility of near- infrared hyperspectral imaging to differentiate Canadian wheat classes. *Biosystems Engineering*, **101**, 50-57.

Manley, M., Williams, P., Nilsson, D. & Geladi, P. (2009). Near infrared hyperspectral imaging for the evaluation of endosperm texture in whole yellow maize (Zea maize L.) kernels. *Journal of Agricultural and Food Chemistry*, **57**, 8761-8769.

McGoverin, C.M., Engelbrecht, P., Geladi, P. & Manley, M. (2011). Characterisation of non-viable whole barley, wheat and sorghum grains using near-infrared hyperspectral data and chemometrics. *Analytical and Bioanalytical Chemistry*, 1-7.

McGoverin, C.M. & Manley, M. (2012). Classification of maize kernel hardness using near infrared hyperspectral imaging. *Journal of Near Infrared Spectroscopy*, **20**, 529-535.

Mehl, P.M., Chen, Y.-R., Kim, M.S. & Chan, D.E. (2004). Development of hyperspectral imaging technique for the detection of apple surface defects and contaminations. *Journal of Food Engineering*, **61**, 67-81.

Mendoza, F., Verboven, P., Mebatsion, H.K., Kerckhofs, G., Wevers, M. & Nicolaï, B. (2007). Three- dimensional pore space quantification of apple tissue using x-ray computed microtomography. *Planta*, **226**, 559-570.

Mestres, C., Louis-Alexandre, A., Matencio, F. & Lahlou, A. (1991). Dry-milling properties of maize. Cereal chemistry, 68, 51-56.

Mestres, C. & Matencio, F. (1996). Biochemical basis of kernel milling characteristics and endosperm vitreousness of maize. *Journal of Cereal Science*, **24**, 283-290.

Moghaddam, T.M., Razavi, S.M. & Taghizadeh, M. (2013). Applications of hyperspectral imaging in grains and nuts quality and safety assesment: a review. *Journal of Food Measurement and Characterization*, **7**, 129-140.

Mohan, A. (2008). Pre-harvest sprouting in cereals: a global scenario. Current Science, 94, 704-705. Moot, D.J. & Every, D. (1990). A comparison of bread baking, falling number, α-amylase assay and visual method for the assessment of pre-harvest sprouting in wheat. Journal of Cereal Science, 11, 225-234.

Mousavi, R., Miri, T., Cox, P.W. & Fryer, J.P. (2005). A novel technique for ice crystal visualization in frozen solids using x-ray micro computed tomography. *Journal of Food Science*, **70**, 437-
442.

Neethirajan, S., Jayas, D.S. & White, N.D.G. (2007). Detection of sprouted wheat kernels using softX-ray image analysis. Journal of Food Engineering, 81, 509-519.

Nicolaï, B.M., Beullens, K., Bobelyn, E., Peirs, A., Saeys, W., Theron, K.I. & Lammertyn, J. (2007).Nondestructive measurement of fruit and vegetable quality by means of NIR spectroscopy: A review. Postharvest Biology and Technology, 46, 99-118.

Nonogaki, H., Bassel, G.W. & Bewley, J.D. (2010). Germination—still a mystery. Plant Science, 179, 574-581.

O'Kennedy, K. (2011). Characterisation of zein from South African maize of varying endosperm texture. MSc in Food Science, University of Stellenbosch: Stellenbosch.

Ohnson, L.A. & Fox, S.R. (1991). Relationships among maize quality factors. Cereal chemistry, 68, 602-605.

Oldewage-Theron, W.H., Dicks, E.G. & Napier, C.E. (2006). Poverty, household food insecurity and nutrition: Coping strategies in an informal settlement in the Vaal Triangle, South Africa. *Public Health*, **120**, 795-804.

Orman, B.A. & Schumann, R.A. (1991). Comparison of near-infrared spectroscopy calibration methods for the prediction of protein, oil, and starch in maize grain. *Journal of Agricultural and Food Chemistry*, **39**, 883-886.

Pagano, E.A., Benech-Arnold, R.L., Wawrzkiewicz, M. & Steinbach, H.S. (1997). Alpha-amylase activity in developing sorghum caryopses from sprouting resistant and susceptible varieties. The role of ABA and GAs on its regulation. *Annals of Botany*, **79**, 13-17.

Paulsen, M.R. & Hill, L.D. (1985). Corn quality factors affecting dry milling performance. Journal of Agricultural Engineering Research, 31, 255-263.

Pomeranz, Y., Czuchajowska, Z. & Lai, F. (1986a). Comparison of methods for determination of hardness and breakage susceptibility of commercially dried corn. *Cereal chemistry*, **63**, 39-43.

Pomeranz, Y., Hall, G., Czuchajowska, Z. & Lai, F. (1986b). Test weight, hardness, and breakage susceptibility of yellow dent corn hybrids. *Cereal chemistry*, **63**, 349-351.

Pomeranz, Y., Martin, C., Traylor, D. & Lai, F. (1984). Corn hardness determination. *Cereal chemistry*, **61**, 147-150.

Qin, J. (2010). Hyperspectral imaging instrument. In: Hyperspectral Imaging for Food Quality Analysis and Control (edited by D.-W. Sun). Pp. 129-172. UK: Academic Press.

Radosavljević, M., Bekrić, V., Božović, I. & Jakovljević, J. (2000). Physical and chemical properties of various corn genotypes as a criterion of technological quality. *Genetika*, **32**, 319-329.

Reich, G. (2005). Near-infrared spectroscopy and imaging: Basic principles and pharmaceutical applications. *Advanced Drug Delivery Reviews*, **57**, 1109-1143.

Renu, R. & Chidanand, D.V. (2013). Internal quality classification of agricultural produce using non- destructive image processing technologies (soft X-ray). *International Journal of Latest Trends in Engineering and Technology*, **2**, 535-543.

Ritchie, S., Swanson, S.J. & Gilroy, S. (2000). Physiology of the aleuron layer and starchy endosperm during grain development and early seedling growth: new insights from cell and molecular biology. *Seed science research*, **10**, 193-212.

Ritman, E.L. (2004). Micro-computed tomography - current status and developments. Annual Review of Biomedical Engineering, 6, 185-208.

Robutti, J., Borrás, F., González, R., Torres, R. & De Greef, D. (2002). Endosperm properties and extrusion cooking behavior of maize cultivars. *LWT - Food Science and Technology*, **35**, 663-669.

Robutti, J.L. (1995). Maize kernel hardness estimation in breeding by near-infrared transmission analysis. *Cereal chemistry*, **72**, 632-636.

Sabelli, P.A. & Larkins, B.A. (2009). The development of endosperm in grasses. Plant Physiology, 149, 14-26.

Sahai, D., Mua, J.P., Surjewan, I., Buendia, M.O., Rowe, M. & Jackson, D.S. (2001). Alkaline processing (Nixtamilization) of white mexican corn hybrids for tortilla production: Significance of corn physicochemical characteristics and process conditions. *Cereal chemistry*, **78**, 116-120.

Salvo, L., Suéry, M., Marmottant, A., Limodin, N. & Bernard, D. (2010). 3D imaging in material science: application of x-ray tomography. *Computer Rendus Physique*, **11**, 641-649.

Sasov, A. & van Dyck, D. (1998). Desktop x-ray microscopy and microtomography. Journal of Microscopy, 191, 151-158.

Schambach, S.J., Bag, S., Schilling, L., Groden, C. & Brockmann, M.A. (2010). Application of micro- CT in small animal imaging. *Methods*, **50**, 2-13.

Serna-Saldivar (2010). Cereal grains: the staff of life. In: Cereal Grains Properties, Processing and Nutritional Attributes. Pp. 1-40. Monterrey, Mexico: CRC Press: Taylor & Francis Group.

Shackelford, S., Wheeler, T. & Koohmaraie, M. (2004). Development of optimal protocol for visible and near-infrared reflectance spectroscopic evaluation of meat quality. *Meat Science*, **68**, 371-381.

Shephard, G.S., van der Westhuizen, L., Gatyeni, P.M., Somdyala, N.I.M., Burger, H.M. & Marasas, W.F.O. (2005). Fumonisin mycotoxins in traditional Xhosa maize beer in South Africa. *Journal of Agricultural and Food Chemistry*, **53**, 9634-9637.

Sierra, V., Aldai, N., Castro, P., Osoro, K., Coto-Montes, A. & Oliván, M. (2008). Prediction of the fatty acid composition of beef by near infrared transmittance spectroscopy. *Meat Science*, **78**, 248-255.

Singh, C.B., Jayas, D.S., Paliwal, J. & White, N.D.G. (2009). Detection of sprouted and midge-damaged wheat kernels using near-infrared hyperspectral imaging. *Cereal chemistry*, **83**, 256-260.

Singh, C.B., Jayas, D.S., Paliwal, J. & White, N.D.G. (2010). Detection of midge-damaged wheat kernels using short-wave near-infrared hyperspectral and digital colour imaging. *Biosystems Engineering*, **105**, 380-387.

Singletary, G.W., Banisadr, R. & Keeling, P.L. (1994). Heat stress during grain filling in maize: effects on carbohydrate storage and metabolism. *Functional Plant Biology*, **21**, 829-841.

Skerritt, J.H. & Heywood, R.H. (2000). A five-minute field test for on-farm detection of pre-harvest sprouting in wheat. *Crop science*, **40**, 742-756.

Smail, V.W., Fritz, A.K. & Wetzel, D.L. (2006). Chemical imaging of intact seeds with NIR focal plane array assists plant breeding. *Vibrational spectroscopy*, **42**, 215-221.

Subedi, C.K. & Bhattarai, T. (2003). Effect of gibberellic acid on reserve food mobilization of maize(Zea mays L. var Arun-2) endosperm during germination. Himalayan Journal of Sciences, 1,99-102.

Symes, K. (1961). Classification of Australian wheat varieties based on the granularity of their wholemeal. *Animal Production Science*, **1**, 18-23.

Taina, I.A., Heck, R.J. & Elliot, T.R. (2008). Application of x-ray computed tomography to soil science: a literature review. *Canadian Journal of Soil Science*, **88**, 1-20.

Tallada, J.G., Palacios-Rojas, N. & Armstrong, P.R. (2009). Prediction of maize seed attributes using a rapid single kernel near infrared instrument. *Journal of Cereal Science*, **50**, 381-387.

Tetlow, I.J. (2011). Starch biosynthesis in developing seeds. *Seed science research*, **21**, 5.

Tnani, H., López, I., Jouenne, T. & Vicient, C.M. (2011). Protein composition analysis of oil bodies from maize embryos during germination. *Journal of Plant Physiology*, **168**, 510-513.

Tran, T.L., deMan, J.M. & Rasper, V.F. (1981). Measurement of corn kernel hardness. CanadianInstitute of Food Science and Technology Journal, 14, 42-48.

van der Merwe, B., Erasmus, C. & Taylor, J.R.N. (2001). African maize porridge: a food with slow in vitro starch digestibility. *Food Chemistry*, **72**, 347-353.

Wang, Y. & Petrova, V. (2012). Scanning electron microscopy. In: *Nano Technology Research Methods for Food and Bioproducts* (edited by G.W. Padua & Q. Wang). Pp. 103-126. USA: John Wiley & Sons.

Watson, S.A. (1987). Structure and composition. In: Corn: chemistry and technology (edited by S.A. Watson & P.E. Ramstad). Pp. 53-82. St. Paul, MN: American Association of Cereal Chemists. Inc.

Wehling, R., Jackson, D. & Hamaker, B. (1996). Prediction of corn dry-milling quality by near-infrared spectroscopy. *Cereal chemistry*, **73**, 543-546.

Westneat, M.W., Socha, J.J. & Lee, W., -K (2008). Advances in biological structure, function andphysiology using synchroton X-ray imaging. Annual Review of Physiology, 70, 119-142.

Williams, P., Geladi, P., Fox, G. & Manley, M. (2009). Maize kernel hardness classification by near infrared (NIR) hyperspectral imaging and multivariate data analysis. *Analytica Chimica Acta*,
653, 121-130.

Williams, P.J. (2013). Near infrared (NIR) hyperspectral imaging and X-ray computed tomography combined with statistical and multivariate data analysis to study Fusarium infection in maize. Stellenbosch: University of Stellenbosch.

Wold, S., Esbensen, K. & Geladi, P. (1987). Principal component analysis. Chemometrics and Intelligent Laboratory Systems, 2, 37-52.

Wu, D. & Sun, D.-W. (2013a). Advanced applications of hyperspectral imaging technology for food quality and safety analysis and assessment: a review - part I: fundamentals. *Innovative Food Science and Emerging Technologies*, **19**, 1-14.

Wu, D. & Sun, D.-W. (2013b). Advanced applications of hyperspectral imaging technology for food quality and safety analysis and assessment: a review - part II: applications. *Innovative Food Science and Emerging Technologies*, **19**, 15-28.

Xing, J., Van Hung, P., Symons, S., Shahin, M. & Hatcher, D. (2009). Using a Short Wavelength Infrared (SWIR) hyperspectral imaging system to predict alpha amylase activity in individual Canadian western wheat kernels. *Sensing and Instrumentation for Food Quality and Safety*, **3**, 211-218.

Yin, L. (2012). X-ray computerized microtomography. In: *Nanotechnology Research Methods for Food and Bioproducts* (edited by G.W. Padua & Q. Wang). Pp. 215-234. USA: John Wiley & Sons.

Yoo, Y.J., Hong, J. & Hatch, R.T. (1986). Comparison of α-amylase activities from different assay methods. *Biotechnology and Bioengineering*, **30**, 147-151.

Zhang, X., Lui, F., He, Y. & Li, X. (2012). Applications of hyperspectral imaging and chemometric calibrations for variety discrimination of maize seeds. *Sensors*, **12**.

Zhu, L.-J., Dogan, H., Gajula, H., Gu, M., -H, Liu, Q.-Q. & Shi, Y.-C. (2012). Study of kernel structure of high-amylose and wild-type rice by x-ray microtomography and SEM. *Journal of Cereal Science*, **55**, 1-5.

Chapter 3

Impact of pre-germination on maize kernel hardness using near infrared hyperspectral imaging

Abstract

Kernel hardness is an essential maize attribute to the milling industry. This requires factors that may negatively impact it to be investigated. In this study white maize kernels with varying hardness levels were incubated for an extended period of time at 30°C to induce pre-germination. A representative sample was taken out two-hourly from 0 to 22 h and scanned using a near infrared (NIR) hyperspectral imaging instrument. Clear separation between the three types of endosperm (vitreous, floury and transitional) within the maize kernel was observed on cleaned principal component analysis (PCA) score plots and score images. This enabled the determination of the percentage vitreous (%vitreous) endosperm depicted by the percentage pixels representing this type. A decreasing trend in %vitreous endosperm could also be observed from 0 to 22 h. By means of 95% confidence interval calculations, all the projected %vitreous endosperm data points were within the positive and negative confidence intervals. The R^2 from the projected data matrices were 0.78, 0.77; 0.75, 0.74; 0.73, 0.71; 0.71 and 0.70 for the 2 hard, 2 intermediate and 2 soft maize hybrids respectively. The decrease in the vitreousness of the maize kernels as the kernels were allowed to pre-germinate should be of major concern to the milling industry. Should pre-germination commence without being detected before milling, it will lead to great losses in yield and quality of the production of the end-product.

Introduction

Maize kernel hardness is an important quality attribute and of great importance to the dry maize milling industry. In South Africa, hard maize kernels are preferred for the production of maize meal, a primary staple food in the form of breakfast porridge, and maize grits, a raw material for the traditional Xhosa beer (Mestres *et al.*, 1995; Shephard *et al.*, 2005). Hard maize kernels have been described as those that contain higher ratios of vitreous-to-floury endosperm (Manley *et al.*,2009; Williams *et al.*, 2009; McGoverin & Manley, 2012). Variation between the endosperm types lies in the arrangement of the starch and protein macromolecule arrangement, i.e. the macromolecules of the vitreous endosperm are more

tightly packed as opposed to those of the floury endosperm (Watson, 1987; Bewley & Black, 1994; Srivastava, 2002).

Pre-germination is the process that mature maize kernels can experience during humid conditions prior to the harvesting period (Smail *et al.*, 2006). During pre-germination the endosperm's macromolecules are degraded by the synthesized and secreted hydrolytic enzymes to provide nutrients to the growing embryo. The embryo's growth is depended on the degradation of starch by alpha-amylases (to provide sugars) and protein by proteases (to provide amino acids), until the seedling can undergo the process of photosynthesis to sustain its growth (Dure, 1960; Asiedu *et al.*, 1993; Ritchie *et al.*, 2000; Wang *et al.*, 2005; Ranal & Santana, 2006; Fang & Chu, 2008; Mares & Mrva, 2008). The hydrolysis of starch and protein during pre-germination raised concerns about the changes on the texture of the endosperm and thus maize kernel hardness.

The impact of pre-germination on cereal grains such as wheat, barley, sorghum and rice has been studied and revealed as decrease in grain weight, yield and functionality (Mohan, 2008). Using conventional methods such as α-amylase activity determination and Falling Number it was shown that pre-germinated wheat grains decrease the flour's baking quality (Moot & Every, 1990). In the brewing industry with the help of the Rapid Visco Analyser (RVA), the malting quality of barley and sorghum was shown to decrease due to the degradation of the starch necessary for the malting process (Bueckert *et al.*, 2007). More recently, near infrared (NIR) hyperspectral imaging was used to investigate the viability of wheat, barley and sorghum grains after pre-germination had taken place (McGoverin *et al.*, 2011).

NIR hyperspectral imaging allows the visualisation of the spatial distribution (x,y) of chemical components within a sample. The spatial images collected by hyperspectral sensors at various wavelengths are superimposed to create a three dimensional (3D) image cube or hypercube (reviewed by: Elmasry *et al.*, 2012; Huang *et al.*, 2014). A hypercube contains information where each pixel (x,y coordinate) is a complete spectrum. Due to the large amounts of data acquired using a NIR hyperspectral imaging system, it is necessary to reduce the data into manageable sets using chemometric techniques such as principal component analysis (PCA). PCA is one of the most useful and widespread techniques within the frame of food science based on the number of papers published (Amigo *et al.*, 2013). It (PCA) generates a range of analysis outputs including score images, score plots and loading line plots enabling efficient means of data interpretation.

PCA allows for the decomposition of large quantity of data obtained from the objects and variables (I X J) matrix into manageable data sets that can be easily explored (Wold *et al.*, 1987; Gowen *et al.*, 2008). PCA decomposes the data to form scores, loadings and a residual matrix where $\mathbf{X = t_1p_1' + t_2p_2' + \cdots + t_np_n' + E}$ (Geladi, 2003) where:

X = the data matrix of I rows or objects x J columns or variables

T = the matrix of score vectors (I x A [A = components chosen by eigenvalues of the matrix and standardised eigenvalues])

P = the matrix of loading vectors (J x A)

E = the residual matrix of I x J

n = 1, 2, 3, ….., N

The scores of PCA indicate the presence of variation between samples and loadings express the variation accountable and establishes which wavelengths are contirbuting (Williams, 2009). The results are presented in the form of score plots and score images of various principal components (PCs) (Wold *et al.*, 1987; Francis & Wills, 1999; Davies & Fearn, 2004; Rodionova *et al.*, 2005). The score plots and images can be used interactively to explore samples investigated. Score plots of two different PCs (e.g. PC1 vs. PC2 or PC1 vs. PC6) allows visualisation of the sample's special features or irregularities (Williams *et al.*, 2012). Pre-processing of mean-centered data (**X**) is essential for the removal of light scattering and dead pixels (pixels caused by detector anomalies) so that the desired information in terms of chemical differences can be emphasised better (Amigo *et al.*, 2013). Techniques such as multiplicative scatter correction (MSC) and standard normal variate (SNV) correct hyperspectral images being analysed removing any non- uniform scattering and edge effects that would interfere with achievement of valued results (Luypaert *et al.*, 2004; Maleki *et al.*, 2007; Elmasry *et al.*, 2012). First and second derivative techniques highlight spectral features of interest (Amigo *et al.*, 2013). Derivatives however increase signal-to-noise ratio and therefore the noise will be amplified.

Effect of germination on cereal grains such as wheat (Moot & Every, 1990; Kruger, 1994; Groos *et al.*, 2002; McGoverin *et al.*, 2011; Huang *et al.*, 2012), barley (Enari & Sopanen, 1986; Kadziola *et al.*, 1994; Woonton *et al.*, 2005; Arngren *et al.*, 2011; McGoverin *et al.*, 2011) and sorghum (McGoverin *et al.*, 2011) have been studied extensively using NIR hyperspectral imaging. McGoverin *et al.* (2011) used a total of 239 wavelengths (from 1000 to 2498 nm) to investigate possible classification between viable (non-germinated) cereal grains (wheat, barley and sorghum) from the non-viable (germinated) grains for the baking and brewing industries. Their results were successful as *ca.* 80% separation could be clearly observed using PC1 and PC5. No research has been performed thus far, using maize kernels as the subject of interest.

With the knowledge that endosperm contents are utilised during pre-germination and endosperm ratios give rise to kernel hardness, it was imperative to study the impact of pre-germination on changes in endosperm texture and thus maize kernel hardness using NIR

hyperspectral imaging.

Materials and Methods

Preliminary study

Thirty randomly selected white maize kernels were placed in a Petri-dish lined with 2 Whatman no.1 filter papers and either 5 or 10 mL distilled water (dH_20) were added to determine sufficient moisture levels for pre-germination. The Petri-dishes were incubated at the optimum seedling growth temperature, i.e. 30^{o}C (Watson, 1987). The kernels were monitored on an hourly basis to determine the time of the radicle emergence.

Maize samples

Six white maize hybrids (H2, H3, H6, H7, H8, H9) from a breeding program kindly supplied by PANNAR (Sasko, Paarl, South Africa) were used. The hybrids belonged to three hardness categories, i.e. H2 and H3 belonged to a hard maize category, H6 and H7 were of intermediate hardness, while H8 and H9 were soft. Hardness categories were pre-determined and provided by experienced maize breeders.

Sample preparation

Once the appropriate pre-germination time period was established, a two-hourly time frame for data collection was decided upon. This requires that every 2 h (starting from 0 h) 80 g of maize kernels was placed in each of 5 Petri-dishes, lined with 2 Whatman no. 1 filter papers, and 10 mL of water was added. The petri-dishes were then incubated at 30^{o}C to induce pre-germination. The staggered pre-germination process allowed all samples to be removed from the incubator simultaneously at the end pre-determined time period. The samples were subsequently drained and freeze dried in preparation for the imaging process. The kernels were freeze dried to stop the germination process after each respective time period and to enable transportation to the site where imaging took place. To ensure fair comparison between all samples, the 0 h samples were also freeze dried. Figure 3.1 illustrates sample preparation in more detail.

a)

Hard				Intermediate				Soft			
H2		H3		H6		H7		H5		H9	
0 h	80 g	0 h	80 g	0 h	80 g	0 h	80 g	0 h	80 g	0 h	80 g
2 h	80 g	2 h	80 g	2 h	80 g	2 h	80 g	2 h	80 g	2 h	80 g
4 h	80 g	4 h	80 g	4 h	80 g	4 h	80 g	4 h	80 g	4 h	80 g
6 h	80 g	6 h	80 g	6 h	80 g	6 h	80 g	6 h	80 g	6 h	80 g
8 h	80 g	8 h	80 g	8 h	80 g	8 h	80 g	8 h	80 g	8 h	80 g
10 h	80 g	10 h	80 g	10 h	80 g	10 h	80 g	10 h	80 g	10 h	80 g
12 h	80 g	12 h	80 g	12 h	80 g	12 h	80 g	12 h	80 g	12 h	80 g
14 h	80 g	14 h	80 g	14 h	80 g	14 h	80 g	14 h	80 g	14 h	80 g
16 h	80 g	16 h	80 g	16 h	80 g	16 h	80 g	16 h	80 g	16 h	80 g
18 h	80 g	18 h	80 g	18 h	80 g	18 h	80 g	18 h	80 g	18 h	80 g
20 h	80 g	20 h	80 g	20 h	80 g	20 h	80 g	20 h	80 g	20 h	80 g
22 h	80 g	22 h	80 g	22 h	80 g	22 h	80 g	22 h	80 g	22 h	80 g

b)

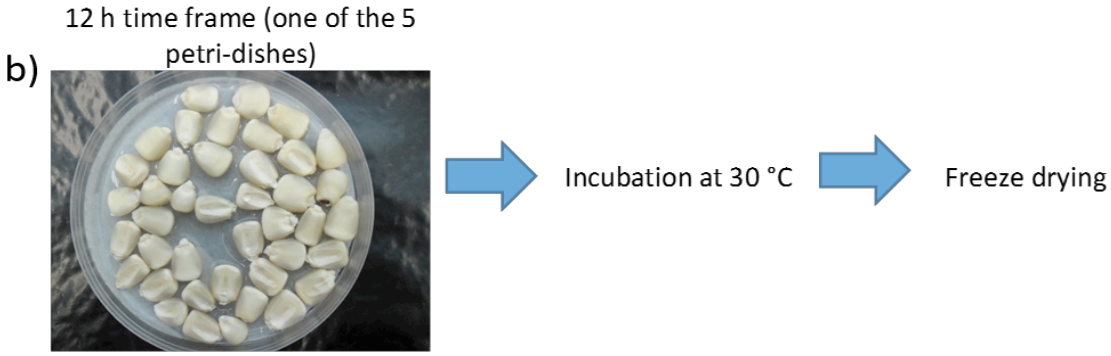

Figure 3.1. a) Sample compilation as used in the study where every time period from every hybrid comprised of 80 g white maize and b) illustration of steps from Petri-dish lined with 2 Whatman no. 1 filter papers, 10 mL of water, incubated and freeze dried.

Near infrared hyperspectral imaging and data analysis

An Umbio Inspector shortwave infrared (SWIR) hyperspectral camera (Umbio, Umeå, Sweden) was used. This is a line scanner with a spectrograph coupled to a 2D array Mercury-Cadmium-Telluride (HgCdTe) detector and quartz-halogen lamps with regulated current to ensure a stable light output. The halogen cycle causes the light output to remain almost constant throughout the lamp's life. Three randomly selected maize kernels from each hybrid and time period were placed germ down on a plastic sample holder, secured with double sided tape and clearly marked. Samples moved on a conveyer belt and images of 320 spatial pixels at 239 wavebands (region 1000-2498 nm) were obtained (Fig. 3.2). An internal dark reference was obtained whilst the camera shutter was closed and an external white reference was collected using a Spectralon (ACAL BFi Nordic, Uppsala, Sweden) strip) before sample imaging. Image collection were performed randomly with respect to the incubation time periods.

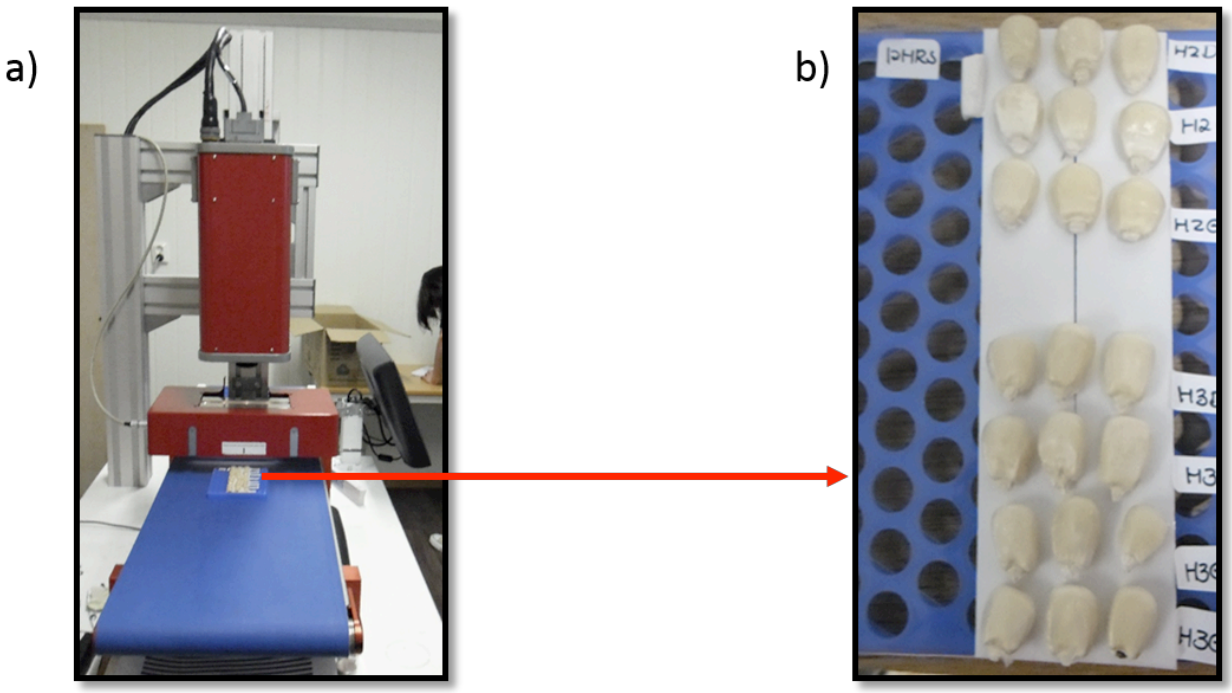

Figure 3.2. a) An Umbio Inspector shortwave infrared instrument used for imaging purposes and b) a plastic sample holder with 3 maize kernels per hybrid secured with double sided tape and clearly marked.

Data processing and analysis of hyperspectral image datasets were carried out using Evince software (version 2.5.0, Umbio AB, Umeå, Sweden). PCA scores plots and images (Fig. 3.3) could be used interactively by means of a technique referred to as brushing for image cleaning, i.e. once a region of pixels are selected on the score plot, the associated area that is represented on the score image is also highlighted. It was possible to select clusters in the score plot that could be associated with difference parts of the image. PCA thus allowed for the classification of the different parts of the image for easy removal of classes that were not vital for this study such as pixels dedicated to background information (plastic sample holder, double sided tape and labels), dead pixels and illumination errors. Typically three PCs would be adequate to remove the background. Colours were assigned to each class to illustrate the different parts of the image. PCA was then re-calculated on the cleaned images with six PCs for futher analysis. In this case prior expert knowledge of the samples and sample presentation is required. Whereas with masking threshold values are used.

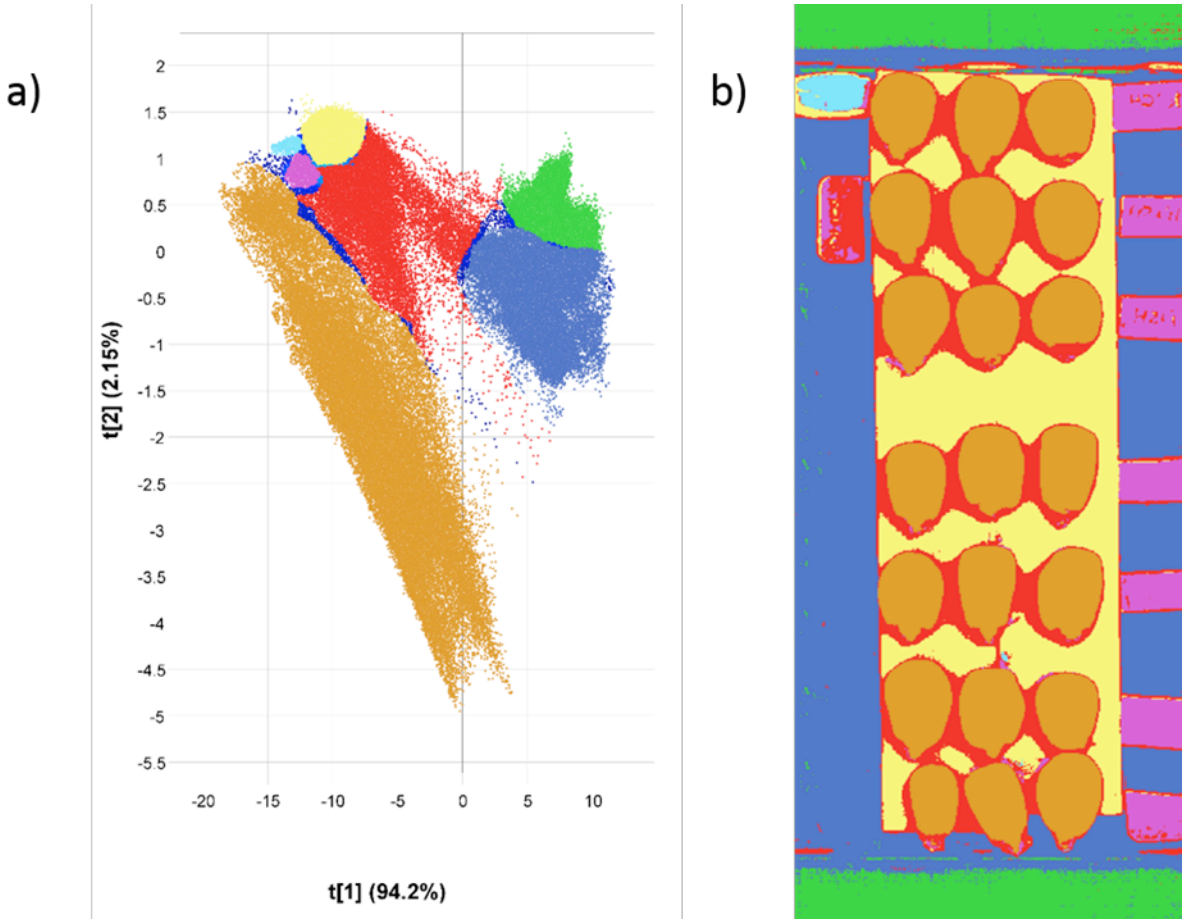

Figure 3.3. PCA classification (a) score plot of PC1 vs. PC2 with the corresponding (b) score image. All parts of the image were colour coded in the score plot and projected to the image space. Maize kernels = brown, labels = purple, plastic sample holder = blue, double sided tape = yellow and the red = unidentified. This enabled efficient cleaning (removal of unwanted information) of the image.

Individual images were combined to construct mosaic images using Evince. Maize kernels were arranged, for each hybrid, according to incubation time for the first set of mosaics (Fig. 3.4a). A subsequent mosaic combined the three maize hardness categories and various incubation time periods in a single image (as per Fig. 3.4b). Mosaic image corrections were performed in Evince using the following algorithm:

$$I_{\lambda,n} = -\log_{10}\left(\frac{S_{\lambda,n} - B_{\lambda,n}}{W_{\lambda,n} - B_{\lambda,n}}\right)$$ ...equation 1

n = number of pixels generated (n=1……N)

$I_{\lambda,n}$ = standard absorbance pixel intensity, pixel n and wavelength λ

$S_{\lambda,n}$ = sample image, pixel n at wavelength λ

$B_{\lambda,n}$ = dark reference image, pixel n at wavelength λ

$W_{\lambda,n}$ = white reference image, pixel n at wavelength λ

a)

0 h	H2	H2	H2
2 h	H2	H2	H2
4 h	H2	H2	H2
6 h	H2	H2	H2
8 h	H2	H2	H2
10 h	H2	H2	H2
12 h	H2	H2	H2
14 h	H2	H2	H2
16 h	H2	H2	H2
18 h	H2	H2	H2
20 h	H2	H2	H2
22 h	H2	H2	H2

b)

	Hard maize kernels			Intermediate maize kernels			Soft maize kernels		
0 h	H2	H2	H2	H6	H6	H6	H9	H9	H9
2 h	H2	H2	H2	H6	H6	H6	H9	H9	H9
4 h	H2	H2	H2	H6	H6	H6	H9	H9	H9
6 h	H2	H2	H2	H6	H6	H6	H9	H9	H9
8 h	H2	H2	H2	H6	H6	H6	H9	H9	H9
10 h	H2	H2	H2	H6	H6	H6	H9	H9	H9
12 h	H2	H2	H2	H6	H6	H6	H9	H9	H9
14 h	H2	H2	H2	H6	H6	H6	H9	H9	H9
16 h	H2	H2	H2	H6	H6	H6	H9	H9	H9
18 h	H2	H2	H2	H6	H6	H6	H9	H9	H9
20 h	H2	H2	H2	H6	H6	H6	H9	H9	H9
22 h	H2	H2	H2	H6	H6	H6	H9	H9	H9

Figure 3.4. A schematic representation of mosaic construction in Evince. (a) Mosaic of a single hybrid, H2, from 0 – 22 h and (b) three hardness categories were placed next to each other with H2 = hard maize kernels, H6 = intermediate maize kernels and H9 = soft maize kernels.

Once the mosaic images were constructed, new PCA models were calculated with 6 PCs, pre-processed with SNV and comparisons of two different PCs at a time allowed for further removal of undesired pixels from the scores plot. Pixel clusters observed on PCA scores plots were used to identify and classify components of the maize kernels. This was achieved by highlighting a cluster on the scores plot and simultaneously, the score image would be activated and the location of the clustered pixels on it (i.e. scores image) would be highlighted and visualised. Classes were then assigned and projected onto the PCA scores images. The region- of-interest (ROI) for this study was the vitreous endosperm. For ease of visualisation, the intermediate and floury endosperm clusters were subsequently removed. The percentage pixels representing the vitreous endosperm were calculated according to equation 2:

$$\%vit = \frac{pixels\ dedicated\ to\ the\ vitreous\ enodsperm}{pixels\ dedicated\ to\ the\ whole\ maize\ kernel} \quad \text{...equation 2}$$

Where:

%vit = percentage of vitreous endosperm

Plots were created to establish a trend in the %vitreous data using MATLAB v 7.10 (The MathWorks, Massachusetts, USA). Polynomial curves were established to determine the best fitting line to a series of data points obtained and coefficients calculated using the equation 3.

$$\mathbf{b} = \mathbf{X}/\mathbf{h}$$ ...equation 3

Where:

X = polynomial degree of curves

h = is the %vitreous endosperm.

New values were then predicted to compensate for the non-linearity of the data using equation 4.

$\hat{h}$(hat)= X x b ...equation 4

Where:

X = polynomial degree of curves

b = coefficients of the best fitting line.

Standard deviations were also determined to accommodate the variation of the data and the R^2 to ensure a stable model of prediction using equation 5.

R^2 = std (hhat)^2 / std (h)^2, ...equation 5

The residual value was calculated according to equation 6.

e = h-hhat. ...equation 6

Root mean square error was determined using equation 7.

(**sqrt (e * e/11)**, ...equation 7

where 11 represents the number of incubation time periods).

Using a quadratic root calculation (equation 8) the point at which the deterioration or breakdown of the vitreous endosperm is believed to be of concern could be determined .

(X = (-b(2) + sqrt(b2)^2 – 4 * dev b(3) * 2 * b(3)) …equation 8

Results and discussions

From the preliminary study conducted, radicle emergence was noted at 22 h of incubation, which led to the decision of incubating maize kernels for 0, 2, 4, 6, 8, 10, 12, 14, 16, 18, 20 and 22 h time periods.

Near infrared hyperspectral image analysis

To minimise variation between the samples due to moisture content, all samples from 0 h to 22 h were freeze dried. In comparison to other pre-processing techniques, SNV resulted in the clearest clusters of the maize kernels (Fig. 3.5a). The PCA plot of PC 1 vs PC2 showed clearly distinct clusters and a gradient on the score plot (with 91.34% variation explained). The clusters belonged to the 3 types of endosperm present within a maize kernel. This observation was made with the help of a classification score plot and image (Fig. 3.5b). The scores images also indicated the decrease in the endosperm content (depicted in green) as pre-germination time increased, a hypothesis was thus made that pre-germination negatively affects vitreous endosperm content within the maize kernel. Similar results were observed in all hybrids examined. Again expert cereal science knowledge is required for such evaluation and interpretation of scores plots and images using brushing.

PC1 depicts scattering information, therefore the information obtained from PC1 (which depicts endosperm variation) is based on the differences between the types of endosperm present within the maize kernel. The vitreous endosperm (more dense) is made up of tightly packed starch granules surrounded by protein matrix, while the soft endosperm (less dense) is made up of loosely packed starch granules surrounded by a protein matrix (McGoverin and Manley, 2012). McGoverin and Manley (2012) illustrated that NIR hyperspectral imaging could be used to determine the hardness of individual maize kernels without sample destruction or the need for reference data. They illustrated that it was possible to determine the percentage vitreous and floury endosperm from images after principal component analysis was applied. Manual kernel dissection, the only reference method of determining proportions of endosperm, was used to validate this method.

During pre-germination, the endosperm are broken down into monomers that can be utilised by the growing embryo (Fincher, 1989), leading to the hypothesis that loss of compactness can be experienced by the vitreous endosperm.

(a)

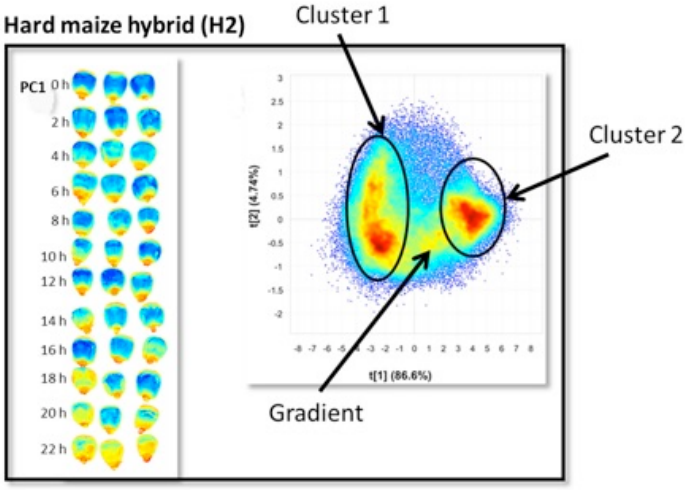

(b)

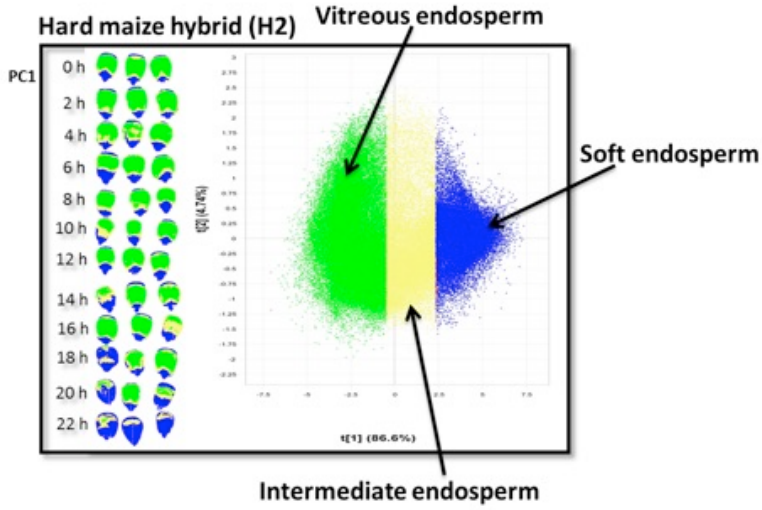

(c)

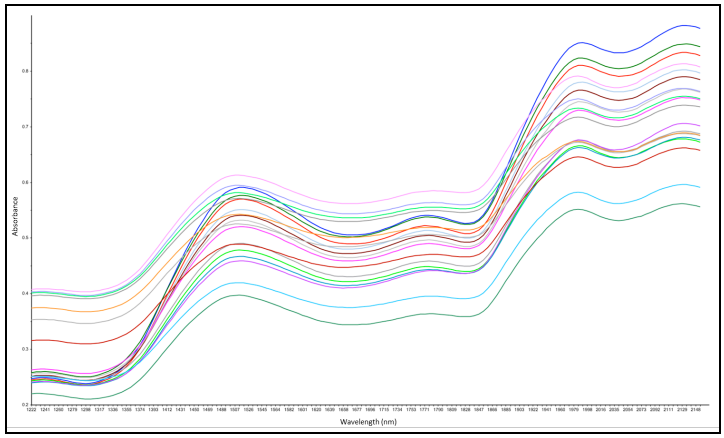

Figure 3.5. (a) PCA scores image from PC1 (left) and scores plot of PC1 vs PC2 (right), of the pre-germinated kernels of a hard maize kernel hybrid, (H2). Dark blue indicate vitreous endosperm. Decrease in vitreous endosperm with increasing incubation time period is clear in this image. Different colours in the scores plot indicate density of pixels with red being the densest and blue the least dense. (b) Classification scores image and scores plot illustrating two clear clusters (Cluster 1 = vitreous endosperm; Cluster 2 = floury endosperm) with the gradient region (intermediate endosperm) in-between. (c) Whole maize kernel spectra of a range of the maize kernels.

A mosaic comprising of the three hardness categories was constructed (Fig. 3.6a) to illustrate the different types of endosperm, and the changes occurring as pre-germination time increased. Employing the histological knowledge of the maize endosperm allowed for the classed (clusters) to be assigned (Fig. 3.6b) and the classes were then projected onto the scores image situated on the right side of figure 3.6b. PCA classification plots (PC 1 vs. PC 2 which explained 91.37% of the variation) indicated that the assigned classes belonged to the various endosperm types present within the maize kernels. The various endosperm types were classed as green = vitreous endosperm, yellow = transitional (or intermediate) endosperm and blue = soft endosperm and pedicle. The two types of endosperm were previously observed by other researchers (Manley *et al.*, 2009; Williams *et al.*, 2009) using PCA score plots and score images. This way of using PCA for classification purposes was illustrated by McGoverin and Manley (2012). The authors used PCA to illustrate that maize hardness was related to the ratio of the vitreous-to-floury endosperm within a maize kernel. Williams *et al.* (2009) developed a partial least square discriminant analysis (PLS-DA) model that was able to distinguish between floury and vitreous endosperm. The model was built by assigning a certain portion of the images to the training set and the rest to a test set. The PLS-DA model was 88% successful in endosperm discrimination (Williams *et al.*, 2009). The third type of endosperm was also observed by O'Kennedy (2011), who termed it the transitional endosperm. Using the SEM technique she noted the intermediate endosperm to be in-between the vitreous and soft endosperm types. The transitional phase endosperm was reported to comprise of small starch granules that are less compact than the vitreous endosperm and less loosely packed when compared to the floury endosperm. It was again noticed that as degree of germination increased, loss of vitreousness occurred. This was attributed to the diminishing dark green classed section as one progressed down with increasing degree of germination on the scores image, i.e. 0 to 22 h (Fig. 3.6b).

More observations made on the scores images were, some of the maize kernels showed an increase in the soft and transitional endosperm content, observable on the scores image from 8 h onwards (Fig. 3.6b). The increase in the transitional endosperm was observed more on the intermediate maize hybrids when compared to the hard and soft maize hybrids (Fig. 3.6b). The soft hybrids showed an increase in the soft endosperm (Fig. 3.6b). Similar results were observed when comparing H3 (hard hybrid), H7 (intermediate hybrid) and H5 (soft hybrid).

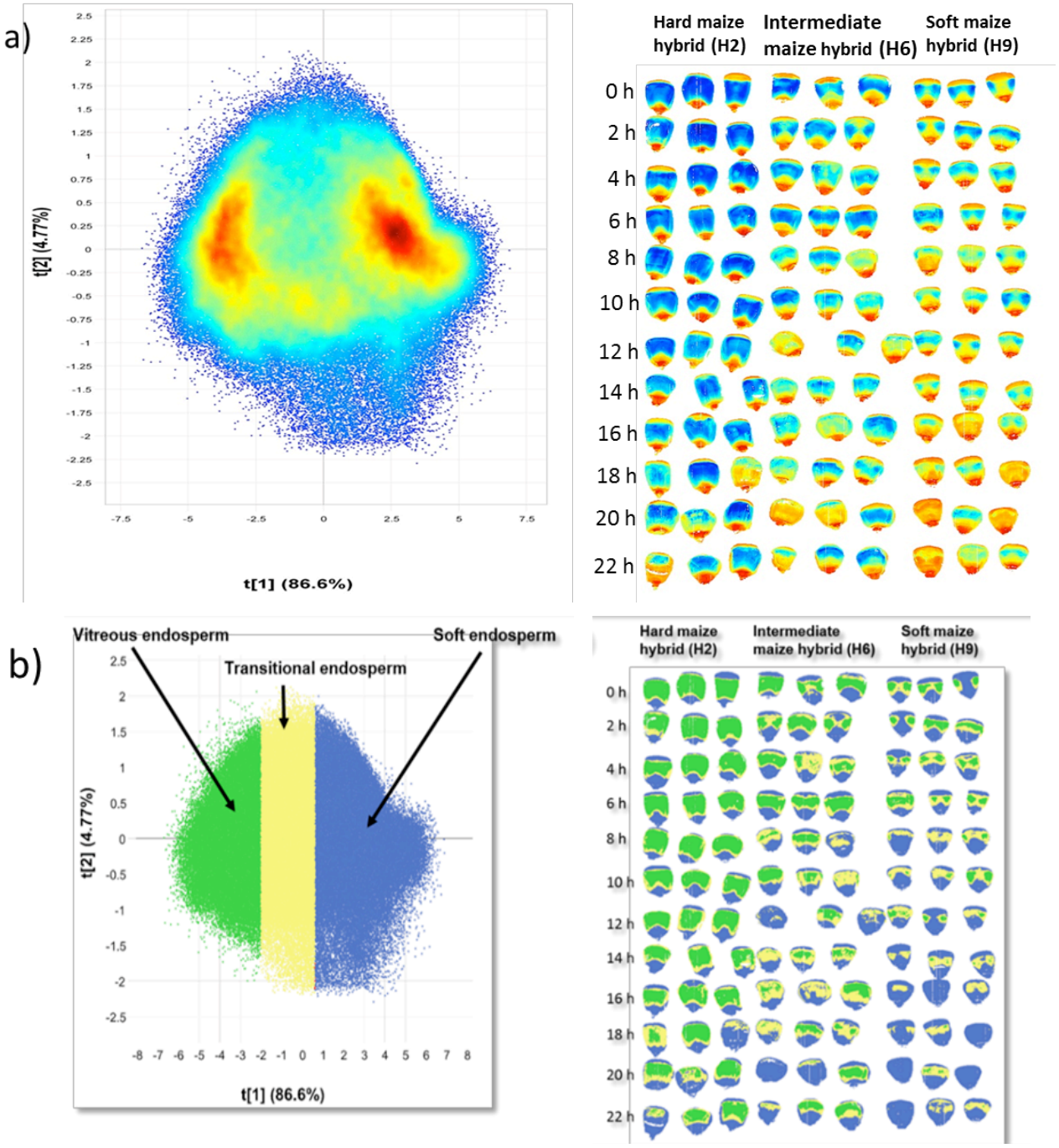

Figure 3.6 (a) PCA scores plot (left) and mosaic scores image (right) of three different maize hybrids (H2 = hard maize hybrid, H6 = intermediate maize hybrid and H9 = soft maize hybrid), pre-germinated from 0 to 22 h. Two distinct clusters and a gradient are again observed. (b) Classification scores plot (left) of PC1 vs PC2 used to project the classes onto the score image (right) revealing three different types of endosperm in a maize kernel (green = vitreous endosperm, yellow = intermediate endosperm and blue = soft endosperm and pedicle. On the scores image s pre-germination increases the content of the intermediate endosperm increases in the intermediate and hard maize hybrids. Soft endosperm increase in the soft maize hybrids.

A new separate PCA model was constructed by removing unwanted classes (soft and intermediate endosperm classes) and the score images indicated a decrease in the content of the vitreous endosperm within the maize kernels as pre-germination progressed (Fig. 3.7). From 12 h onwards the number of pixels representative of the vitreous endosperm (particularly in the soft and intermediate hybrid) seemed to be diminishing on PCA score images (Fig. 3.7). Calculations of the % vitreous endosperm within the maize kernels indicated that the content of the vitreous endosperm decreased from 70 – 20 % in hard maize hybrids, 60 – 20 % in the intermediate maize hybrids and 46 – 11 % in soft maize hybrids. With the knowledge of the pre-germination process, it was hypothesised that as the enzymes degrade the maize endosperm, a porous structure of the protein matrix and starch granules (similar to that of the floury endosperm) was being formed. Zein is stored in the protein bodies that are arranged to form the matrix. The zein proteins become degraded during the germination process to create nutrients for the growing embryo (Mitsuhashi & Oaks, 1994). The zein chain is degraded by proteases into monomers which are transported to the growing embryo. No other polypeptides will replace the ones transported into the growing embryo (which led to the hypothesis of the porous structure development). Similarly, starch granules filled with the glucose polymers (amylose and amylopectin) are degraded by amylolytic enzymes. The simple sugars produced from the degradation of starch molecules are also transported to the growing embryo (Bewley & Black, 1994) and will not be replaced.

Light penetration of the NIR radiation travels to a specific depth to yield information of the sample, e.g. in fruits, NIR radiation depth has been studied to be between 2–4 mm using the wavelength region between 500 – 1900 nm (ElMasry & Sun, 2010). Shorter wavelengths (between 700 – 900 nm) were able to penetrate to 4 mm into the fruit. To be able to observe microstructural changes within the maize kernel an instrument with short wavelength radiation to provide deeper penetration would be ideal. An instrument such as the X-ray micro computed tomography imaging system (Butz *et al.*, 2005) uses short wavelengths and high frequencies, X-rays to penetrate through material in search of information (Lim & Barigou, 2004).

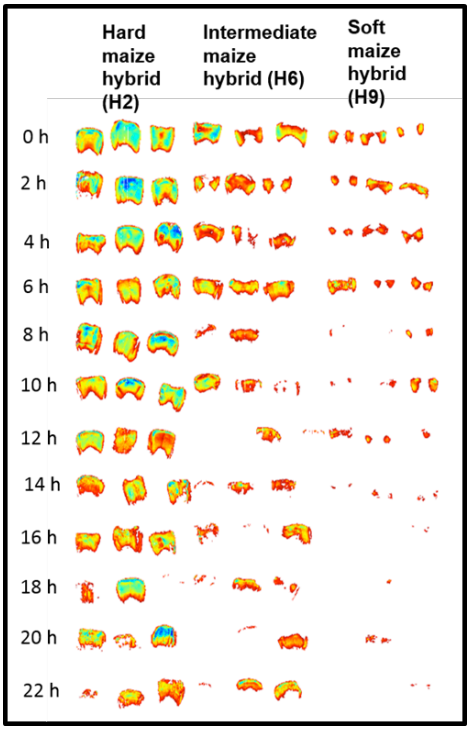

Figure 3.7. A score image of PC1 indicating the decrease of the vitreous endosperm experienced by the hard, intermediate and soft maize kernels as the degree of pre-germination increased. After 12 h of incubation of the soft maize kernels, there was almost no vitreous endosperm left.

The polynomial curves created with the data from the projection matrix (percentage vitreous pixels vs incubation time period) also indicated a decreasing trend in all hybrids analysed. The reliability of the projected matrix was tested with 95% confidence intervals and data points fell within the parameters of the negative (green) and positive (red) confidence bands, the black line was the best fitting line (Fig. 3.8). The hard hybrids (i.e. H2 and H3) data points at the 4 h interval fell out of the confidence interval (Fig. 3.8). Reason for this deviation could not be established. Percentage vitreous endosperm in hard (i.e. H2 and H3), intermediate (H7) and soft hybrids (H9) depicted a decreasing polynomial curve trends (Fig. 3.8). A quadratic root calculation revealed that a point of concerning deterioration in hardness was at 10 h. It is known that maize hardness influences the efficiency of production and quality of the final product. Maize that has pre- germinated to a degree similar to that of 10 h in this experiment will yield end products of low quality. With the help of NIR hyperspectral imaging, the exclusion of these kernels from the line is possible. Ensuring that only maize kernels of desired quality is used, optimal equipment efficiency and quality of the end product.

H2 (hard maize hybrid)

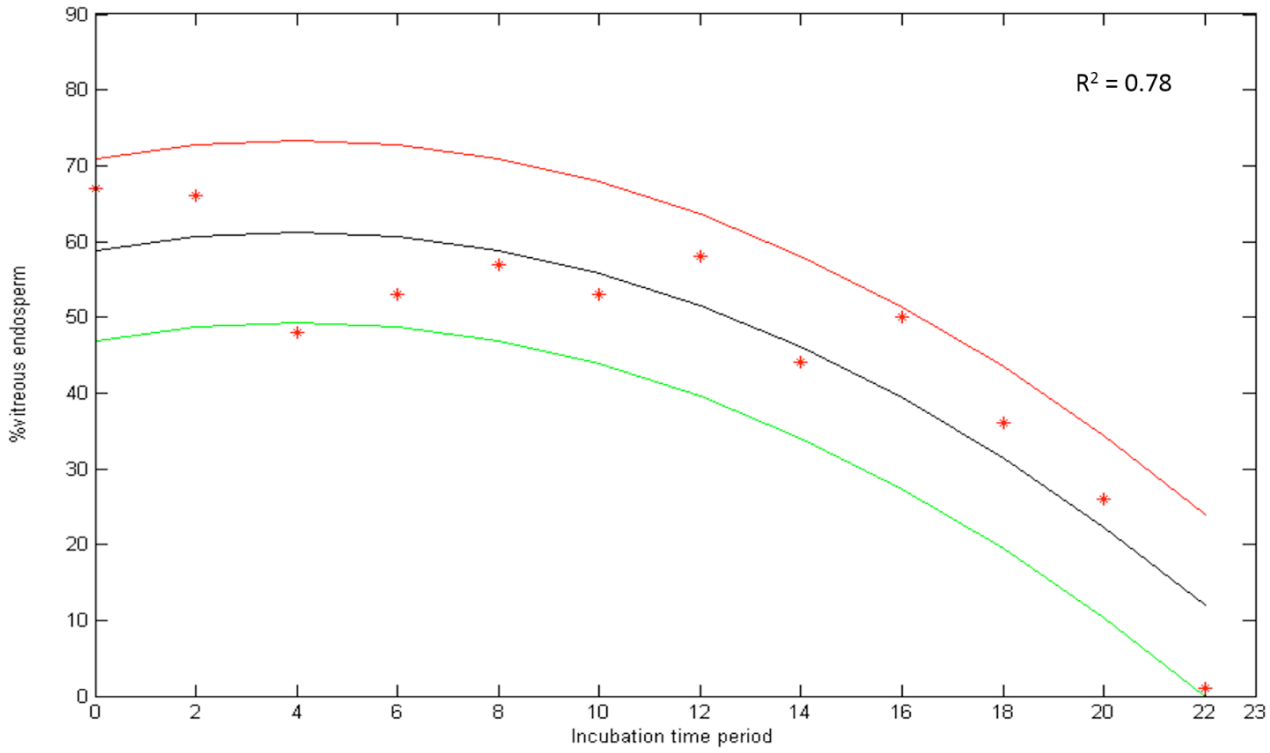

H3 (hard maize hybrid)

b)

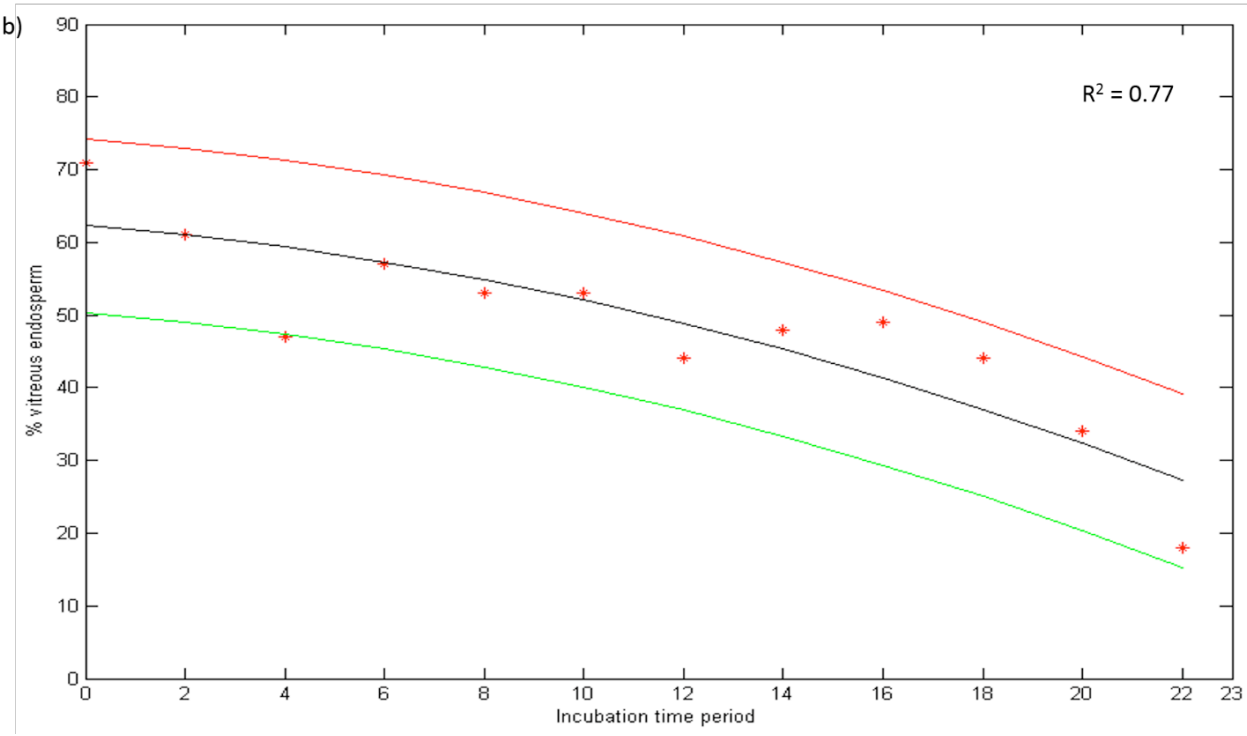

c)

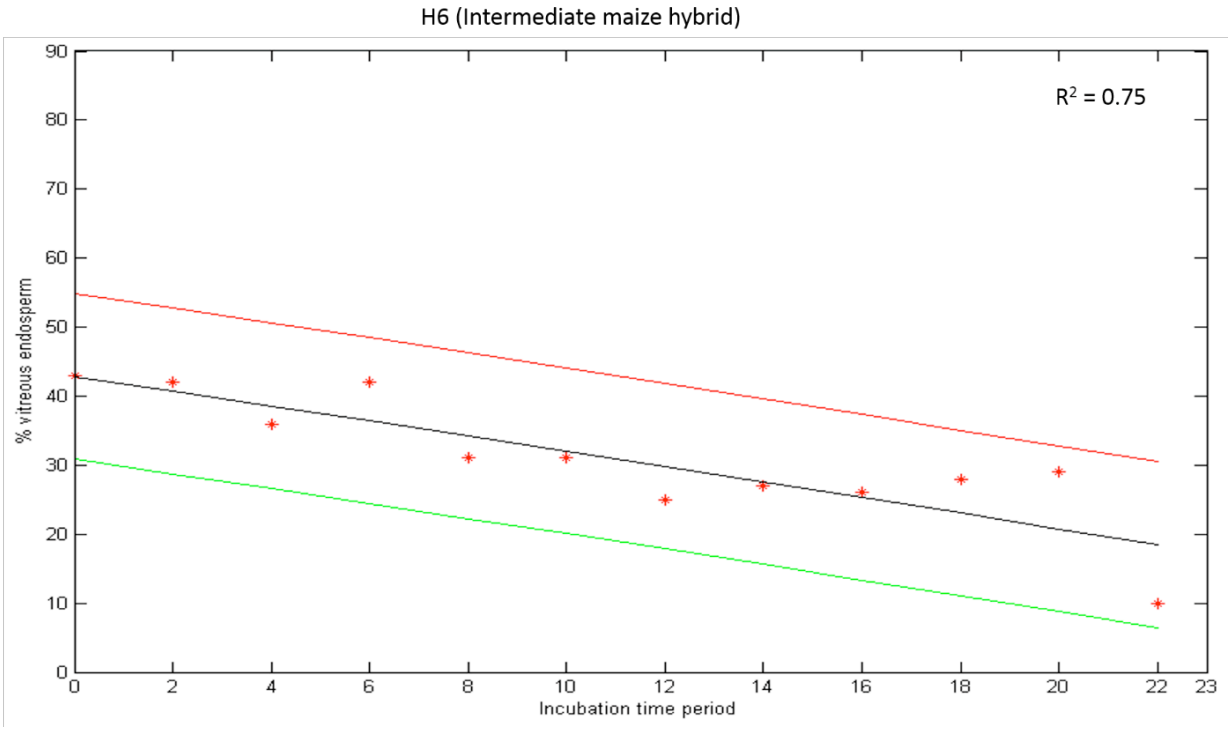

d)

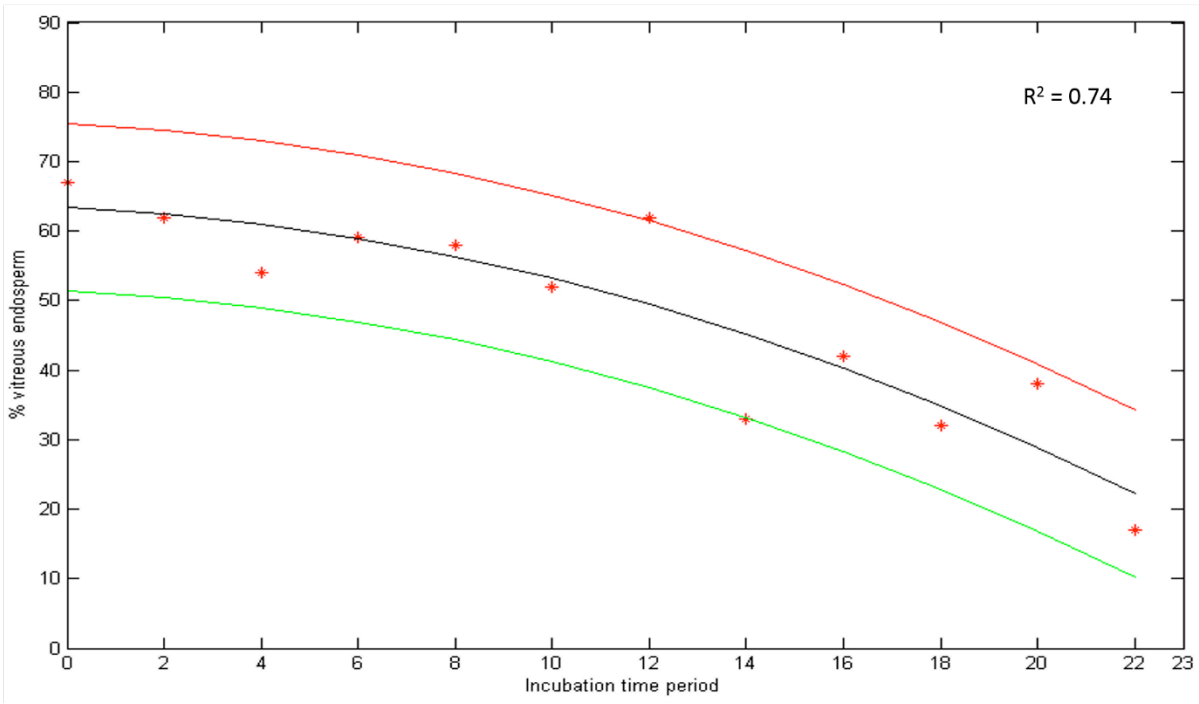

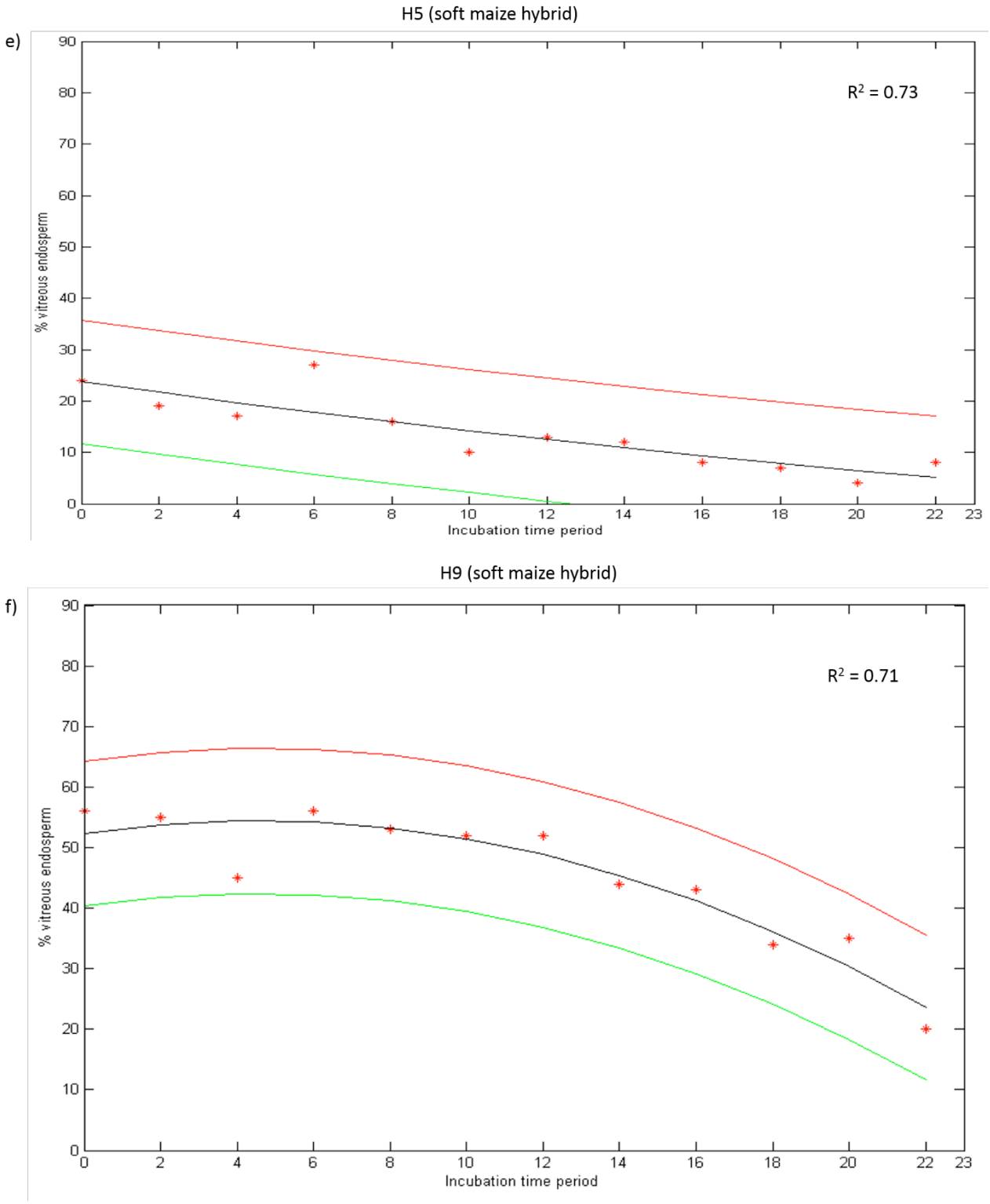

Figure 3.8. Projection matrix plot of percentage vitreous endosperm versus incubation time with 95% negative (green line) and positive (red line) confidence intervals and best fitting line (black) indicating a decreasing trend in the %vitreous endosperm calculations data obtained. A decrease in % vitreous endosperm was observed for the (a and b) hard maize hybrids, (c and d) intermediate maize hybrids, as well as for the (e and f) soft maize hybrids.

Conclusions

Deterioration in the vitreousness of the maize kernels could be observed on all imaged samples. Increase in the soft and intermediate endosperm content was noted. As pre-germination increased, the vitreous endosperm was degraded and it became similar in texure to that of the intermediate and soft endosperm. In the dry milling industry, maize hardness is defined as the maize with the higher ratio of the vitreous endosperm. Polynomial curves created using projected matrix data with 95% confidence intervals indicated a decreasing trend in vitreousness (measured as %vitreous pixels) for all the maize hybrids imaged. Based on the results obtained germination taking place within maize kernels prior to harvesting should be of major concern to the dry milling industry where kernel hardness is of great importance. Other properties such as the quality of starch (in terms of swelling and gelling properties) and protein (to visualise the deterioration of the protein matrix), which have an impact on maize hardness should also be investigated. With the help of loading plots, variation between the starch and protein content should be attainable as well as the wavelengths that are critical to the study. It would be advisable though to use the same kernels in the imaging process from 0 to 22 h, so that variations due to kernel size and original content uncertainty could be eliminated. For the industry purposes, models that help separate germinated maize kernels from the sound maize kernels can be developed with the help of partial least square discriminant analysis (PLS-DA). Due to the knowledge that high energy photons provide deeper penetration into the sample, a technique such as X-ray micro-computed tomography that allows usage of such photons, could be considered in investigating the changes that took place within the maize kernel's microstructure.

With the help of NIR hyperspectral imaging, the exclusion of these kernels from the line is possible. Ensuring that only maize kernels of desired quality is used, optimal equipment efficiency and quality of the end product. There is no official hardness determination method for maize hardness, information obtained and methods used in this study has been based on previous studies performed by referenced authors.

The main focus of this chapter was to illustrate if there are changes within the vitreous endosperm caused by pre-germination. The results obtained from this study concluded that the vitreous endosperm does deteriorate during the process of pre-germination.

References

Amigo, J.M., Martí, I. & Gowen, A. (2013). Hyperspectral imaging and chemometrics: a perfect combination for the analysis of food structure, composition and quality. In: *Chemometrics in Food Chemistry* (edited by F. Marini). Pp. 343-370. UK: Elsevier.

Arngren, M., Hansen, P.W., Eriksen, B., Larsen, J. & Larsen, R. (2011). Analysis of pre-germinated barley using hyperspectral image analysis. *Journal of Agricultural and Food Chemistry*, **21**,11385-11394.

Asiedu, M., Lied, E., Nilsen, R. & Sandnes, K. (1993). Effect of processing (sprouting and/or fermentation) on sorghum and maize: II. Vitamins and amino acid composition and biological utilization of maize protein. *Food Chemistry*, **48**, 201-204.

Bewley, J.D. & Black, M. (1994). *Seeds: physiology of development and germination.* Pp. 372. New York: Plenum Publishing Corporation.

Bueckert, R.A., Lefol, E.B. & Harvey, B.L. (2007). Early detection of non-visible sprouting in barley seed using rapid visco analysis. *Canadian Journal of Plant Science*, **87**, 3-12.

Butz, P., Hofmann, C. & Tauscher, B. (2005). Recent developments in noninvasive techniques for fresh fruit and vegetable internal quality analysis. Journal of Food Science, 70, R131-R141.

Davies, T. & Fearn, T. (2004). Back to basics: the principles of principal component analysis. *Spectroscopy Europe*, **16**, 20-23.

Dure, L.S. (1960). Site of origin and extent of activity of amylases in maize germination. *Plant Physiology*, **35**, 925.

Elmasry, G., Kamruzzaman, M., Sun, D.-W. & Allen, P. (2012). Principles and applications of hyperspectral imaging in quality evaluation of agro-food products: a review. *Critical reviews in food science and nutrition*, **52**, 999-1023.

ElMasry, G. & Sun, D.-W. (2010). Principles of hyperspectral imaging technology. In: *Hyperspectral Imaging for Food Quality Analysis and Control* (edited by S. Professor Da-Wen). Pp. 3-43. San Diego: Academic Press.

Enari, T.M. & Sopanen, T. (1986). Mobilisation of endopsermal reserves during the germination of barley. *Journal of Institute of Brewing*, **92**, 25-31.

Fang, J. & Chu, C. (2008). Abscisic acid and the pre-harvest sprouting in cereals. *Plant signaling & behavior*, **3**, 1046.

Fincher, G.B. (1989). Molecular and cellular biology associated with endosperm mobilization in germinating cereal grains. *Annual Review of Plant Physiology and Plant Molecular Biology*, **40**, 305-346.

Francis, P.J. & Wills, B.J. (1999). Introduction to principal components analysis. *Astrophysics*, **2**, 363-372.

Geladi, P. (2003). Chemometrics in spectroscopy. part 1: classical chemometrics. *Spectrochimica Acta Part B*, **58**, 767-782.

Gowen, A., O'Donnell, C., Taghizadeh, M., Cullen, P., Frias, J. & Downey, G. (2008). Hyperspectral imaging combined with principal component analysis for bruise damage detection on white mushrooms (Agaricus bisporus). *Journal of chemometrics*, **22**, 259-267.

Groos, C., Gay, G., Perretant, M.-R., Gervais, L., Bernard, M., Dedryver, F. & Charmet, G. (2002). Study of the relationship between pre-harvest sprouting and grain color by quantitative trait loci analysis in a white and red grain bread-wheat cross. *Theoretical and Applied Genetics*, **104**, 39-47.

Huang, H., Liu, L. & Ngadi, M.O. (2014). Recent developments in hyperspectral imaging for assessment of food quality and safety. *Sensors*, **14**, 7248-7276.

Huang, T., Qu, B., Li, H.-P., Zuo, D.-Y., Zhao, Z.-X. & Liao, Y.-C. (2012). A maize viviparous 1 gene increases seed dormancy and preharvest sprouting tolerance in transgenic wheat. *Journal of Cereal Science*, **55**, 166-173.

Kadziola, A., Abe, J.-i., Svensson, B. & Haser, R. (1994). Crystal and molecular structure of barleyα-amylase. . *Journal of Molecular Biology,*, **239**, 104-121.

Kruger, J. (1994). Enzymes of sprouted wheat and their possible technological significance. In: *Wheat: production, properties and quality* (edited by W. Bushuk & V.F. Rasper). Pp. 143-153. US: Springer.

Lim, K.S. & Barigou, M. (2004). X-ray micro-computed tomography of cellular food products. Food Research International, 37, 1001-1012.

Luypaert, J., Heuerding, S., Heyden, Y.V. & Massart, D. (2004). The effect of preprocessing methods in reducing interfering variability from near-infrared measurements of creams. *Journal of pharmaceutical and biomedical analysis*, **36**, 495-503.

Maleki, M., Mouazen, A., Ramon, H. & De Baerdemaeker, J. (2007). Multiplicative scatter correction during on-line measurement with near infrared spectroscopy. *Biosystems Engineering*, **96**, 427-433.

Manley, M., Williams, P., Nilsson, D. & Geladi, P. (2009). Near infrared hyperspectral imaging for the evaluation of endosperm texture in whole yellow maize (Zea maize L.) kernels. *Journal of Agricultural and Food Chemistry*, **57**, 8761-8769.

Mares, D. & Mrva, K. (2008). Late-maturity α-amylase: Low falling number in wheat in the absence of preharvest sprouting. *Journal of Cereal Science*, **47**, 6-17.

McGoverin, C. & Manley, M. (2012). Classification of maize kernel hardness using near infrared hyperspectral imaging. *Journal of Near Infrared Spectroscopy*, **20**, 529-535.

McGoverin, C.M., Engelbrecht, P., Geladi, P. & Manley, M. (2011). Characterisation of non-viable whole barley, wheat and sorghum grains using near-infrared hyperspectral data and chemometrics. *Analytical and Bioanalytical Chemistry*, 1-7.

Mestres, C., Matencio, F. & Louis-Alexandre, A. (1995). Mechanical behavior of corn kernels: development of a laboratory friability test that can predict milling behavior. *Cereal chemistry*, **72**, 652-657.

Mitsuhashi, W. & Oaks, A. (1994). Development of endopeptidase activities in maize (Zea mays L.) endosperms. *Plant Physiology*, **104**, 401-407.

Mohan, A. (2008). Pre-harvest sprouting in cereals: a global scenario. *Current Science*, **94**, 704-705.

Moot, D.J. & Every, D. (1990). A comparison of bread baking, falling number, α-amylase assay and visual method for the assessment of pre-harvest sprouting in wheat. *Journal of Cereal Science*, **11**, 225-234.

O'Kennedy, K. (2011). Characterisation of zein from South African maize of varying endosperm texture. MSc in Food Science, University of Stellenbosch: Stellenbosch.

Ranal, M.A. & Santana, D.G.d. (2006). How and why to measure the germination process? *RevistaBrasileira de Botânica*, **29**, 1-11.

Ritchie, S., Swanson, S.J. & Gilroy, S. (2000). Physiology of the aleuron layer and starchy endosperm during grain development and early seedling growth: new insights from cell and molecular biology. *Seed science research*, **10**, 193-212.

Rodionova, O.Y., Houmøller, L.P., Pomerantsev, A.L., Geladi, P., Burger, J., Dorofeyev, V.L. & Arzamatsev, A.P. (2005). NIR spectrometry for counterfeit drug detection: a feasability study. *Analytica Chimica Acta*, **549**, 151-158.

Shephard, G.S., van der Westhuizen, L., Gatyeni, P.M., Somdyala, N.I.M., Burger, H.M. & Marasas, W.F.O. (2005). Fumonisin mycotoxins in traditional Xhosa maize beer in South Africa. *Journal of Agricultural and Food Chemistry*, **53**, 9634-9637.

Smail, V.W., Fritz, A.K. & Wetzel, D.L. (2006). Chemical imaging of intact seeds with NIR focal plane array assists plant breeding. *Vibrational spectroscopy*, **42**, 215-221.

Srivastava, L.M. (2002). Seed Development and Maturation. In: *Plant Growth and Development*. Pp. 431-446. San Diego: Academic Press.

Wang, X.F., Jing, X.M. & Lin, J. (2005). Starch mobilization in ultradried seed of maize (Zea mays L.) during germination. *Journal of Integrative Plant Biology*, **47**, 443-451.

Watson, S.A. (1987). Structure and composition. In: *Corn: chemistry and technology* (edited by S.A. Watson & P.E. Ramstad). Pp. 53-82. St. Paul, MN: American Association of Cereal Chemists. Inc.

Williams, P., Geladi, P., Fox, G. & Manley, M. (2009). Maize kernel hardness classification by near infrared (NIR) hyperspectral imaging and multivariate data analysis. *Analytica Chimica Acta*, **653**, 121-130.

Williams, P.J. (2009). Near infrared (NIR) hyperspectral imaging for evaluation of whole maize kernels: chemometrics for exploration and classification. Stellenbosch: University of Stellenbosch.

Williams, P.J., Geladi, P., Britz, T.J. & Manley, M. (2012). Investigation of fungal development in maize kernels using NIR hyperspectral imaging and multivariate data analysis. *Journal of Cereal Science*, **55**, 272-278.

Wold, S., Esbensen, K. & Geladi, P. (1987). Principal component analysis. *Chemometrics and Intelligent Laboratory Systems*, **2**, 37-52.

Woonton, B., Jacobsen, J., Sherkat, F. & Stuart, I. (2005). Changes in germination and malting quality during storage of barley. *Journal of the Institute of Brewing*, **111**, 33-41.

Chapter 4

Evaluation of the effect of pre-germination on whole maize kernels and kernel hardness using X-ray micro-computed tomography (X-ray µCT)

Abstract

Endosperm microstructure is an agglomerate of starch and protein molecules which has been shown to be related to maize kernel hardness. During the pre-germination process, starch and protein molecules are utilised for seedling development. The aim of this study was to investigate the effect of pre-germination (0, 10 and 22 h) on maize kernel hardness using X-ray micro computed tomography (X-ray µCT). A total of 36 maize kernels from different hardness categories were scanned during this study. Maize anatomical parts could be distinguished on 2D greyscale image slices and inadequate filled endosperm appeared as black regions. Radicle elongation in the germ area in maize kernels pre-germinated for 10 and 22 h was noticeable mainly on maize hybrids of soft and intermediate hardness. Hard and intermediate maize hybrids seemed to have experienced more starch deterioration than the soft hybrids in the 10 and 22 h pre-germinated samples. Starch deterioration was noted in the form of fissures caused by pre-germination and shrinkage cracks due to the drying process. Scanning electron microscopy (SEM) was used to validate the presence of fissures and shrinkage cracks within the endosperm. A real-time experiment validated endosperm deterioration that took place within pre-germinated maize kernels with fissures developing from 21 h of pre-germination till 143 h when the radicle protruded. The fissures propagated and shrinkage cracks also developed after the single kernels were freeze dried. Pre-germination effects should be of great concern to the dry milling industry because crevices that develop increase undesirable breakage during the milling process leading to decreased yields of desired particle size.

Introduction

Germination is an essential growth process in nature as it ensures the survival of the maize crop (Fincher, 1989). It starts with the imbibition of water by the maize kernel and ends with the protrusion of the radicle (Subedi & Bhattarai, 2003; Mei & Song, 2008; Nonogaki *et al.*, 2010). The pre-germination process takes place in three phases: Imbibition and activation, intra-seminal

growth and embryo/radicle protrusion (Labouriau & Osborn, 1984; Bewley, 1997; Gallardo *et al.*, 2002; Finch-Savage & Leubner-Metzger, 2006). The anatomical parts involved are the aleurone layer situated on the peripheral area of the kernel and the scutellar epithelium situated on the interface of the embryo and endosperm (Harvey & Oaks, 1974; Fincher, 1989; Nonogaki *et al.*, 2010).

During germination, the maize kernel's endosperm microstructure is broken down to provide food for the growing embryo (Subedi & Bhattarai, 2003; Sánchez-Linares *et al.*, 2012). Endosperm comprised an agglomerate of macromolecules called polysaccharides (that make up the starch granules) as well as polypeptides (that make up the protein bodies found in the protein matrix) which have been related to maize kernel hardness (Falcone *et al.*, 2006; Gaytán-Martínez *et al.*, 2006; Narváez-González *et al.*, 2006; Li *et al.*, 2007). The process of endosperm stored material being broken down to simple components is called mobilisation (Subedi & Bhattarai, 2003; Sánchez- Linares *et al.*, 2012).

Pre-germination is the untimely germination of mature maize kernels that have been subjected to wet or humid conditions prior to the harvest period (Smail *et al.*, 2006). Scanning electron microscopy (SEM) has been employed to investigate the starch and protein molecules (Fannon *et al.*, 1992; Gallant *et al.*, 1997; Huber & BeMiller, 2000; Sujika & Jamroz, 2007) in the pursuit of linking maize kernel hardness to starch and protein morphology. SEM images are based on the interaction between electrons emitted by the electron gun and the sample material being analysed. SEM has also been used to investigate the morphology of starch granules attacked by the alpha-amylase (Sujika & Jamroz, 2007).

The effect of the germination process on cereal grains such as wheat has been investigated by a few researchers in the past. Tkachuk *et al.* (1991) indicated germinated wheat grains decreased in density in relation to sound wheat grains using specific gravity tables. Martin *et al.* (1998) used a micropycnometer to relate the volume of the liquid displaced by the wheat grain to the density of the wheat grain, indicating germinated grains decreased in density. In a study conducted by Neethirajan *et al.* (2007) germinated wheat kernels were investigated using soft X-rays found between 1 – 100 nm on the electromagnetic spectrum. The focus part of the wheat kernel during their study was the endosperm due to its relation to kernel hardness. X-ray images of Neethirajan *et al.* (2007) illustrated the endosperm region of the germinated wheat grain appeared lighter when compared to sound kernels, indicating loss of density. They also observed white specks on the germinated wheat kernels which was attributed to endosperm degradation by the α-amylase enzyme.

X-ray technology is fast becoming the most preferred technique for the study of food products due to the X-ray's ability to acquire the microstructure of the sample material and depict the results in the form of 2D and 3D images (Zwiggelaar *et al.*, 1996; Barcelon *et al.*, 1999; Falcone *et al.*, 2004; Falcone *et al.*, 2005; Babin *et al.*, 2006; Falcone *et al.*, 2006; Babin *et al.*, 2007; Dogan, 2007; Mendoza *et al.*, 2007; Haff & Toyofuku, 2008; Laverse *et al.*, 2012; Williams, 2013). X-ray micro computed tomography (µCT) is a miniaturised version of the medical computed axial tomography. The difference between the µCT and the medical axial tomography is that the spatial resolution of the µCT is in the micrometer region and the sample rotates around its axis instead of the detector and X-ray tube rotating (Landis & Keane, 2010; Santos Garcés, 2012). During sample rotation, shadow images called radiographic projections are obtained from all angular rotations (Sasov & van Dyck, 1998). The 2D images are then reconstructed for the production of 3D reconstructed virtual representations of the imaged sample, comprising 2D slice images or 3D renderings.

An interpretation of an X-ray CT image can be done based on attenuation of the X-rays photons interacting with the material of the object being studied (Dyck, 1998; Bouxsein *et al.*, 2010) and on a grey colour scale, with white colour indicating areas of high density (i.e. high attenuation) and black colour indicating air spaces (no attenuation) (Sasov & van Dyck, 1998; Lim & Barigou, 2004; Landis & Keane, 2010).

Using greyscale 3D reconstructed volume images and threshold attenuation restrictions, different types of endosperm could be isolated and their volumes measured (Gustin *et al.*, 2013). The segmentation was done in the following manner; on the greyscale images the germ appeared white proving to be of higher density than the rest of the kernel and air spaces appeared black. This meant that they could be segmented from the rest of the virtual image with the help of the X-ray µCT dedicated software tools, leaving only the vitreous and floury endosperm. Kernel density significantly correlated with bulk density ($r=0.80$) proving single kernel measure of density with the help of X-ray µCT a viable technique (Gustin *et al.*, 2013).

Based on the penetration abilities and success of X-ray µCT technique in analysis of various food products, the aim of this study was to investigate the microstructure of pre-germinated maize kernels at various pre-determined incubation time periods. The results were validated using SEM. Real-time lapse scans were performed to correlate features observed and record various pre- germination stages (i.e. intra-seminal growth and radicle protrusion).

Materials and Methods

Pre-germination at 30°C

Sample

The sample set for this study was made up of six white hybrid maize samples, i.e. two hard (H2 and H3), two intermediate (H6 and H7) and two soft (H5 and H9) hardness categories. The maize samples were categorised by experienced breeders from PANNAR (PANNAR Seed, Greytown, South Africa) and pre-germinated for 0 h (control), 10 h (middle of process and point of significant difference as per Chapter 3) and 22 h (radicle protrusion (Fig 4.1)

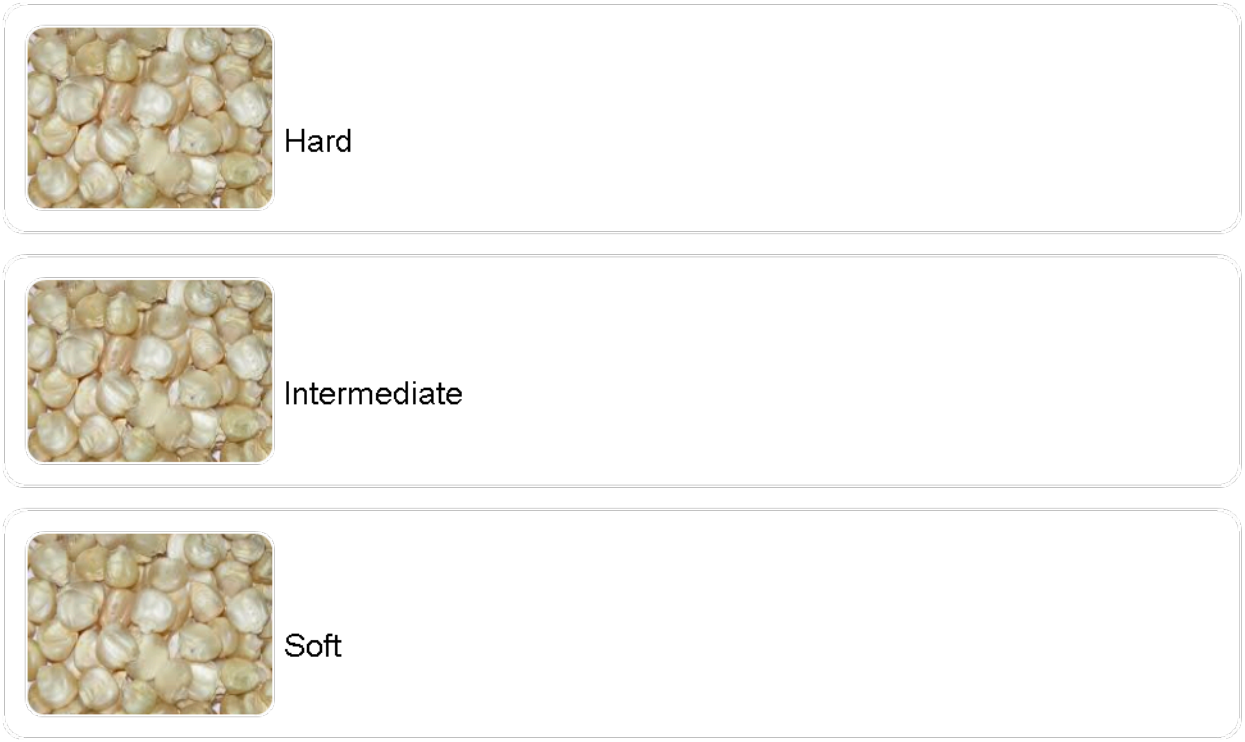

Figure 4.1. Three hardness categories were included in this study to illustrate the effect of pre-germination on the different kernel hardnesses.

Sample preparation

An imaging session involved scanning three kernels from different incubation time periods stacked on top of each other on a rod with a known density (Fig. 4.2). The control kernel (0 h) was placed at the bottom, followed by a 10 h kernel and lastly on top was the 22 h kernel.

X-ray µCT

A General Electric Phoenix model V|Tome|X L240, micro focus system (General Electric Sensing and Inspection Technologies / Phoenix X-ray, Wunstorff, Germany) from the Central Analytical Facility (CAF), Stellenbosch University (Stellenbosch, South Africa) was used (Fig. 4.2 b). The Phoenix Datos|x 2, software package (General Electric Sensing and Inspection Technologies / Phoenix X-ray, Wunstorff, Germany) was used for data acquisition and image reconstruction. The Phoenix Datos|x 2 software is a fully automated software package integrated within the X-ray system and uses programmed algorithms to perform reconstruction from the projection data acquired (Park *et al.* (2003).

The following settings were used: 160 kV, 70 µA for X-ray generation using the nano tube with a Tungsten target (transmission type). Image acquisition was performed at 500 ms and 11.8 µm scan resolution per image. A total of 2000 image projections were recorded during one rotation of 360°. There was no averaging or skipping of images and a full scan took approximately 25 min. Prior to the scanning process taking place, the CT scanner had to be calibrated to account for background information to be removed from sample information on the projection images during the reconstruction process. To calibrate the instrument, scanning had to take place without the sample being in the X-ray unit. Once the initial calibration scan had taken place, the kernels on the rod were then placed on a turn table that rotated till 360 degrees.

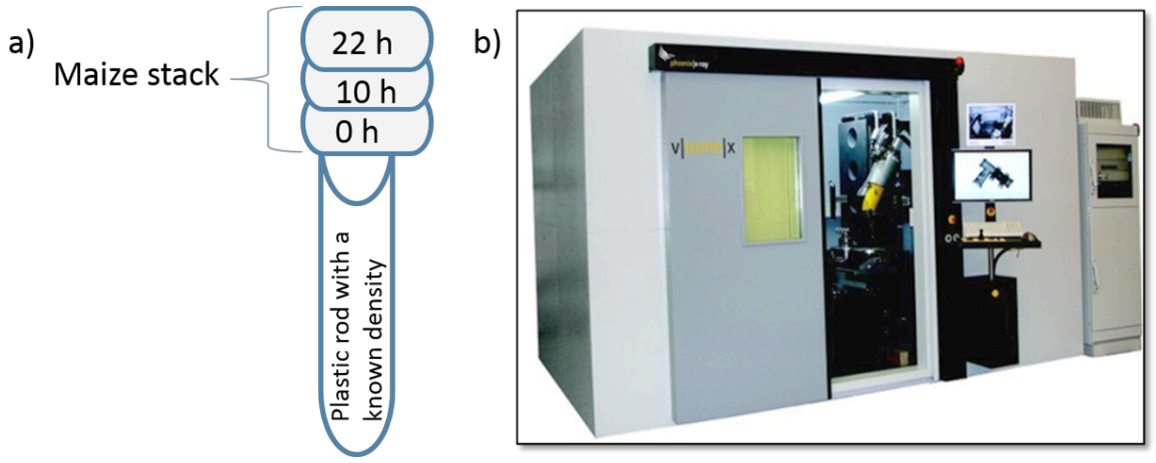

Figure 4.2. a) Depiction of the imaged maize sample arrangement. b) A General Electric Phoenix model V|Tome|X L240, micro focus system used for acquiring X-ray images.

Image processing

From 0° to 360°, numerous of 2D image projections were gathered, fed into a computer (with Phoenix Datos|x 2 software installed) and used for the reconstruction of 3D volumes depicting the internal microstructure of the maize kernels. The Phoenix Datos|x 2 reconstruction algorithms, using a modified filtered back projection algorithm (Park *et al.* (2003) allowed for the reconstruction to take place in the form of a set of flat cross sections. The cross sections contain voxel information of grey values on a 16-bit grey scale (0-65536 grey values). Scan optimisation and beam hardening correction was set at 3.5. At the end of the automated reconstruction process, 3D virtual images (also called 3D volumes) of the samples and 2D CT image slices were obtained and used for analysis.

Image analysis

Images were segmented to remove background noise and further analysis (2D slice images and 3D volumes) was performed using the Volume Graphics VGStudio Max 2.1 software package (Volume Graphics GmbH, Heidelberg, Germany). The Volume Graphics VGStudio Max 2.1 software allowed for simultaneous analysis of greyscale 3D volumes and greyscale 2D image slices (Fig. 4.3) from various orientations (top, front and side). To minimise artefacts caused by the instrument and smooth the images, a Gaussian filter was used on a 5 x 5 x 5 voxel range.

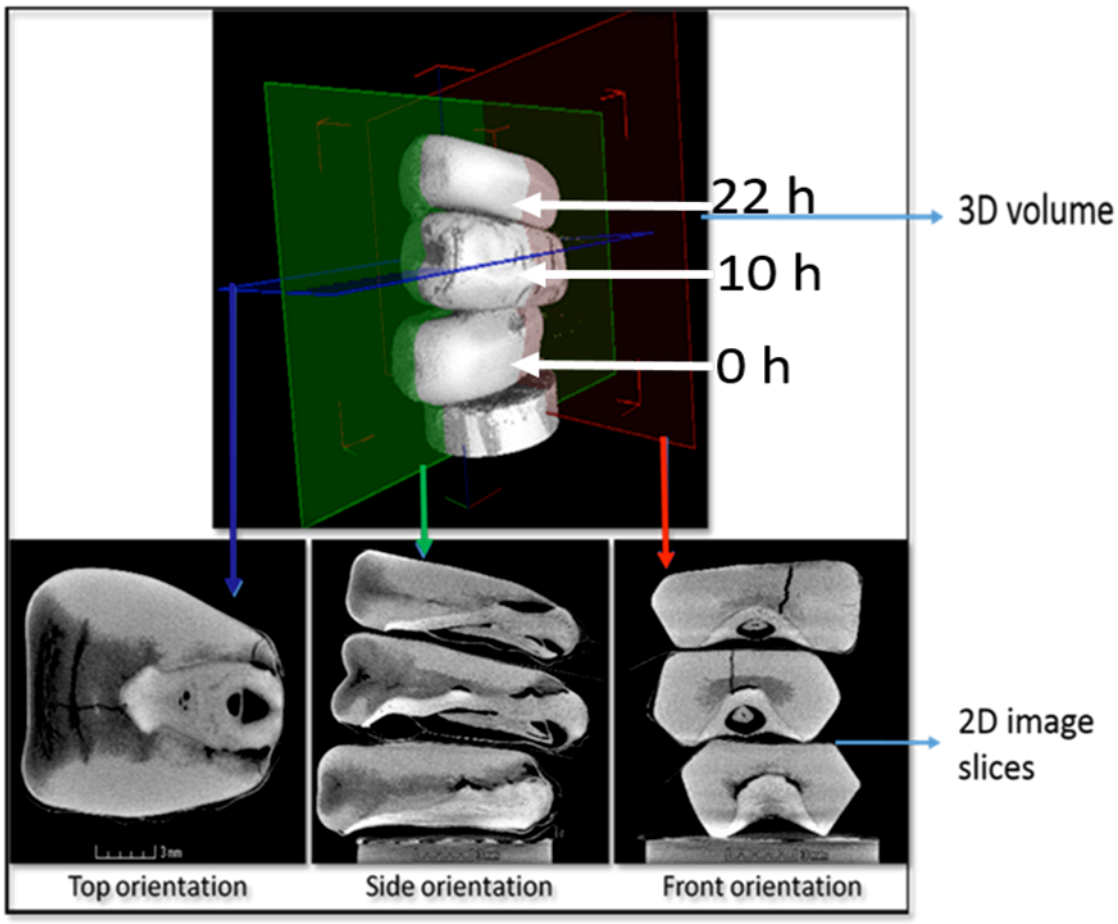

Figure 4.3. 3D reconstructed volume image of 3 stacked imaged maize kernels, the kernel at the bottom of the pile is the 0 h kernel, followed by the 10 h kernel. The kernel on top of the pile is the 22 h kernel, indicated using the white arrows. 2D image slices were obtained from various orientations, i.e. top orientation obtained from the blue block area in the 10 h kernel indicated by the blue arrow; side orientation obtained from the green block of all three kernels indicated with the green arrow and front orientation obtained from the red block of all three kernels indicated with the red arrow.

Scanning electron microscopy

Maize kernels were cut vertically (approximately yielding two equal parts) and sputter coated with gold. Imaging took place using a Leo® 1430VP Scanning Electron Microscope (Zeiss, Germany) instrument. Beam conditions during the imaging process were 7.00 KV, 3pA, working distance of 8 mm and a spot size of 112 µm.

Pre-germination at 19°C (Real-time scanning)

Sample preparation

White maize kernels of the hard and intermediate category were utilised for this study. The experiment was performed at 19°C, which is the constant temperature kept in the X-ray housing cabinet. A single maize kernel was placed inside a sample holder with wet cotton wool placed at the bottom to provide humidity for the pre-germination process (Fig. 4.4). The sample holder was sealed to ensure that the humidity environment created was kept constant. The maize kernel was scanned every 3 h from 0 to143 h (point at which the radicle protruded),

without removing the kernel from the sample holder. X-ray scanning conditions were similar to those utilised for the 30°C pre-germination process along with the image processing conditions. Immediately after 143 h, the single kernels were freeze dried similar to the 30°C samples' drying conditions.

Image analysis

Analysis of 2D slice images and 3D volumes was performed using analysis tools in Volume Graphics VGStudio Max 2.1 software (Volume Graphics GmbH, Heidelberg, Germany). Images were segmented to remove background noise, sample holder and wet cotton wool information. Segmentation of just the maize kernel allowed for optimum analysis of the maize kernel. Fissure measurement was performed at various time periods. The percentages (%) of the vitreous endosperm were also recorded at 5 various time intervals (Table 4.1).

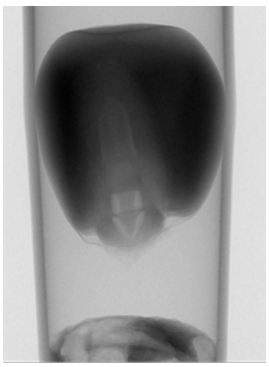

Figure. 4.4. A shadow projection of the scanned maize kernel in a sample holder and a wet cotton wool at the bottom of the kernel, generated by the X-ray CT scanner.

Table 4.1 A measure of the % vitreous endosperm volume of various time series

Time period
T1 = 0 h
T6 = 15 h
T12 = 75 h
T15 = 123 h
T19 = 143 h

The time periods selected for analysis were based on the following; T1 is the beginning of the incubation time period while T19 is the extreme. T12 is mid-way between 0 and 143 h, T6 is mid-way scan between 0 h and 75 h and T15 is the scan between 75 h and 143 h.

Results and discussions

Pre-germination at 30°C

Using 2D slice images, various anatomical parts of the maize kernel could be easily identified (Fig. 4.5) due to their attenuation coefficient variation. An attenuation coefficient is defined as the quantity that describes the ease with which an X-ray beam can penetrate through sample material (Sasov & van Dyck, 1998). The ease of penetration is dependent on the material's density. The relation between density and attenuation coefficient lies in the interaction between the X-rays and sample matter. X-ray photons emitted from the X-ray tube interact with various atoms within the sample causing the photons to lose energy while passing through the sample (Santos Garcés, 2012). The decrease in the energy experienced by the X-ray photons is attributed to the atomic number, thickness and density of the sample matter. The higher the atomic number, thickness and density, the more attenuated the X-ray photons will be.

Due to the knowledge that energy is not lost, the sample material's atoms interacting with the X-ray photons become excited and emit energy. The scintillator found in the X-ray detector re-emits the energy from the atoms in the form of light and the X-ray photons then become attenuated (i.e weakened). Areas with high attenuation within the sample are therefore registered as bright areas (i.e. areas of high density due to the energy transfer between the X-ray photons and sample atoms) whereas those with low attenuation are registered as dark areas (Cnudde & Boone, 2013).

Black areas were also observed in the crown area and several other regions of the 2D maize kernel slice image (Fig. 4.5). An assumption was made that the black areas developed due to inadequate grain filling, therefore there was no matter to attenuate the X-rays. Heat stress during maize development can interfere with endosperm starch biosynthesis (Singletary *et al.*, 1994). Grain filling takes place after the differentiation of the aleurone and starchy endosperm cells. The maize kernel is filled in the form of storage products (i.e. starch and protein) accumulated from glucose and amino acids (Wilson, 1997). Andronescu (1919), Jones and Brenner (1987) and Sabelli and Larkins (2009), explained the starch filling process in detail. The possibility of the black areas also being due to imaging artefacts could also not be omitted.

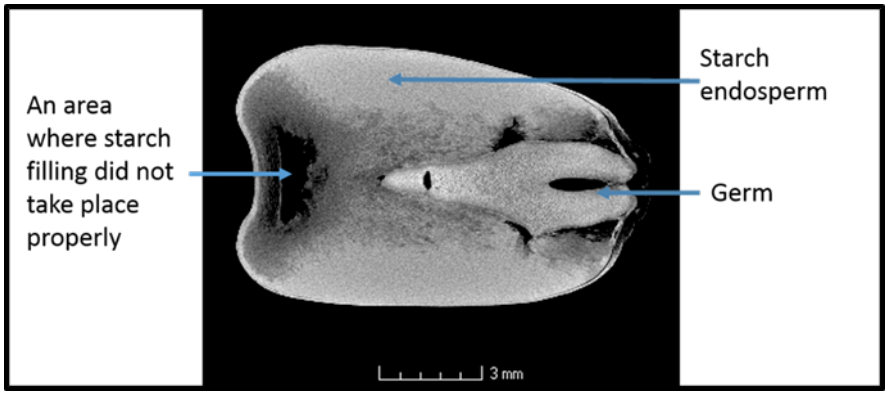

Figure 4.5. 2D slices taken approximately from the middle of a non-germinated 3D virtual maize kernel to illustrate the kernel's various anatomical parts.

Based on the knowledge of the location of the various endosperm types, both the vitreous and floury endosperms could be visualised (Fig. 4.6). The vitreous endosperm appeared lighter while the floury endosperm appeared darker, indicating the vitreous endosperm was made up of material of higher density than the floury endosperm. The random selection of maize kernels from the three pre-determined hardness categories validated that the maize kernels were correctly classified (Fig. 4.6). The separation of the three maize hardness categories are based on the ratio of the two types of endosperm present within the maize kernel, hard hybrid maize kernels comprise more vitreous endosperm than the floury endosperm (Fig. 4.6). The soft hybrid maize kernels comprise more of the floury than the vitreous endosperm and the intermediate hybrid maize kernels comprised of what is believed to be approximately equal amounts of each endosperm type. Again areas of inadequate starch filling or imaging artefacts were observed in Fig. 4.6 and were circled in yellow.

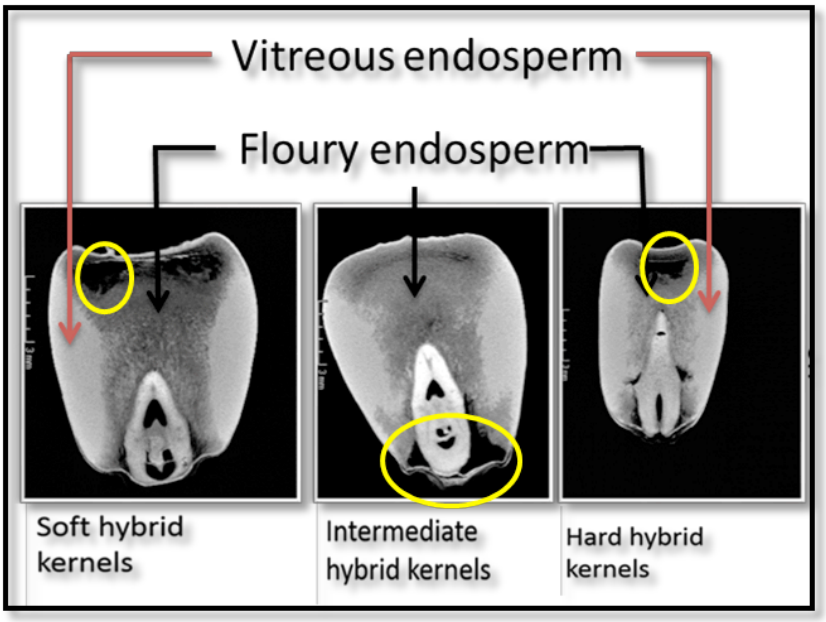

Figure 4.6. 2D slice image indicating various anatomical parts of maize kernels of various hardness levels, with the different endosperm types indicated. The yellow circles are deemed to be areas of inadequate starch filling during endosperm development.

When analysing X-ray side orientation 2D slice images (Fig. 4.7), the germ appeared to be losing its brightness which could be translated into loss of density. Germ morphological changes were evident after 10 h of incubation. At the 10 h interval, the radicle seemed to have grown but had not extended to the exterior of the kernel. The germ also seemed to have developed "black spots" that could be translated into loss of attenuation, indicating the germ could have developed a porous structure. These “black spots” were more prominent in the soft hybrid kernels and they indicated there was no matter for the X-ray photons to react with at those particular areas. The last phase of the germination process is called the embryo protrusion which was seen 22 h after the incubation period (Fig. 4.7) and was again more prominent in the soft hybrid kernels (Fig. 4.7).

Empty spaces depicted in the form of “black holes or empty spaces” could also be observed in the intermediate and soft maize hybrid (Fig. 4.7). The observations were made in kernels incubated for 10 and 22 h maize samples of the intermediate and soft hybrid, in the vitreous and floury endosperm area (Fig. 4.7). These are areas where loss of endosperm content could have taken place leading to decreased endosperm yields and perhaps loss of endosperm hardness because during pre-germination starch and protein molecules (contents of the endosperm) are broken down (Fincher, 1989).

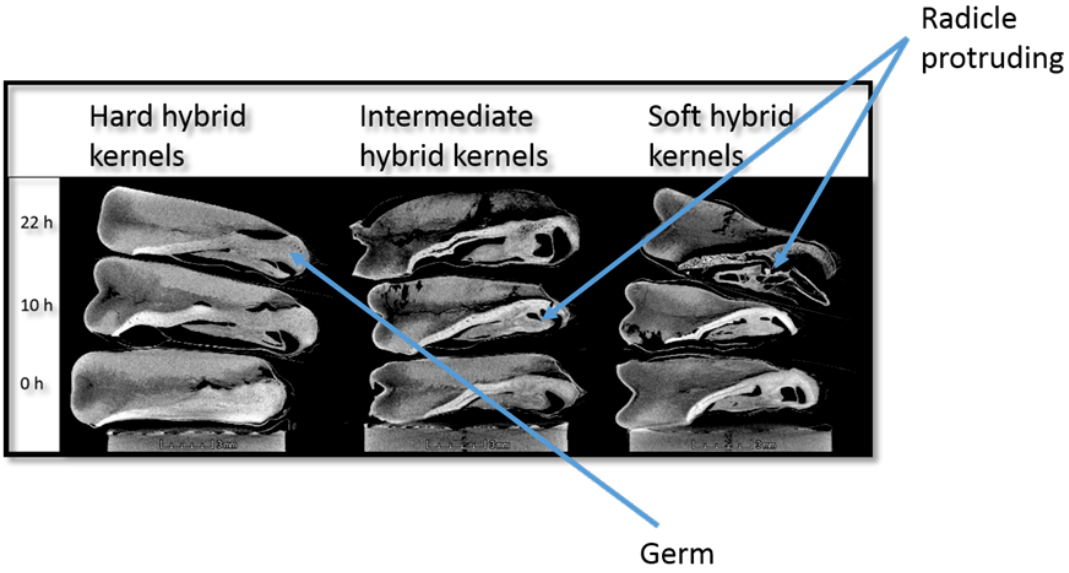

Figure 4.7. 2D slices of maize kernels obtained from the side orientation indicating the intra-seminal growth phase where the germ undergoes transformation after 10 h and 22 h of incubation period within the hard, intermediate and soft hybrid kernels. Loss of endosperm content depicted as black empty spaces

Endosperm deterioration could be observed in all hybrids pre-germinated for 10 and 22 h (Fig.4.8a). Voids above the germ area could also be seen (Fig. 4.8a). Crevices that could either be explained as shrinkage cracks caused by the drying process or fissures due to pre-germination, were evident in the endosperm area of the maize kernels incubated for 10 and 22 h (Fig. 4.8a). Shrinkage cracks differ from fissures as shrinkage cracks (caused by moisture loss) originate from the surface of the maize kernel and propagate towards the inner part of the maize kernel (De Carvalho *et al.*,1999). Similar to shrinkage cracks, the fissures could increase the susceptibility of the maize kernels to unwanted kernel breakage during the mechanical handling, increase microbial contamination and lower yields of the desired dry milling particle sizes (Davidson *et al.*, 2000). Therefore some of the crevices observed in Figure 4.8a, could be due to the loss of moisture during the drying of the kernel and some could be fissures caused by the pre-germination process. The preferred moisture content of the maize kernel at harvest is below 12% (Song & Litchfield, 1994), therefore maize kernels harvested at high moisture levels (due to high humidity conditions during harvest) are subjected to drying meaning the germinated kernels' integrity would further be compromised in terms of kernel hardness. Similar results were obtained for all hybrids if similar hardness.

SEM images validated the presence of the crevices (Fig. 4.8b) and increased magnification into the SEM images indicated starch granule deterioration (Fig. 4.8c).

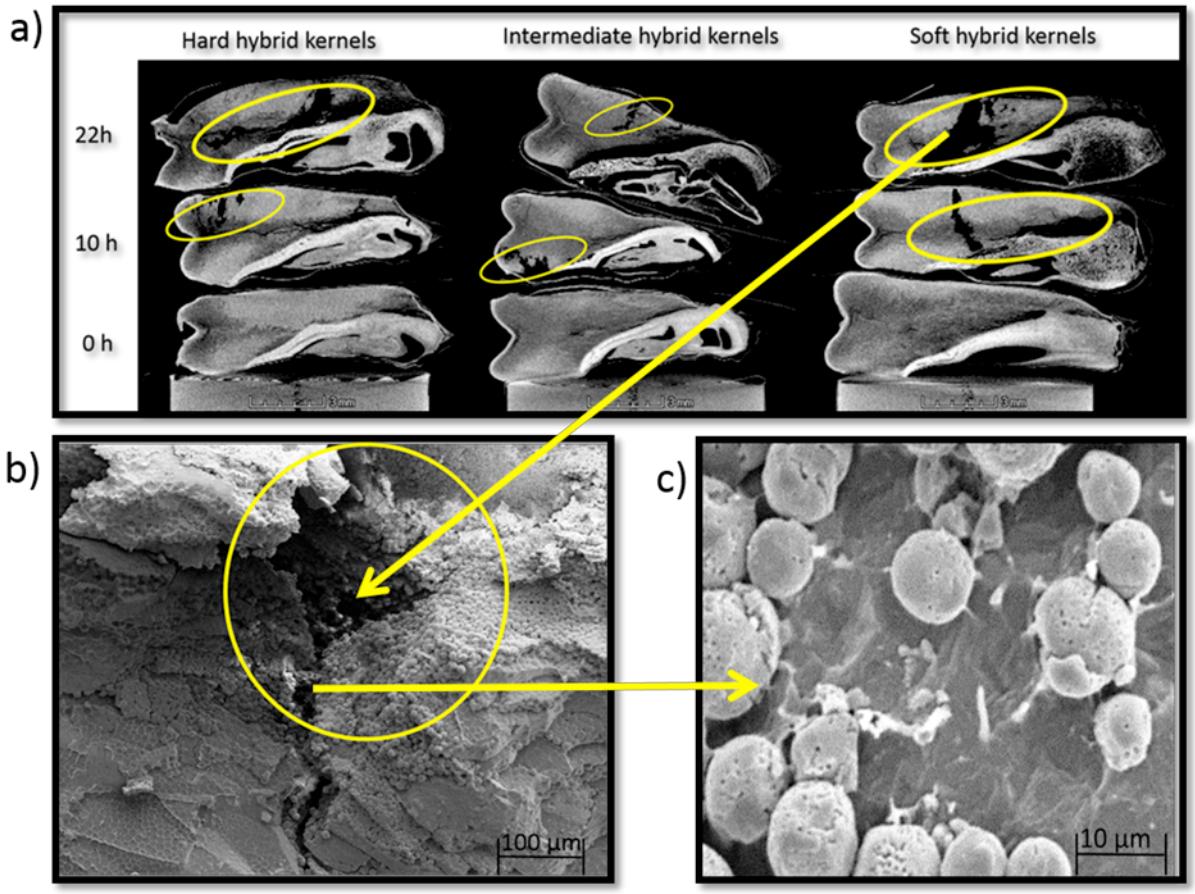

Figure 4.8. a) 2D image slices of the various hardness levels maize kernels at various incubation time periods, indicating endosperm degradation of the maize kernels circled in yellow. The circled areas are voids created during the germination process and they appear black because there was no endosperm material for the X-ray photons to interact with. b) A SEM image illustrating and validating the fissures and a void observed in the 2D image slice of the 22 h soft hybrid maize kernel. c) A SEM image illustrating the deterioration of the granules inside voids of the 22 h soft hybrid maize kernel.

Top orientation of the 2D slices exhibited that crevices took place in a plane formation, spreading throughout the maize kernels (Fig. 4.9). Hard and intermediate maize hybrids seemed to have developed more crevices compared to the soft maize hybrids. The 10 and 22 h maize kernels of the hard and intermediate hybrid kernels developed crevices within the endosperm area and an empty space was observed within the soft endosperm area of the 22 h maize kernel belonging to the hard maize sample.

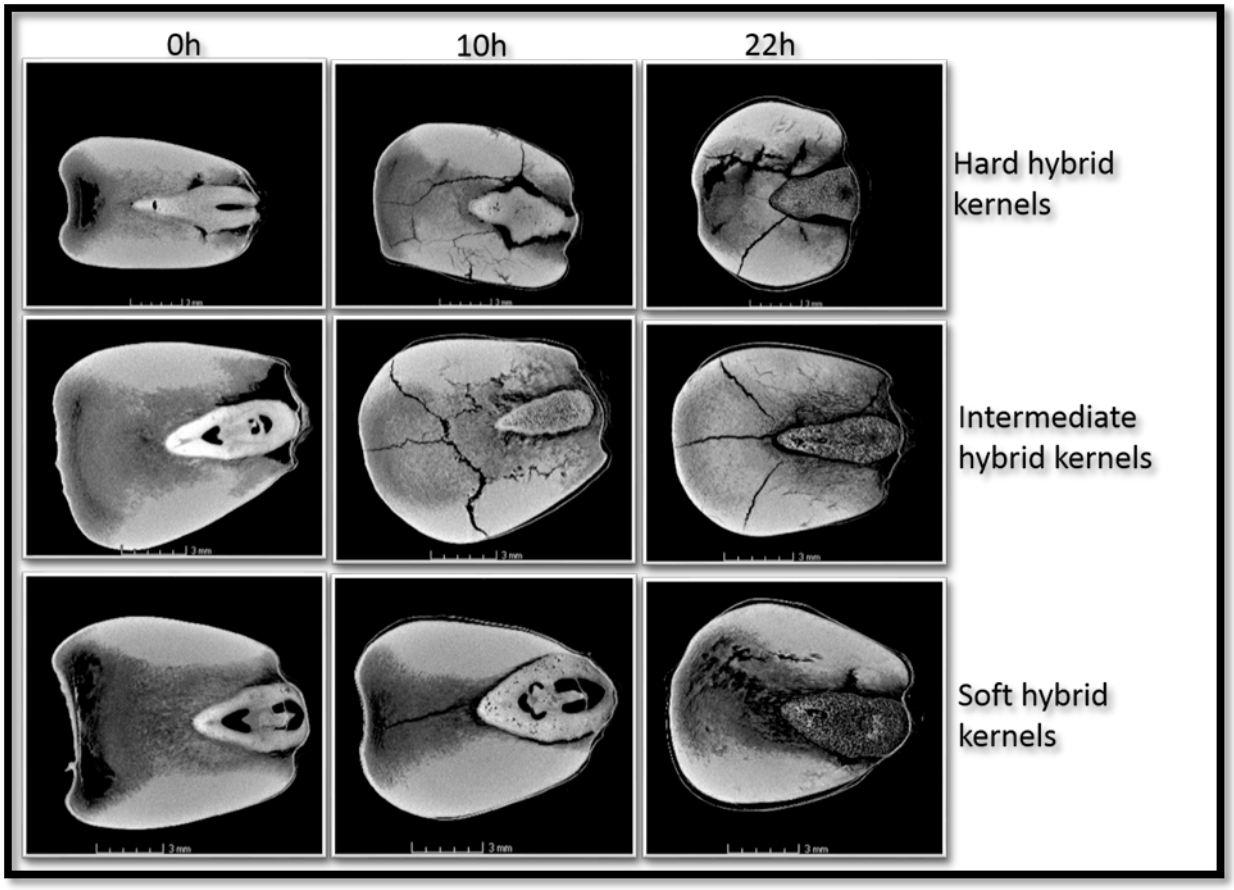

Figure 4.9. 2D slice images of the hard, intermediate and soft kernels at 0, 10 and 22 h germination time period illustrating the changes that took place within a maize kernel and could be related to negative implication on maize kernel hardness. These 2D image slices were obtained from the top orientation.

Front orientation 2D slices indicated crevices developed in the centre of the maize kernels were perpendicular to the germ (Fig. 4.10). Another crevice was seen on a cube sectioned 3D volume at the interface of the germ and floury endosperm (coloured in yellow), with parts of the floury endosperm located below the crevice. This revelation further indicated the destruction of the endosperm during the pre-germination process.

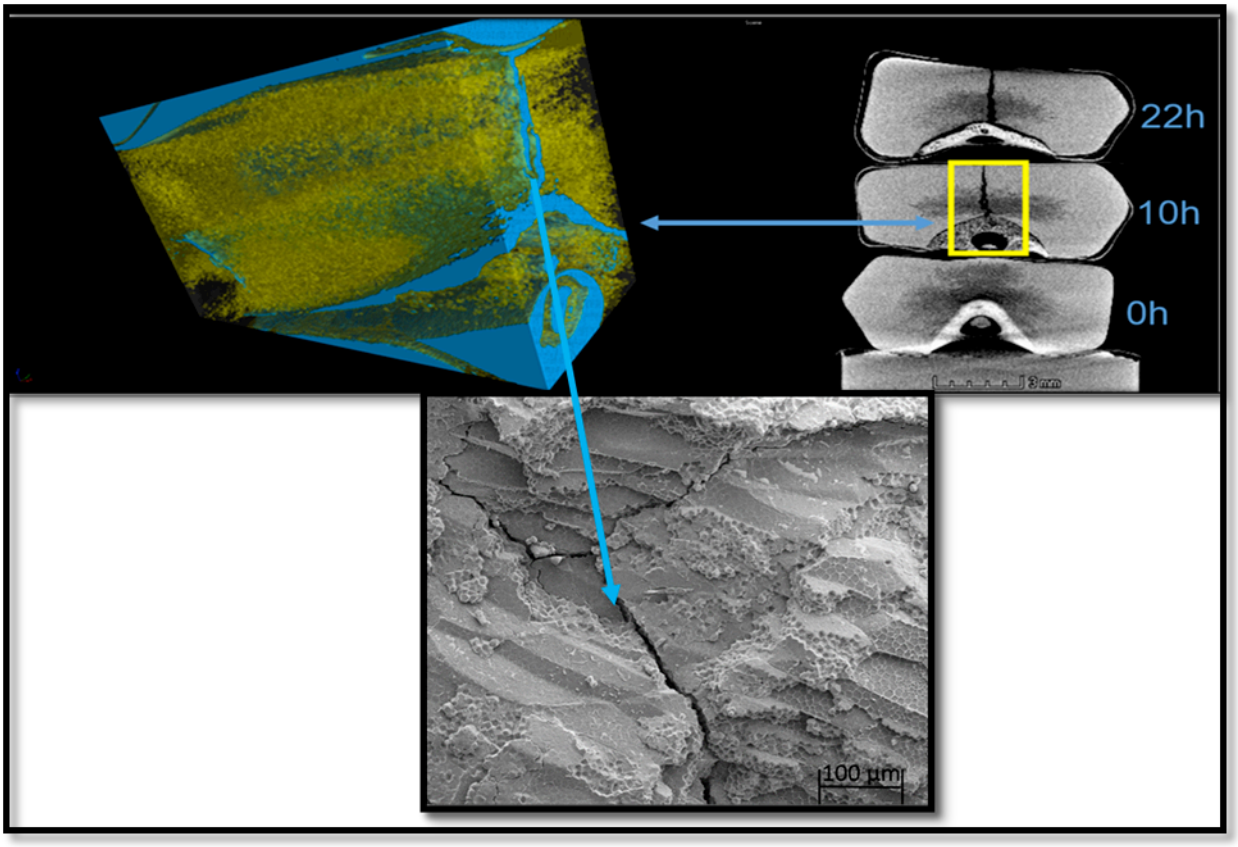

Figure 4.10. An enlarged void from the intermediate maize kernel hybrid incubated for 10 h. The blue areas indicate crevice while the yellow parts indicate the less dense material, i.e. floury endosperm. SEM image located at the bottom validates the presence of the crevice.

Higher magnifications of the SEM images revealed the 0 h starch granules of the hard, intermediate and soft maize hybrids were sound and intact (Fig. 4.11a). The 10 h maize kernels of all the hybrids shown in Figure 4.11a, also appeared to be sound. At 22 h maize kernel hybrids, the starch granules showed morphological changes in the form of apertures developing around the starch granules. The apertures formed are believed to be the hydrolytic act of the pre-germination process. A 22 h SEM image of a soft maize hybrid kernel, showed degradation of the protein matrix in the form of apertures (Fig. 4.11b). The apertures were believed to have occurred as a result of proteolytic enzymes. Starch and protein molecules arrangement have been related to maize kernel hardness (Watson, 1987; Fincher, 1989; Fox & Manley, 2009; Williams *et al.*, 2009), therefore any form of starch and/or protein deterioration taking place will have a negative impact on kernel hardness.

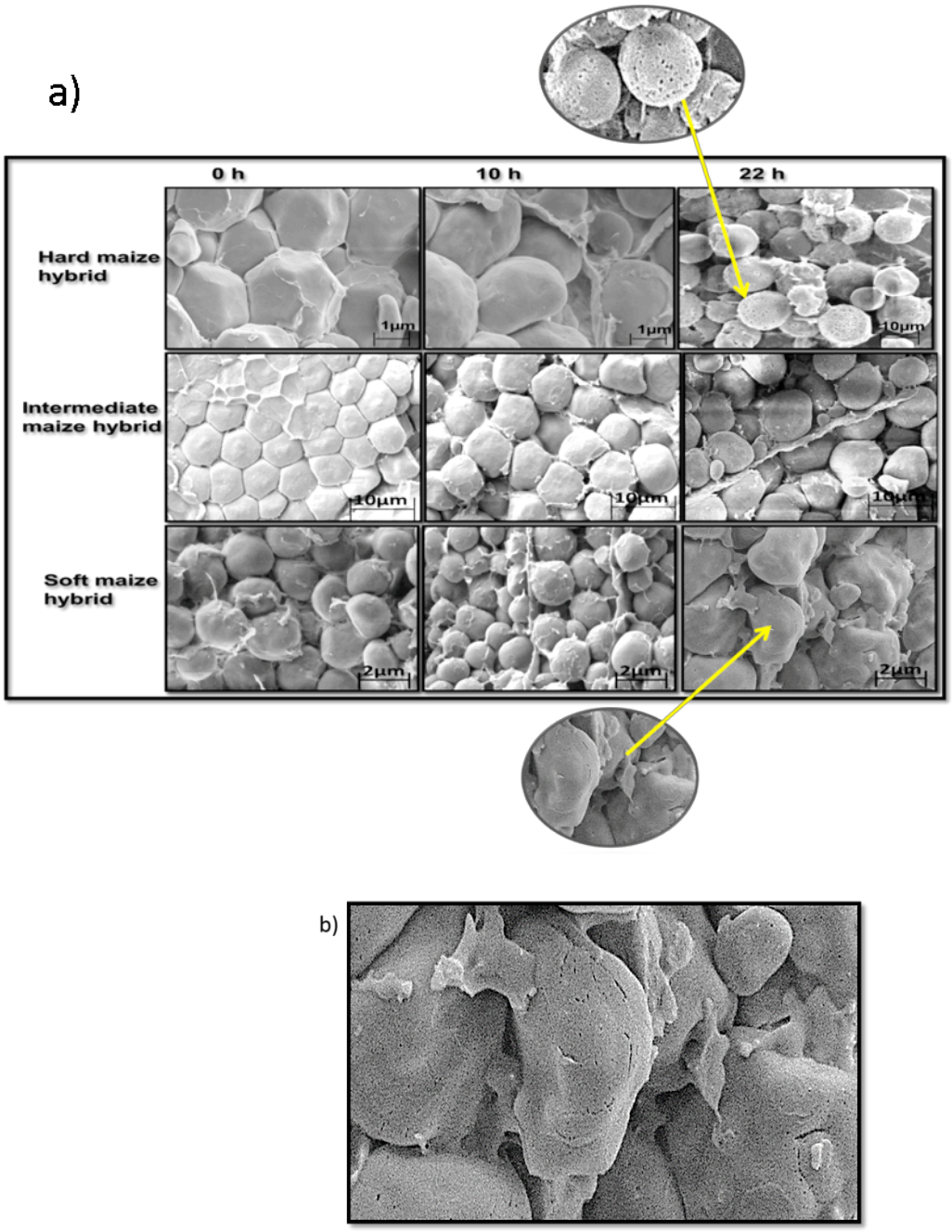

Figure 4.11. a) SEM image comparison of various hybrids (hard, intermediate and soft) at various incubation time periods (0, 10 and 22 h) illustrating the morphological changes that the starch granules undergoes during the germination process. b) A SEM image illustrating what seems to be degradation of the protein matrix at 22 h maize kernel of the soft hybrid.

More apertures were observed on the surface of the 0 h hard hybrid floury starch granule (Fig.4.12a). These sort of pin size apertures have been previously observed and reported as surface pores (Fannon *et al.*, 1992; Gallant *et al.*, 1997; Huber & BeMiller, 1997; Huber & BeMiller, 2000). The pores are believed to be the point of entry for the hydrolytic enzymes such as α-amylase, released during the germination process. Alpha-amylase is known to be the most abundant type of hydrolytic enzyme released during the germination process (Dure, 1960). It is the first enzyme to catalyse the crystalline structure of the starch granules, making visible the α(1→6) glycosidic bonds to be catalised by other hydrolytic enzymes such as the iso-amylase or pullulanase. The alpha- amylase is an endo-acting enzyme, i.e. it breaks the α(1→4) glycosidic bonds of the starch granules (Oates, 1997; Tester *et al.*, 2006; Blazek & Gilbert, 2010; Shrestha *et al.*, 2012). When observing the SEM image of starch granules of the 22 h maize kernels from the same hard hybrid, the pores of the starch granules' become deeper to the point where the granules disintegrated (Fig. 4.12b). Hydrolysis of the starch granules subsequently decreases the molecular weight, leading to decreased maize kernel hardness.

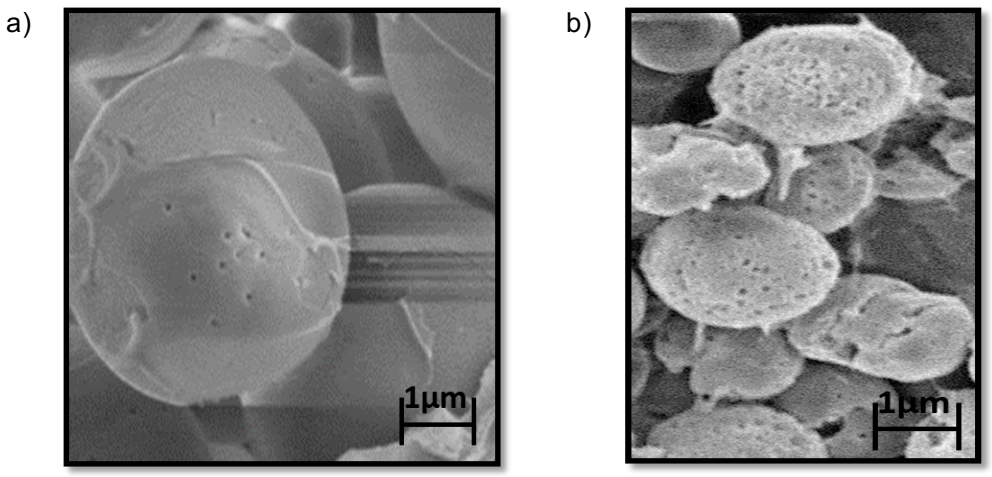

Figure 4.12. a) A SEM image of a 0 h hard hybrid maize kernel with pores on the surface of the floury starch granule. b) A SEM image of the same hard hybrid after 22 h of incubation indicating the effect of germination on the starch granules.

When investigating the front orientation 2D slices further, the global pre-germination process could be seen. This process is described in detail by Toole *et al.* (1956) and Bewley (1997). Observations on Figure 4.13 revealed void creation took place on the peripheral area of the kernel. The voids were evident in kernels that had been incubated for 10 and 22 h only and not in the 0 h kernels, indicating the kernels had indeed undergone the germination process. The aleurone layer

situated on the peripheral area of the maize kernel is made up of lipid and protein rich tissues that remain cellular and viable even during the quiescent stage of the kernel. Upon imbibition, the aleurone layer is stimulated by gibberellic acid generated from the embryo to use its lipids and protein tissues to synthesise and release digestive enzymes that mobilise the insoluble reserves of the starchy endosperm (Ritchie *et al.*, 2000). The endosperm top section below the aleurone layer is made up of a thick protein matrix and small starch granules. This layer is termed the subaleurone, which becomes hydrolysed by the digestive enzymes released by the aleurone layer (Fincher, 1989). The hydrolytic enzymes degrade the endosperm components into their simplest form so that they growing embryo can utilise the nutrients for growth. This would be seen as an explanation to voids created around the peripheral area, evident in all hybrids analysed during the study.

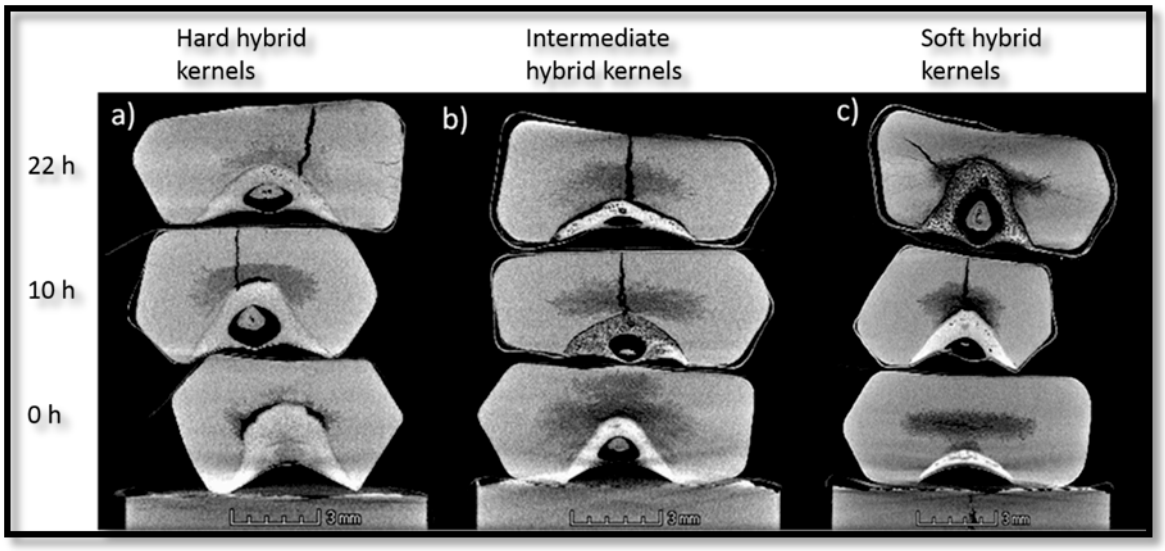

Figure 4.13. A 2D slice of; maize kernels indicating voids that have developed around the peripheral area of the 10 and 22 h maize kernels in all the various hybrids. These images are approximately middle slices viewed from the front orientation of the 3D volumes of the maize kernels.

Pre-germination at 19°C (Real-time scans)

The first set of results presented in figure 4.14 were from a hard maize hybrid pre-germinated for only 24 h. Large crevices were observed on 2D images (Fig. 4.14) and noted as fissures as opposed to shrinkage stress cracks because the maize kernel was not dried. It was then decided to repeat the experiment using a different maize kernel and scanning the sample every 3 h to determine the time period at which the fissures can be clearly seen to be developing. The rest of the results given in this section will be from the intermediate maize hybrid to illustrate changes that took place within the vitreous and floury endosperm of the

kernel. The intermediate hybrid kernel was chosen as it contains approximately equal amounts of the two types of endosperm.

Comparison between the 0 h slice images and 24 h slice images from all different orientations proved that endosperm deterioration in maize kernels could take place as early as 24 h.

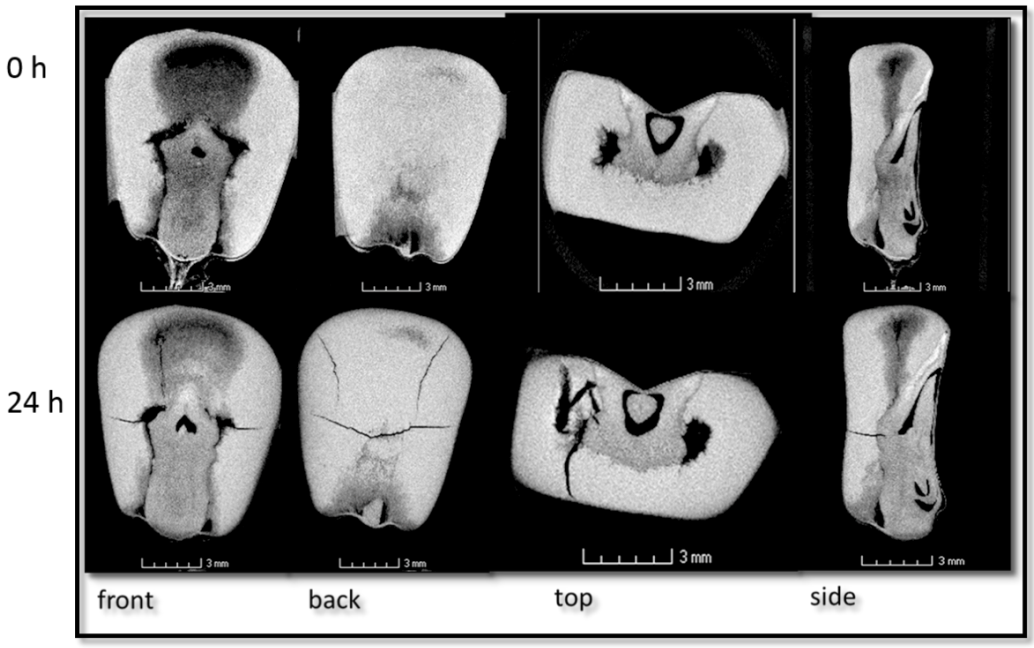

Figure. 4.14. 2D images obtained from all orientations (front, back, top and side of the kernel) used to depict changes that took place in the endosperm area of the pre-germinated maize kernel. The fissures were noticed 24 h in the pre-germination process. The kernel used was of a hard category. The top 4 images were obtained from T1 = 0h and the bottom 4 images were obtained from T9 = 24 h using the temperature of 19°C.

Figure 4.15 is made up of images taken from slice no. 425 of T1 = 0 h (not freeze dried) to T20 = freeze dried maize kernel. When observing 2D real-time slice images from the front orientation of the kernel (Fig 4.17), deterioration presented itself in the form of fissures. The fissures seem to be developing from the central area of the endosperm stretching to the peripheral area of the endosperm. Fissure development circled in turquoise could be observed from T8 = 21 h after the induced pre-germination process had initiated till T19 = 143 h, and are believed to be a pathway used for the transportation of the hydrolytic and proteolitic enzymes released by the scutellar epithelium layer and aleurone layer in order to degrade the endosperm (Labouriau & Osborn, 1984;
Bewley, 1997; Gallardo *et al.*, 2002; Finch-Savage & Leubner-Metzger, 2006). At T20 (freeze dried

kernel at the culmination of the pre-germination process) the fissures had expanded all over the maize sample. The spread of the fissures was believed to be due to either loss of moisture from the drying process (i.e. stress cracks) or could have been created but hidden by the swollen neighbouring polymers (i.e. starch) during water imbibition. Koster and van Dalen (2013) and Kidmose and Martens (1999) investigated the microstructural changes that take place in a carrots after blanching and freeze drying to prove that freeze drying causes minimal destruction to the microstructure of food products. They used freezing temperatures of -70 to -150°C similar to those used to perform this experiment (i.e. -80°C). Their results indicated minimal structural damage using SEM technique as well as µCT.

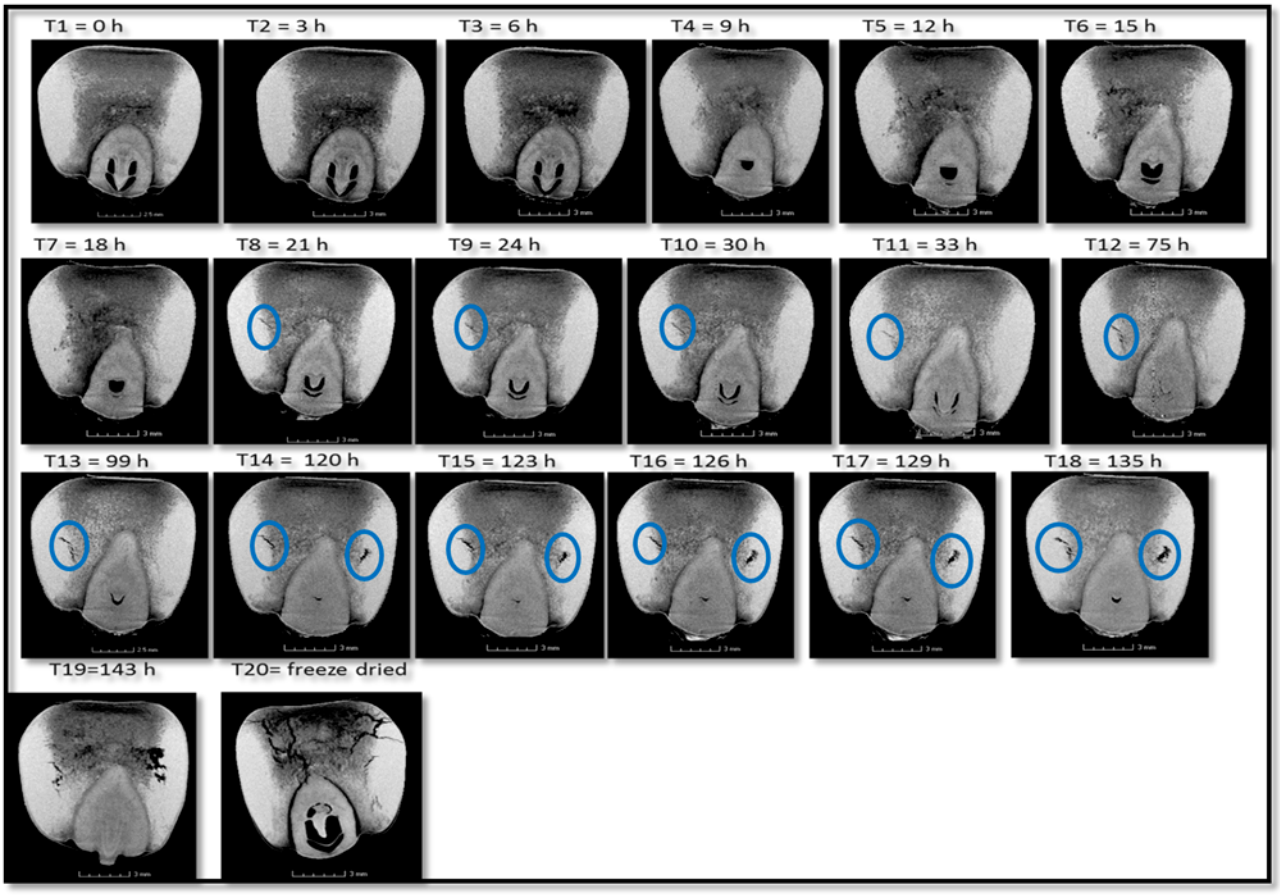

Figure. 4.15. 2D image obtained from front orientation of slice nr. 425, used to depict changes that took place in the endosperm area of the germinated maize kernel. T1 signaled the beginning of the process prior to any water imbibition, T8 was the point at which the fissures started to develop, while T 20 was the freeze dried kernel indicating the expansion of the fissures throughout the maize kernel. The maize sample was taken from the intermediate category.

A closer look at a 2D slice image obtained from the 3D volume image of T13 = 99 h (Fig.4.16a) revealed on the distal area, some form of layer separation believed to be a degraded subaleurone layer. The layer separation was more pronounced at the bottom part of the maize kernel (Fig. 4.16a) and was encircled in red, while the green rectangle on the 3D volume indicated the origin of the 2D slice image. Along the side of the maize kernel there is an attenuation contrast between the area where the vitreous endosperm is situated and the area where the subaleurone layer is situated. The subaleurone layer part seems to be darker indicating that the X-rays were attenuated less compared to the rest of vitreous endosperm. Loss of attenuation was related to loss of density due to the knowledge that attenuation variation relates to material density variation (Dyck, 1998; Cnudde *et al.*, 2006; Kalender, 2006). Virtual slicing of the T13 = 99 h maize kernel indicated fissures throughout the 3D volume (Fig. 4.16b).

a)

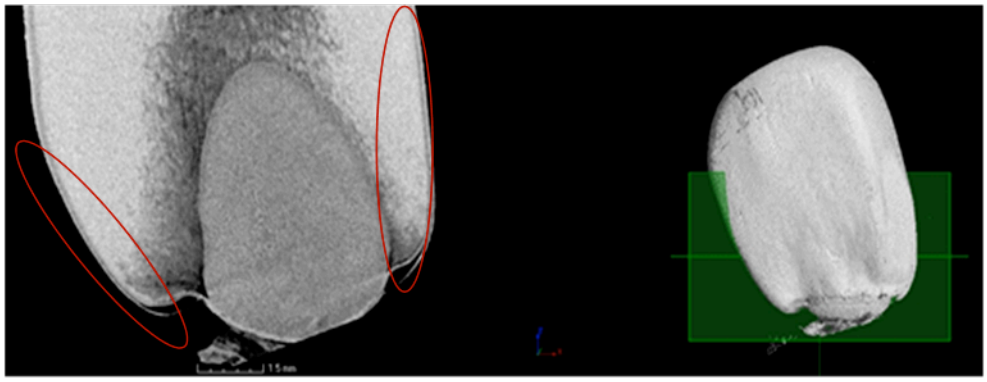

b)

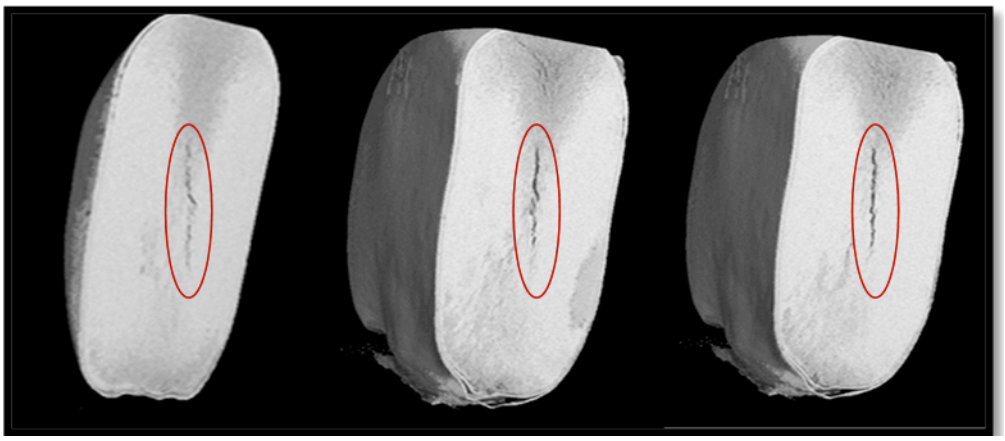

Figure. 4.16. a) 2D slice image and 3D maize kernel volume of the intermediate hybrid indicated layer separation that took place during the germination process at T13 = 99 h. The red circles on the 2D image slices indicate the layer separation while the green block on the 3D volume indicated the origin of the 2D image slice. b) 3D volumes of the same maize kernel being virtually clipped from the right to the left indicating that the fissures (indicated in red circles) that developed were on a plane field at T13 = 99 h.

Observing the front orientation T17 = 129 h 2D slice images, fissure location and indication of propagation could be depicted after every 11 or 22 slice images (Fig 4.17). Only six 2D image slices were used to illustrate the observations. At T18 = 135 h fissure propagation had increased and 2D slice image used to depict the observations is selected after every 15 slice images (i.e. from slice image nr. 336 – 351, the difference is 15 slice images. Lastly, at T19 = 143 h every second slice could be used to depict the severity of endosperm deterioration.

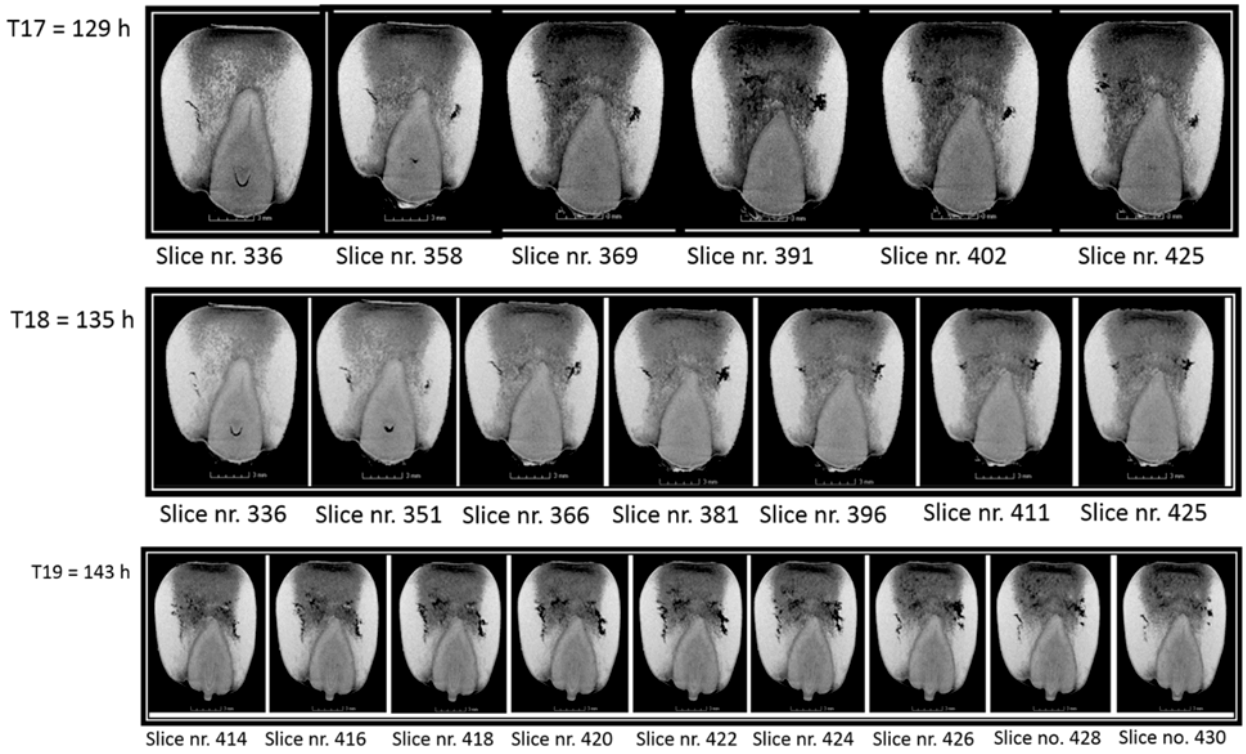

Figure. 4.17. 2D image obtained from front orientation of an intermediate hybrid, used to depict changes that took place in the endosperm area of the germinated maize kernel. T17 depicted the floury endosperm degradation that took place 129 h into the germination process, T18 showed degradation on both sides of the maize kernel endosperm, while T 19 was the extreme case.

Fissures developed were measured to track their progress over a period of time. The fissures seem to develop at a random manner and not in a particular order. However their origin seems to be closer to the germ area extending away from the germ. From T8 = 21 h to T12 = 75 h, the fissures were too small to measure. At T13 = 99 h the fissures appeared as parallel lines of 1.51 mm (left) and 1.86 mm (right) starting from the top of the green line ending at the bottom of it, for T15 = 123 h the measures were 3.93 mm (left), 1.62 mm (middle) and 3.29 mm (right). Lastly at T19 = 143 h the measure were 4.21 mm (left), 4.30 mm (middle) and 3.65 mm (right) (Fig 4.18).

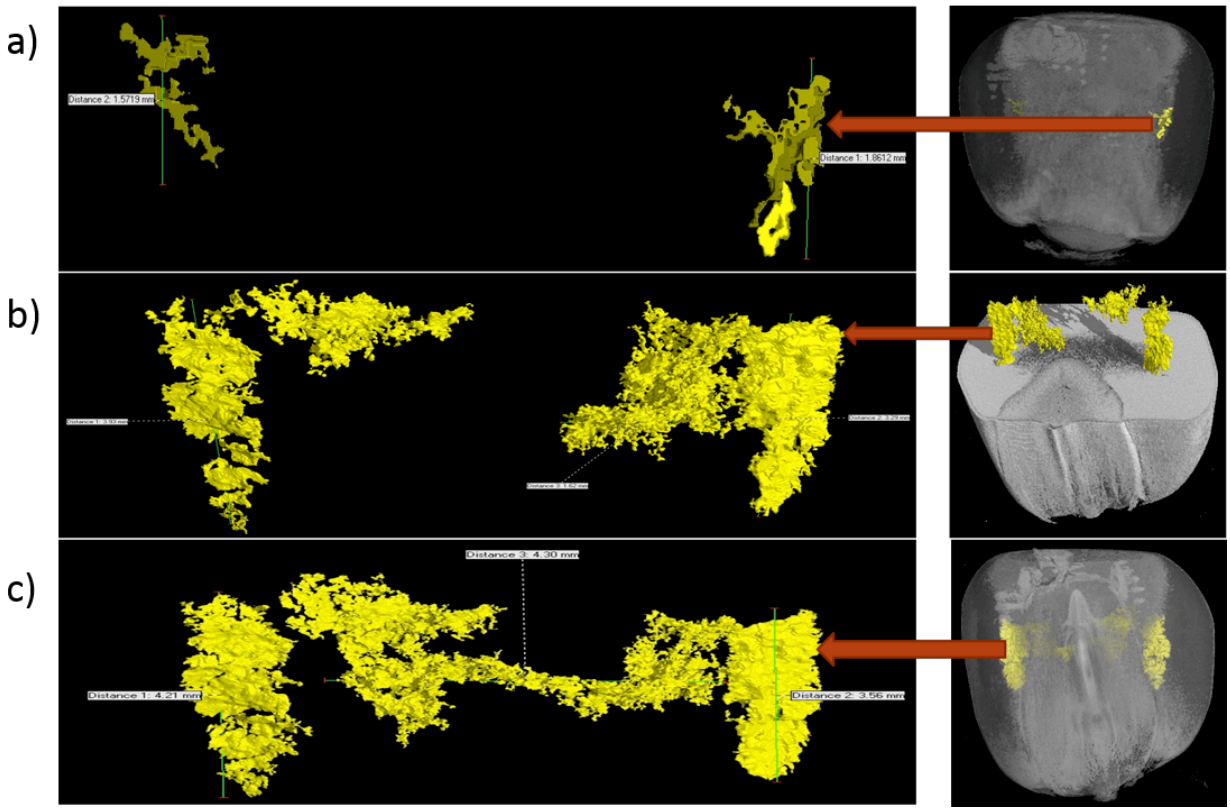

Figure. 4.18. a) At T13 = 99 h the fissures appeared as parallel lines of 1.51 mm (left) and 1.86 mm (right) starting from the top of the green line ending at the bottom of it with a corresponding 3D image to indicate where the fissures were virtually extracted from. The white material is the floury endosperm, b) T15 = 123 h with the measures as 3.93 mm (left), 1.62 mm (middle) and 3.29 mm (right) along with a virtually sliced 3D volume to indicate where the fissures were extracted. c) T19 = 143 h the measure were 4.21 mm (left), 4.30 mm (middle) and 3.65 mm (right) along with a 3D volume of a swollen maize kernel with a protruding radicle. (The white blocks on the image were in actual fact the measurements of the fissures, however they could not appear clear enough on the image.

The results from the measuring of the vitreous endosperm volume indicated that as germination process progressed, the maize kernel experienced a decrease in the volume attributed to the vitreous endosperm (Table 4.2) due to endosperm hydrolysis.

Table 4.2 A measure of the % vitreous endosperm volume of various time series

Time period	% vitreous endosperm volume
T1 = 0 h	64.70
T6 = 15 h	63.15
T12 = 75 h	58.70
T15 = 123 h	52.57
T19 = 143 h	50.46

Similarities could be observed between the freeze dried hard maize kernel hybrids incubated at 30°C as well as the slow process (19°C) of real-time scanning (Fig. 4.19).

The middle sample slice image (10 h maize sample) of the 30°C pre-germination process, depicted a massive fissure from the peripheral area of the kernel towards the germ, while the 19°C one appeared to be smaller in size. This indicted the drying process caused shrinkage cracks in the 30°C pre-germination process.

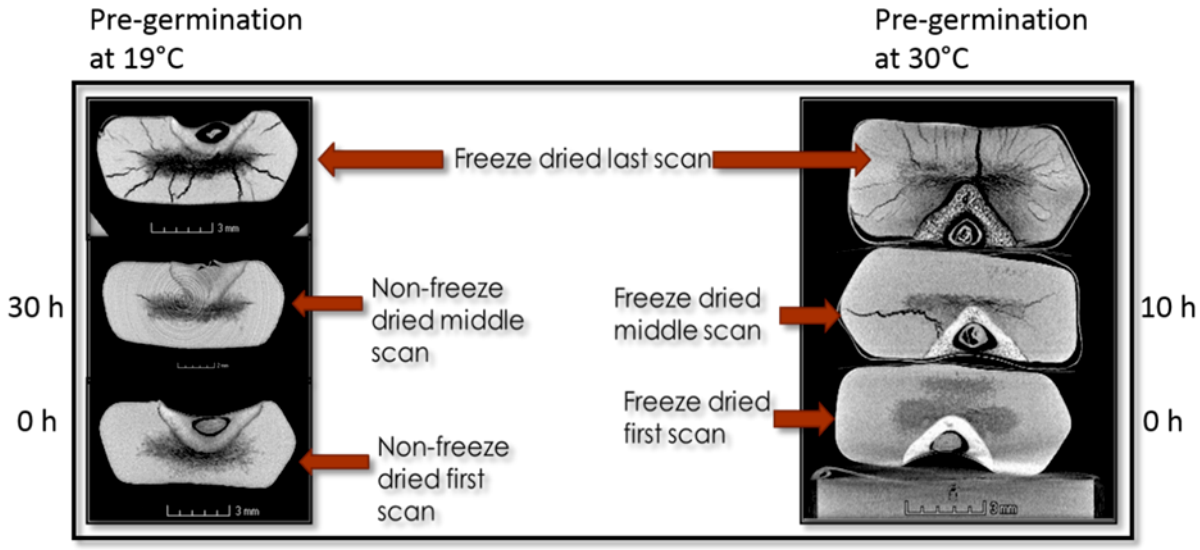

Figure. 4.19. 2D image obtained from front orientation, used to depict changes that took place in the endosperm area of the germinated maize kernel. T1 and 0 h signaled the beginning of the process prior to any water imbibition, T8 was the point at which the fissures started to develop in the non-freeze dried sample and 10 h depicted fissures that took place during the middle of the preset pre-germination time period, and T 20 and 22 h were the freeze dried kernel indicating the expansion of the fissures throughout the maize kernel, once the pre-germination process had culminated.

Comparison of an X-ray image and SEM image validated the germ's porous structure and radicle elongation (Fig. 4.20a and b). Sánchez-Linares *et al.* (2012) investigated the germination process of a maize kernel destructively and compared germ properties between the various incubation time periods (Fig. 4.20c). The investigation of this phase was based on the radicle elongation supported by the sucrose depletion using the sucrose staining method (indicated by the black arrows in the figure). The germ utilised the sucrose from the scutellum and diminished the sucrose after 8 h of incubation (Sánchez-Linares *et al.*, 2012). After 8 h sucrose stains increased again indicating the presence of sucrose from the hydrolysation of the endosperm. The results obtained from this non-destructive study were similar to those observed destructively by Sánchez- Linares *et al.* (2012), proving the non-destructive capabilities of X-ray.

Radicle elongation takes place with the help of plasmodesmata (i.e. channels that connect plant cells, allowing the exchange of nutrients and signals responsible for plant growth and development to take place) (Cilia & Jackson,2004; Wang *et al.*, 2005). Radicle plasmodesmata plays a vital role in radicle growth.

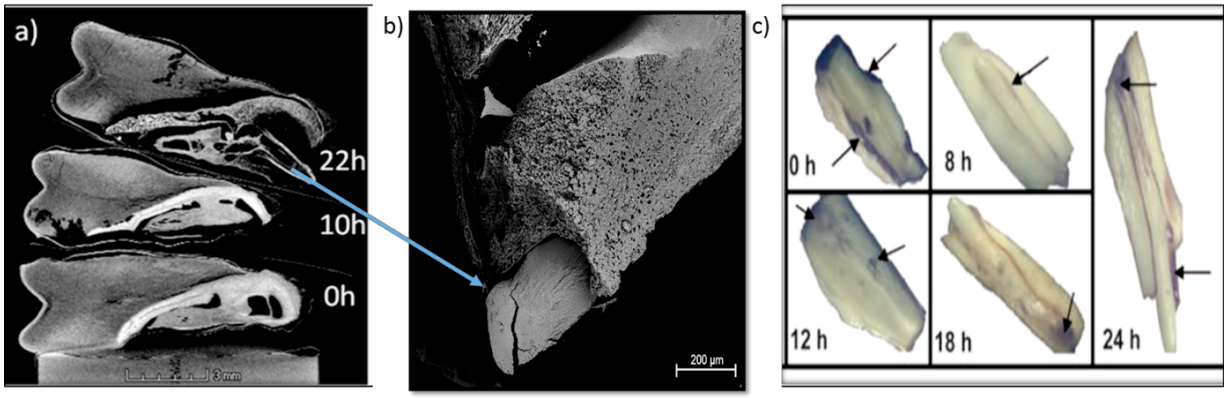

Figure 4.20. a) 2D slices of a maize kernel indicating the intra-seminal growth phase where the germ undergoes transformation after 10 h and 22 h of incubation; b) SEM image validating the germ's porous structure that developed after 22 h incubation time and radicle protrusion, c) morphological changes of the germ, evident after 8 h of incubation, the black arrows indicate the sucrose stains as an indication of the hydolysation of the starchy endosperm. The stains decrease in intensity after 8 h but increase again from 12 h till 24 h of incubation indicating that the sucrose must have come from the hydrolysation of the endosperm Image (b) was modified from (Sánchez-Linares *et al.*, 2012).

What could only be explained as a new plant was observed in one of the 22 h intermediate hybrid stacks (Fig. 4.21). A hypothesis was then made that the maize kernel was dormant. Dormant maize kernels are able to undergo pre-germination, however the embryo of a dormant kernel is constrained by its surrounding structures (Bewley, 1997). This means that the radicle will not protrude through the seed coat to signal the end of the pre-germination process. Hormones that regulate seed dormancy have been reviewed (Kucera *et al.*, 2005 : invited review),however information on new plant development in dormant seeds could not be obtained.

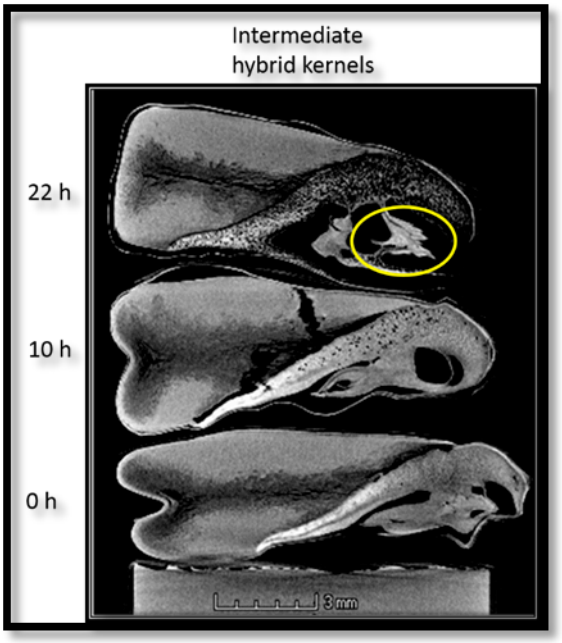

Figure 4.21. 2D slices of maize kernels obtained from the side orientation indicating what is thought to be a new plant developing, circled in yellow in the 22 h incubated maize kernel from the intermediate hybrid kernels

Conclusion

The various anatomical parts of the maize kernel were clearly observed from the 2D image slices due to attenuation coefficient variation including the areas where inadequate starch filling took place. Germ morphological changes in the form of radicle growth could be clearly noticed on the 2D slice images throughout the pre-germination process. Radicle elongation was evident after 10 h of maize kernel incubation and protrusion noticed after 22 h of maize kernel incubation. Another morphological variation noticed in the germ was the attenuation variation that took place between the 0, 10 and 22 h pre-germinated maize kernels. As the pre-germination time period increased, the germ lost its density indicated by the loss of attenuation (the germ appeared darker). What seemed like a development of a new seedling could be observed on various maize kernels incubated for 22 h and subaleurone layer deterioration could be visualised and validated using real-time scanning slice images.

Endosperm degradation was evident at the germ interface in 10 and 22 h maize kernel 2D image slices. All 3 orientations (front, side and top) indicated crevices developed throughout the floury and vitreous endosperm, with the hard and intermediate maize hybrids proving to be more susceptible to endosperm deterioration during pre-germination as opposed to soft hybrids. Endosperm deterioration was depicted in the form of attenuation variation where degraded areas appeared as dark areas on the 2D slice images. The loss of attenuation indicated loss of density which indirectly showed loss of hardness for the 10 and 22 h pre-geminated kernels. SEM images validated endosperm deterioration in the 10 and 22 h

pre-germinated maize kernels in the form of starch and protein matrix degradation. Apertures present on 0 h maize kernels assisted with the breakdown of starch granules and protein matrix observed in 10 and 22 h samples, by allowing hydrolysing enzymes entry to these macromolecules.

Crevices developed in the endosperm were more due to fissures as opposed to the shrinkage cracks. Real-time X-ray scans validate the formation of fissures during pre-germination prior to the drying process. Fissure development in the hard maize hybrid was noticed 24 h after pre- germination began while in the intermediate hybrid, the fissures were noticed at T8 = 21 h 2D slice images. This indicated that hard maize kernel deteriorate more rapidly in the endosperm than the intermediate hybrid. Observations made on the T19 = 143 h 2D slice image depicted radicle protrusion and higher endosperm deterioration. Fissure measurement at T13, 15 and 19 indicated development starting first as parallel lines and a mid-section horizontal one developing as pre- germination progresses. While fissure development increased, vitreous endosperm volume decreased.

With the help of the real-time experiment conducted, the results obtained from the freeze dried samples could be verified. The crevices that develop increase the chances of undesired breakage taking place during the milling process.

References

Andronescu, D.I. (1919). Germination and further development of the embryo of Zea mays separated from the endosperm. *American Journal of Botany*, **6**, 443-452.

Babin, P., Della Valle, G., Chiron, H., Cloetens, P., Hoszowska, J., Pernot, P., Réguerre, A., Salvo, L. & Dendievel, R. (2006). Fast X-ray tomography analysis of bubble growth and foam setting during breadmaking. *Journal of cereal science*, **43**, 393-397.

Babin, P., Della Valle, G., Dendievel, R., Lourdin, D. & Salvo, L. (2007). X-ray tomography study of the cellular structure of extruded starches and its relations with expansion phenomenon and foam mechanical properties. *Carbohydrate polymers*, **68**, 329-340.

Barcelon, E.G., Tojo, S. & Watanabe, K. (1999). X-ray computed tomography for internal quality evaluation of peaches. *Journal of Agricultural Engineering Research*, **73**, 323-330.

Bewley, J.D. (1997). Seeds germination and dormancy. *The Plant Cell*, **9**, 1055-1066.

Blazek, J. & Gilbert, E.P. (2010). Effect of enzymatic hydrolysis on native starch granule structure.Biomacromolecules, 11, 3275-3289.

Bouxsein, M.L., Boyd, S.K., Christiansen, B.A., Guldberg, R.E., Jepsen, K.J. & Müller, R. (2010). Guidelines for assessment of bone microstructure in rodents using micro–computed tomography. Journal of bone and mineral research, 25, 1468-1486.

Cilia, M.L. & Jackson, D. (2004). Plasmodesmata form and function. Current Opinion in Plant Biology, 16, 500-506.

Cnudde, V. & Boone, M. (2013). High-resolution X-ray computed tomography in geosciences: a review of the current technology and applications. *Earth-Science Reviews*, **123**, 1-17.

Cnudde, V., Masschaele, B., Dierick, M., Vlassenbroeck, J., Hoorebeke, L.V. & Jacobs, P. (2006).Recent progress in X-ray CT as a geosciences tool. *Applied Geochemistry*, **21**, 826-832.

Davidson, V.J., Noble, S.D. & Brown, R.B. (2000). PH—Postharvest technology: effects of drying air temperature and humidity on stress cracks and breakage of maize kernels. *Journal of Agricultural Engineering Research*, **77**, 303-308.

De Carvalho, M.L.M., Van Aelst, A.C., Van Eck, J.W. & Hoekstra, F.A. (1999). Pre-harvest stress cracks in maize (Zea mays L.) kernels as characterized by visual, X-ray and low temperature scanning electron microscopical analysis: effect on kernel quality. *Seed Science Research*, **9**, 227-236.

Dogan, H. (2007). Nondestructive imaging of agricultural products using X-ray microtomography. *Microscopy and Microanalysis*, **13**, 1316-1317.

Dure, L.S. (1960). Site of origin and extent of activity of amylases in maize germination. *Plant Physiology*, **35**, 925.

Dyck, V. (1998). Desktop X-ray microscopy and microtomography. *Journal of microscopy*, **191**, 151-158

Falcone, P., Baiano, A., Zanini, F., Mancini, L., Tromba, G., Montanari, F. & Nobile, M. (2004). A novel approach to the study of bread porous structure: phase contrast X-ray microtomography. *Journal of Food Science*, **69**, FEP38-FEP43.

Falcone, P.M., Baiano, A., Conte, A., Mancini, L., Tromba, G., Zanini, F. & Del Nobile, M.A. (2006). Imaging techniques for the study of food microstructure: a review. In: *Advances in Food and Nutrition Research* (edited by L.T. Steve). Pp. 205-263. USA: Academic Press.

Falcone, P.M., Baiano, A., Zanini, F., Mancini, L., Tromba, G., Dreossi, D., Montanari, F., Scuor, N.& Nobile, M.A.D. (2005). Three-dimensional quantitative analysis of bread crumb by X-ray microtomography. *Journal of Food Science*, **70**, E265-E272.

Fannon, J.E., Hauber, R.J. & BeMiller, J.N. (1992). Surface pores of starch granules. *CerealChemistry*, **69**, 284-288.

Finch-Savage, W.E. & Leubner-Metzger, G. (2006). Seed dormancy and the control of germination. New Phytologist, 171, 501 - 523

Fincher, G.B. (1989). Molecular and cellular biology associated with endosperm mobilization in germinating cereal grains. *Annual Review of Plant Physiology and Plant Molecular Biology*, **40**, 305-346.

Fox, G. & Manley, M. (2009). Hardness methods for testing maize kernels. *Journal of Agricultural and Food Chemistry*, **57**, 5647-5657.

Gallant, D.J., Bouchet, B. & Baldwin, P.M. (1997). Microscopy of starch: evidence of a new level of granule organization. *Carbohydrate polymers*, **32**, 177-191.

Gallardo, K., Job, C., Groot, S.P., Puype, M., Demol, H., Vandekerckhove, J. & Job, D. (2002). Proteomics of Arabidopsis seed germination. A comparative study of wild-type and gibberellin-deficient seeds. *Plant Physiology*, **129**, 823-837.

Gaytán-Martínez, M., Figueroa-Cárdenas, J., Reyes-Vega, M., Rincón-Sánchez, F. & Morales- Sánchez, E. (2006). Microstructure of starch granule related to kernel hardness in corn. *Revista Fitotecnia Mexicana*, 135-139.

Gustin, J.L., Jackson, S., Williams, C., Patel, A., Armstrong, P.R., Peter, G.F. & Settles, A.M. (2013). Analysis of maize (Zea mays) kernel density and volume using micro-computed tomography and single-kernel near infrared spectroscopy. *Journal of Agricultural and Food Chemistry*,**61**, 10872-10880.

Haff, R. & Toyofuku, N. (2008). X-ray detection of defects and contaminants in the food industry. *Sensing and Instrumentation for Food Quality and Safety*, **2**, 262-273.

Harvey, B. & Oaks, A. (1974). The role of gibberellic acid in the hydrolysis of endosperm reserves in Zea mays. *Planta*, **121**, 67-74.

Huber, K.C. & BeMiller, J.N. (1997). Visualization of channels and cavities of corn and sorghum starch granules1. *Cereal Chemistry Journal*, **74**, 537-541.

Huber, K.C. & BeMiller, J.N. (2000). Channels of maize and sorghum starch granules. *Carbohydrate Polymers*, **41**, 269-278.

Jones, R.J. & Brenner, M.L. (1987). Distribution of abscisic acid in maize kernel during grain filling. Plant Physiology, 83, 905-909.

Kalender, W.A. (2006). X-ray computed tomography. *Physics in medicine and biology*, **51**, R29.

Kidmose, U. & Martens, H.J. (1999). Changes in texture, microstructure and nutritional quality ofcarrot slices during blanching and freezing. *Journal of the Science of Food and Agriculture*,**79**, 1747-1753.

Koster, M. & van Dalen, G. (2013). Study of the water vapour sorption of freeze dried carrots using micro-CT. *Unilever Research*, 1-7.

Kucera, B., Cohn, M.A. & Leubner-Metzger, G. (2005). Plant hormone interactions during seed dormancy release & germination. Seed Science Research, 15, 281-307

Labouriau, L.G. & Osborn, J.H. (1984). Temperature dependence of the germination of tomato seeds. *Journal of Thermal Biology*, **9**, 285-294.

Landis, E.N. & Keane, D.T. (2010). X-ray microtomography. *Materials Characterization*, **61**, 1305-1316.

Laverse, J., Frisullo, P., Conte, A. & Nobile, M. (2012). X-ray microtomography for food quality analysis. In: *Food Industrial Processes–Methods and Equipment* (edited by V. Benjamin). Pp. 339-362. Croatia: InTech.

Li, D., Wang, L.-J., Wang, D.-C., Dong Chen, X. & Mao, Z.-H. (2007). Microstructure analysis of rice kernel. *International Journal of Food Properties*, **10**, 85-91.

Lim, K.S. & Barigou, M. (2004). X-ray micro-computed tomography of cellular food products. *FoodResearch International*, **37**, 1001-1012.

Martin, C., Herrman, T.J., Loughin, T. & Oentong, S. (1998). Micropycnometer measurement of single-kernel density of healthy, sprouted, and scab-damaged wheats 1. *Cereal Chemistry*, **75**, 177-180.

Mei, Y.-Q. & Song, S.-Q. (2008). Early morphological and physiological events occurring during germination of maize seeds. *Agricultural Sciences in China*, **7**, 950-957.

Mendoza, F., Verboven, P., Mebatsion, H.K., Kerckhofs, G., Wevers, M. & Nicolaï, B. (2007). Three- dimensional pore space quantification of apple tissue using X-ray computed microtomography. *Planta*, **226**, 559-570.

Narváez-González, E.D., de Dios Figueroa-Cárdenas, J., Taba, S., Tostado, E.C., Peniche, R.Á.M. & Sánchez, F.R. (2006). Relationships between the microstructure, physical features, and chemical composition of different maize accessions from Latin America. *Cereal chemistry*, **83**, 595-604.

Neethirajan, S., Jayas, D. & White, N. (2007). Detection of sprouted wheat kernels using soft X-ray image analysis. *Journal of Food Engineering*, **81**, 509-513.

Nonogaki, H., Bassel, G.W. & Bewley, J.D. (2010). Germination—still a mystery. *Plant Science*, **179**,574-581.

Oates, C.G. (1997). Towards an understanding of starch granule structure and hydrolysis. *Trends in Food Science & Technology*, **8**, 375-382.

Park, S.C., Park, M.K. & Kang, M.G. (2003). Super-resolution image reconstruction: a technical overview. *Signal Processing Magazine, IEEE*, **20**, 21-36.

Ritchie, S., Swanson, S.J. & Gilroy, S. (2000). Physiology of the aleurone layer and starchy endosperm during grain development and early seedling growth: new insights from cell and molecular biology. *Seed Science Research*, **10**, 193-212.

Sabelli, P.A. & Larkins, B.A. (2009). The development of endosperm in grasses. *Plant Physiology*, **149**, 14-26.

Sánchez-Linares, L., Gavilanes-Ruíz, M., Díaz-Pontones, D., Guzmán-Chávez, F., Calzada-Alejo, V., Zurita-Villegas, V., Luna-Loaiza, V., Moreno-Sánchez, R., Bernal-Lugo, I. & Sánchez- Nieto, S. (2012). Early carbon mobilization and radicle protrusion in maize germination. *Journal of experimental botany*, **63**, 4513-4526.

Santos Garcés, E. (2012). Applications of computed tomography in dry-cured meat products. PhD degree in Technology Chemical Engineering Thesis, University of Girona, Spain.

Sasov, A. & van Dyck, D. (1998). Desktop x-ray microscopy and microtomography. *Journal of Microscopy*, **191**, 151-158.

Shrestha, A.K., Blazek, J., Flanagan, B.M., Dhital, S., Larroque, O., Morell, M.K., Gilbert, E.P. & Gidley, M.J. (2012). Molecular, mesoscopic and microscopic structure evolution during amylase digestion of maize starch granules. *Carbohydrate Polymers*, **90**, 23-33.

Singletary, G.W., Banisadr, R. & Keeling, P.L. (1994). Heat stress during grain filling in maize: effects on carbohydrate storage and metabolism. *Functional Plant Biology*, **21**, 829-841.

Smail, V.W., Fritz, A.K. & Wetzel, D.L. (2006). Chemical imaging of intact seeds with NIR focal plane array assists plant breeding. *Vibrational spectroscopy*, **42**, 215-221.

Song, H.P. & Litchfield, J.B. (1994). Measurement of stress cracking in maize kernels by magnetic resonance imaging. *Journal of Agricultural Engineering Research*, **57**, 109-118.

Subedi, C.K. & Bhattarai, T. (2003). Effect of gibberellic acid on reserve food mobilization of maize(Zea mays L. var Arun-2) endosperm during germination. *Himalayan Journal of Sciences*, **1**, 99-102.

Sujika, M. & Jamroz, J. (2007). Starch granule porosity and its changes by means of amylosis.*International Agrophysics*, **21**, 107-113.

Tester, R., Qi, X. & Karkalas, J. (2006). Hydrolysis of native starches with amylases. *Animal FeedScience and Technology*, **130**, 39-54.

Tkachuk, R., Dexter, J. & Tipples, K. (1991). Removal of sprouted kernels from hard red spring wheat with a specific gravity table. *Cereal Chemistry*, **68**, 390-395.

Toole, E., Hendricks, S., Borthwick, H. & Toole, V.K. (1956). Physiology of seed germination. *Annual review of plant physiology*, **7**, 299-324.

Wang, X.F., Jing, X.M. & Lin, J. (2005). Starch mobilization in ultradried seed of maize (Zea mays L.) during germination. *Journal of Integrative Plant Biology*, **47**, 443-451.

Watson, S.A. (1987). Structure and composition. In: *Corn: chemistry and technology* (edited by S.A. Watson & P.E. Ramstad). Pp. 53-82. St. Paul, MN: American Association of Cereal Chemists. Inc.

Williams, P., Geladi, P., Fox, G. & Manley, M. (2009). Maize kernel hardness classification by near infrared (NIR) hyperspectral imaging and multivariate data analysis. *Analytica Chimica Acta*,
653, 121-130.

Williams, P.J. (2013). Near infrared (NIR) hyperspectral imaging and X-ray computed tomography combined with statistical and multivariate data analysis to study Fusarium infection in maize. PhD in Food ScienceStellenbosch: Stellenbosch University.

Wilson, C.M. (1997). Molecular and cellular studies of early endosperm development in barley(*Hordeum vulgare L.*). PhD Thesis. Durham University, England.

Zwiggelaar, R., Bull, C.R. & Mooney, M.J. (1996). X-ray simulations for imaging applications in the agricultural and food industries. *Journal of Agricultural Engineering Research*, **63**, 161-170.

Chapter 5

General discussion and conclusions

Six white maize hybrids with varying hardness levels (i.e. hard, intermediate and soft) were pre-germinated two-hourly from 0 to 22 h. Three imaging techniques near infrared (NIR) hyperspectral imaging, X-ray micro computed tomography (X-ray μCT) and (Scanning electron microscopy (SEM)) employed for the investigation of the impact pre-germination on maize kernel hardness.

All imaging techniques indicated vitreous endosperm quality deterioration. Score images obtained from using the NIR hyperspectral imaging technique, revealed a decrease in vitreous endosperm content as pre-germination progressed in all tested hybrids. The decrease in vitreous endosperm content (expressed as percentage vitreous endosperm indicated that as pre-germination time period increased, loss vitreousness or hardness in maize kernel hybrids took place. Changes that took place within the maize endosperm as degree of pre-germination increased from 0 to 22 h could be identified and analysed using principal component analysis (PCA) score plots and PCA score images. PCA score plots are able to indicate the presence of variation between samples (Williams, 2009). Isolation of the vitreous endosperm pixels on the PCA score indicated the soft and intermediate maize hybrids had lost vitreousness when comparing imaged maize kernels pre-germinated from 0 h – 22 h. The soft and intermediate maize kernels hybrids seemed to have lost more vitreous endosperm than the hard hybrids. However, it should be noted that the intermediate and soft maize hybrids should comprise of less vitreous endosperm than the hard hybrid. Based on the results obtained it can be noted that, the decrease of the vitreous endosperm led to a decrease in maize kernel hardness and an increase in softness. The degradation of the endosperm renders the quality of the endosperm for the dry milling industry where the endosperm used for the production of maize meal should be of vitreous quality.

X-ray μCT illustrated crevices that could be described as fissures and shrinkage stress cracks occurring as a results of pre-germination and drying process. Fissures were developed due to pre- germination and shrinkage stress cracks from the drying process. Fissures and shrinkage stress cracks were observed in all imaged hybrids pre-germinated for 10 h and 22 h. The side orientation two dimensional (2D) image slices depicted the intermediate and soft maize hybrids micro structure deteriorated more than the hard hybrid at 10 h and 22 h.

The top orientation of the 2D slice images indicated the hard and intermediate deteriorated more than the soft hybrids. Three dimensional image volumes depicted fissures and shrinkage stress

cracks developed on a plane. Fissures could increase the susceptibility of the maize kernels to unwanted kernel breakage during the mechanical handling, increase microbial contamination and lower yields of the desired dry milling particle sizes (Davidson *et al.*, 2000). After drying, more crevices were observed and it was concluded that fissures propagated after the drying process and stress cracks also developed due to the shrinkage of the swollen starch granules. It should be noted however that freeze drying causes minimal destruction to the microstructure of food products (Kidmose & Martens, 1999; Koster & van Dalen, 2013). Another assumption could be made that the growth and development of the germ caused expansion stress cracks to develop as the germ pushed against the endosperm. These expansion stress cracks could be contributing to the large number of crevices observed after the drying process.

Germ morphological changes could also be observed in all hybrids that were pre-germinated in the form of radicle growth. Attenuation decreased as pre-germination increased in the 10 and 22 h maize samples. Areas with high attenuation within the sample were registered as bright areas (i.e. areas of high density due to the energy transfer between the X-ray photons and sample atoms (Cnudde & Boone, 2013)) whereas those with low attenuation are registered as dark areas. SEM images confirmed endosperm degradation in the form of fissures and radicle growth. Furthermore, pores were noted on the surface of the starch granules and protein matrix.

Real time single kernel analysis (performed to investigate the origins of the fissures and shrinkage stress cracks) validated that at T8 = 21 h, crevices started to develop and propagated to T19 = 143 h. Fissure measurement indicated an increment from both sides of the maize kernels, i.e. from the left side of the maize kernel fissures propagated moved from 1.51 mm at 99 h to 4.22 mm at 143 h, on the right side from 1.86 mm at 99 h to 3.65 mm at 143 h. At T15 = 123 h, a horizontal fissure was observed and measured to the 1.62 mm long while at T19 = 143 h it had propagated to 1.30 mm. The crevices noted to be pathways for the hydrolytic enzymes and monomers to be transported to their destined areas. Volumes of the vitreous endosperm were also determined and a decreasing trend was noticed. At T1 = 0 h the content of the vitreous endosperm was 64.7 mm^3 and at T19 = 143 h the content was noted to be 50.5 mm^3.

There is a definite decrease in the vitreousness of maize kernels as a result of pre- germination having taken place. This should be of major concern to the dry milling industry where kernel hardness is of great importance.

Other properties such as starch and protein which have an impact on maize hardness should also be investigated with the help of loading plots. It would be advisable though to use the same kernel in the imaging process from 0 to 22 h, so that variations between samples could be minimised.

Endosperm degradation was evident in 10 and 22 h maize kernel on 2D image slices. All 3 orientations (front, side and top) indicated crevices developed throughout the floury and vitreous endosperm. Endosperm deterioration was depicted in the form of attenuation variation where degraded areas appeared as dark areas on the 2D slice images. The loss of attenuation indicated loss of density which indirectly showed loss of hardness for the 10 and 22 h pre-geminated kernels. SEM images confirmed endosperm deterioration in the 10and 22 h pre-germinated maize kernels in the form of starch and protein matrix degradation noted as pores appearing on the surfaces. Apertures present on 0 h maize kernels starch granules and protein matrix assisted with the degradation observed in 10 and 22 h samples, by allowing hydrolysing enzymes entry to these macromolecules.

Real-time experiment concluded endosperm deterioration within a pre-germinated maize kernel and this should be of great concern to the dry milling industry. The crevices that develop increase the chances of undesired breakage taking place during the milling process leading to decreased yields of desired particle size.

A study such as this one has not yet been performed, therefore there is limited literature on the effect of pre-germination on maize hardness. Studies on the effect of pre-germination on cereal grains have only been limited to wheat, barley and sorghum. To add to that, there is no official stipulated method for maize hardness determination as in the case of wheat, therefore the definition of hardness was based on previous researcher's findings. For future purposes, NIR hyperspectral imaging should be used to further investigate the chemical changes that take place within the maize kernel as pre-germination occurs. It should be noted though that a single maize kernel should be used in the investigation to eliminate kernel size variation as well as endosperm content changes. X-ray µCT should be used to investigate the endosperm further by analysing more than one kernel for real-time lapse experiment. Maize kernel density can also be translated into maize hardness (Gustin *et al.*, 2013), therefore it would be advisable to perform density measurements using X-ray µCT technique.

References

Anonymous. (2014). Total maize: supply and demand. In: *South African maize crop: quality report 2012/2013 season*. Pp. 1-78. Pretoria: South African Grain Laboratory NPC. Bewley, J.D. (1997). Seeds germination and dormancy. *The Plant Cell*, **9**, 1055-1066.

Cnudde, V. & Boone, M. (2013). High-resolution X-ray computed tomography in geosciences: a review of the current technology and applications. *Earth-Science Reviews*, **123**, 1-17.

Davidson, V.J., Noble, S.D. & Brown, R.B. (2000). PH—Postharvest technology: effects of drying air temperature and humidity on stress cracks and breakage of maize kernels. *Journal of Agricultural Engineering Research*, **77**, 303-308.

Fincher, G.B. (1989). Molecular and cellular biology associated with endosperm mobilization in germinating cereal grains. *Annual Review of Plant Physiology and Plant Molecular Biology*,
40, 305-346.

Gustin, J.L., Jackson, S., Williams, C., Patel, A., Armstrong, P.R., Peter, G.F. & Settles, A.M. (2013). Analysis of maize (Zea mays) kernel density and volume using micro-computed tomography and single-kernel near infrared spectroscopy. *Journal of Agricultural and Food Chemistry*, **61**, 10872-10880.

Harvey, B. & Oaks, A. (1974). The role of gibberellic acid in the hydrolysis of endosperm reserves in Zea mays. *Planta*, **121**, 67-74.

Kidmose, U. & Martens, H.J. (1999). Changes in texture, microstructure and nutritional quality of carrot slices during blanching and freezing. *Journal of the Science of Food and Agriculture*, **79**, 1747-1753.

Koster, M. & van Dalen, G. (2013). Study of the water vapour sorption of freeze dried carrots using micro-CT. *Unilever Research*, 1-7.

Lopes, M.A. & Larkins, B.A. (1991). Gamma-zein content is related to endosperm modification in quality protein maize. *Crop science*, **31**, 1655-1662.

Smail, V.W., Fritz, A.K. & Wetzel, D.L. (2006). Chemical imaging of intact seeds with NIR focal plane array assists plant breeding. *Vibrational spectroscopy*, **42**, 215-221.

Watson, S.A. (1987). Structure and composition. In: *Corn: chemistry and technology* (edited by S.A. Watson & P.E. Ramstad). Pp. 53-82. St. Paul, MN: American Association of Cereal Chemists. Inc.

Williams, P.J. (2009). Near infrared (NIR) hyperspectral imaging for evaluation of whole maize kernels: chemometrics for exploration and classification. Stellenbosch: University of Stellenbosch.